This is a preprint, the final version is subject to change, of the American Mineralogist (MSA)
Cite as Authors (Year) Title. American Mineralogist, in press.
DOI: https://doi.org/10.2138/am-2020-7173

REVISION #1—submitted to *American Mineralogist*—07 November 2019

An evolutionary system of mineralogy, part I: stellar mineralogy (>13 to 4.6 Ga)

ROBERT M. HAZEN[1,*] **AND SHAUNNA M. MORRISON**[1]

[1]Geophysical Laboratory, Carnegie Institution for Science,
5251 Broad Branch Road NW, Washington, DC 20015, U. S. A.

"The science of Mineralogy has made rapid progress in the past six years; chemistry has opened to us a better knowledge of the nature and relations of compounds; and philosophy has thrown new light on the principles of classification. To change is always seeming fickleness. But not to change with the advance of science, is worse; it is persistence in error."

James Dwight Dana, *System of Mineralogy*, Third Edition, 1850, p. 5

ABSTRACT

Minerals preserve records of the physical, chemical, and biological histories of their origins and subsequent alteration, and thus provide a vivid narrative of the evolution of Earth and other worlds through billions of years of cosmic history. Mineral properties, including trace and minor elements, ratios of isotopes, solid and fluid inclusions, external morphologies, and other idiosyncratic attributes, represent information that points to specific modes of formation and subsequent environmental histories—information essential to understanding the co-evolving geosphere and biosphere. This perspective suggests an opportunity to amplify the existing system of mineral classification, by which minerals are defined solely on idealized end-member chemical compositions and crystal structures. Here we present the first in a series of

contributions to explore a complementary evolutionary system of mineralogy—a classification scheme that links mineral species to their paragenetic modes.

The earliest stage of mineral evolution commenced with the appearance of the first crystals in the universe at >13 Ga and continues today in the expanding, cooling atmospheres of countless evolved stars, which host the high-temperature ($T > 1000$ K), low-pressure ($P < 10^{-2}$ atm) condensation of refractory minerals and amorphous phases. Most stardust is thought to originate in three distinct processes in carbon- and/or oxygen-rich mineral-forming stars: (1) condensation in the cooling, expanding atmospheres of asymptotic giant branch stars; (2) during the catastrophic explosions of supernovae, most commonly core collapse (Type II) supernovae; and (3) classical novae explosions, the consequence of runaway fusion reactions at the surface of a binary white dwarf star. Each stellar environment imparts distinctive isotopic and trace element signatures to the micro- and nanoscale stardust grains that are recovered from meteorites and micrometeorites collected on Earth's surface, by atmospheric sampling, and from asteroids and comets. Although our understanding of the diverse mineral-forming environments of stars is as yet incomplete, we present a preliminary catalog of 41 distinct natural kinds of stellar minerals, representing 22 official International Mineralogical Association (IMA) mineral species, as well as 2 as yet unapproved crystalline phases and 3 kinds of non-crystalline condensed phases not codified by the IMA.

***E-mail:** rhazen@ciw.edu

Keywords: classification; mineral evolution; mineral ecology; natural kinds; vapor deposition; condensation; astromineralogy; stardust; diamond; graphite; corundum; moissanite; hibonite; amorphous phases

This is a preprint, the final version is subject to change, of the American Mineralogist (MSA)
Cite as Authors (Year) Title. American Mineralogist, in press.
DOI: https://doi.org/10.2138/am-2020-7173

INTRODUCTION

Mineral diversity and distribution have evolved through almost 14 billion years of cosmic history, as a succession of physical, chemical, and ultimately biological processes led to the selection and concentration of mineral-forming elements in varied pressure-temperature-composition environments. As such, minerals and other condensed phases bear vivid testimony to the ancient origins and storied evolution of diverse worlds, both in our Solar System and in star systems far beyond. A central objective of Earth and planetary sciences is to tease out those histories from the rich, revealing mineralogical evidence left behind.

The present system of mineral classification of the International Mineralogical Association's Commission on New Minerals, Nomenclature and Classification (IMA, CNMNC; e.g., Burke 2006; Mills et al. 2009; Schertl et al. 2018) is based on pure end-member chemical compositions and idealized crystal structures—the minimum information necessary to distinguish between any two species. Such a coherent and reproducible framework is essential for the field of mineralogy and it will remain the foundation for mineral nomenclature and classification for decades to come. However, by design the IMA classification system does not incorporate the idiosyncratic compositional variations, distinctive physical properties, and diverse morphological characteristics of minerals and other condensed phases formed under varying environmental conditions at different historical stages of the cosmos (e.g., Santana 2019). Therefore, we have the opportunity to build on the present system of mineralogy, to capture more fully the evolving mineralogical diversity of Earth and other worlds through deep time.

We propose a complementary "evolutionary classification system" of minerals, which catalogues minerals by coupling species with their paragenetic modes. Accordingly, we adopt a binomial nomenclature, with a mineral name preceded by a descriptor of the paragenetic mode,

such as "*impact stishovite*," "*pegmatitic hydroxylapatite*," or "*biogenic pyrite*." The system is divided into chronological parts, each representing a different stage of mineral evolution (Hazen et al. 2008; Hazen and Ferry 2010). In Part I, we consider stellar mineralogy and the earliest condensed phases in the cosmos, to be followed by interstellar and nebular mineralogy (Part II), planetesimal mineralogy (Part III), and a series of subsequent contributions focused on planetary processes. Within each part, minerals are arranged according to the Dana System—Native Elements, followed by Sulfides, Oxides and Hydroxides, etc. (J.D. Dana et al. 1973; Gaines et al. 1997; see www.webmineral.com/danaclass, accessed 28 September 2019).

We employ IMA-approved mineral names for the great majority of species. However, the evolutionary system of mineralogy deviates from IMA nomenclature in three significant ways (Hazen 2019). First, by employing a binomial nomenclature, we split many common minerals into multiple kinds based on their distinctive paragenetic modes. Thus, in our system diamond formed by low-pressure condensation in a stellar atmosphere (e.g., *AGB diamond*; see below) differs from diamond formed by shock alteration of carbon-rich material (*impact diamond*), or crystalized at high pressure and temperature in Earth's mantle (e.g., *Type 1 diamond*).

On the other hand, in some instances two or more IMA species should be lumped because they form by a single process in a continuous phase space. The occurrence of zoned minerals within complex compositional space, for example in the pyroxene, amphibole, mica, and tourmaline groups, often results in multiple IMA species being present in a single mineral grain (e.g., dravite-schorl in zoned tourmaline crystals; Grew et al. 2015). In these instances, we lump two or more compositional end-member mineral species into a single natural kind. We also catalog a variety of non-crystalline condensed phases as natural kinds—materials important in

planetary evolution, even though they are not typically assigned official mineral names by the present IMA procedures.

This contribution is the first in a planned series of publications on an evolutionary system of mineralogy that will examine chronologically the emerging diversity and distribution of condensed phases found on Earth, as well as on other planets, moons, and nebular environments. Here we explore stardust—remnants from the earliest episodes of mineral evolution. Stellar mineralogy, or "astromineralogy" (e.g., DePew et al. 2006; A.P. Jones 2007), encompasses all solid phases that form in the atmospheres of stars—mineralization that commenced more than 13 billion years ago, long before the formation of our solar nebula. At least 41 different natural kinds of stellar minerals, representing 22 IMA-approved mineral species, two crystalline phases not yet approved by the IMA, and three non-crystalline phases (Table 1), formed primarily from 11 relatively abundant chemical elements that emerged from stellar nucleosynthesis—C, N, O, Mg, Al, Si, S, Ca, Ti, Cr, and Fe (e.g., Clayton 1983; Rolfs and Rodney 2005; Schatz 2013; Figure 1A). The expanding, cooling gaseous envelopes of aged stars, characterized by high-temperature (>1000 K) and low-pressure (< 10^{-2} atm) condensation of a few refractory phases (Figure 1B), represent the most ancient mineral-forming environments in the cosmos.

This is a preprint, the final version is subject to change, of the American Mineralogist (MSA)
Cite as Authors (Year) Title. American Mineralogist, in press.
DOI: https://doi.org/10.2138/am-2020-7173

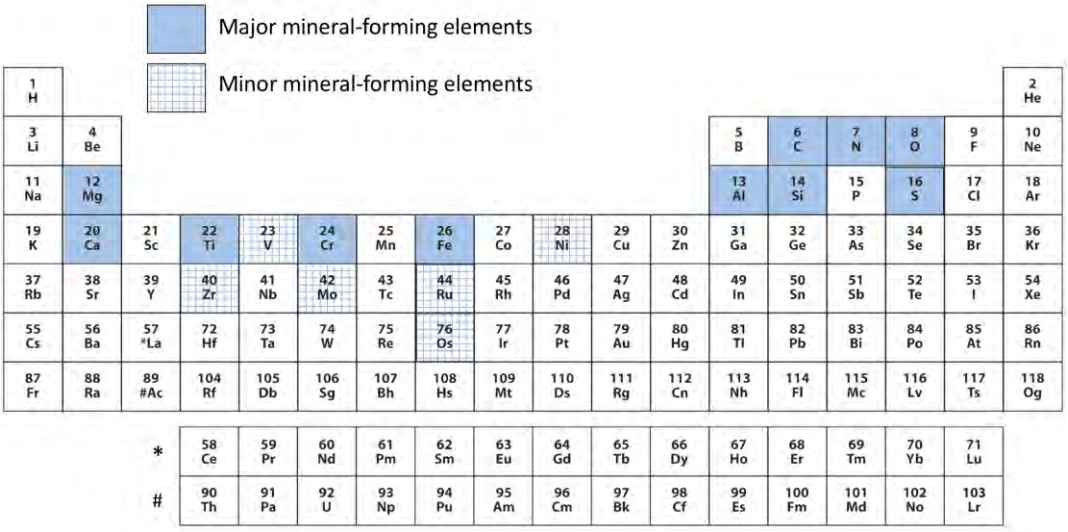

A

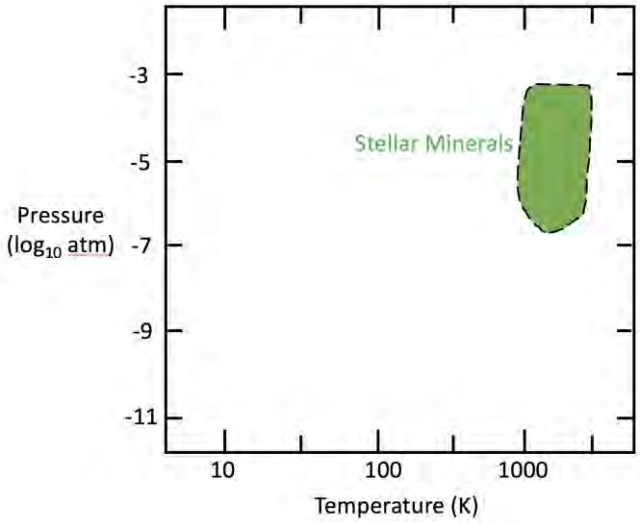

B

Figure 1. Characteristic pressure-temperature-composition regimes of stellar minerals.

A. Eleven major mineral-forming elements and six select minor elements commonly found in stardust.

B. Estimated pressure-temperature formation ranges of most stellar primary condensate minerals, which formed via relatively low-pressure, high-temperature condensation in the turbulent atmospheres of highly evolved stars.

This is a preprint, the final version is subject to change, of the American Mineralogist (MSA)
Cite as Authors (Year) Title. American Mineralogist, in press.
DOI: https://doi.org/10.2138/am-2020-7173

ON THE NATURE OF STARDUST

Stellar minerals must have first formed within a few hundred million years of the Big Bang, as temperatures in the expanding gaseous envelopes of supernovae and early generations of other highly evolved stars (Abel et al. 2002; Robertson et al. 2015; Bowman et al. 2018) fell significantly below the maximum ~1700 K condensation temperature of diamond in a carbon-rich gas at ~10^{-4} atm (Lodders and Amari 2005). Varied nano- and micro-crystalline phases, collectively called the "ur-minerals" (Hazen et al. 2008), represent the earliest condensed matter in the history of the universe—the true beginnings of cosmic mineralogy.

The first evidence for mineral formation around stars came from observations of distinctive infrared absorption features from the dust-rich expanding envelopes of planetary nebulas and supernovae (Gillett et al. 1968; Woolf and Ney 1969; Treffers and Cohen 1974; see Boulanger et al. 2009 and references therein). Donald Clayton subsequently suggested that presolar stellar condensates may be preserved in meteorites and should have significant isotopic anomalies compared to solar abundances (Clayton 1975, 1978; Clayton and Ward 1978)—speculations confirmed by laboratory discoveries in the late 1980s (Lewis et al. 1987; Bernatowicz et al. 1987; Zinner et al. 1987; Amari et al. 1990). These ancient specks of stardust have become the focus of increasingly intense study by both mineralogists and astrophysicists (e.g., Clayton and Nittler 2004; Lodders and Amari 2005; Lugaro 2005; Davis 2011, 2014; Zinner 2014; Nittler and Ciesla 2016; and references therein).

Presolar grains are present in the least processed extraterrestrial materials, including meteorites and micrometeorites collected on Earth's surface (e.g., Yada et al. 2008), interplanetary dust particles collected from Earth's upper atmosphere by high-altitude aircraft (Hodge 1961; Dermott and Liou 1994; Messenger 2002), and samples of comet Wild-2 returned

147 by NASA's *Stardust* mission (e.g., McKeegan et al. 2006; Stadermann et al. 2008). They are
148 identified by their highly anomalous isotopic compositions, compared to materials that formed in
149 the Solar System, which point to an origin in the turbulent winds and/or explosions of previous
150 generations of evolved stars. A significant suite of micro- and nanophases are now recognized
151 by their distinctive chemistries, isotopic compositions, and morphologies—features that point to
152 origins in a variety of carbon- and/or oxygen-rich stellar environments (Table 1). Each individual
153 presolar grain formed during a given time interval in a given evolved star and thus preserves a
154 fossil memory of the physical and chemical conditions of its formation environment
155 (Bernatowicz et al. 2003; Zinner 2014; Takigawa et al. 2018).

156 Studying stellar minerals is challenging on several fronts as a consequence of their diminutive
157 scale. All stellar mineral grains are small, ranging from multi-micrometer-scale grains of
158 graphite and moissanite (SiC) with many trillion atoms to nano-diamonds with fewer than 1000
159 atoms per particle (e.g., Lugaro 2005; Davis 2011). The first identified and best-studied presolar
160 phases (SiC and C allotropes; Lewis et al. 1987; Bernatowicz et al. 1987; Zinner et al. 1987) are
161 highly refractory and acid-resistant, so they can be isolated from meteorites via acid dissolution
162 of the dominant silicate, metal, and sulfide phases ("burning down a haystack to find a needle").
163 The development of nanoscale secondary ion mass spectrometry (NanoSIMS) technology later
164 enabled high-resolution (< 0.1 micron) isotopic mapping of interplanetary dust and meteorites to
165 identify presolar grains *in situ*, especially presolar silicates, as these grains are destroyed by the
166 acid dissolution methods (Messenger et al. 2003; Mostefaoui and Hoppe 2004; Nagashima et al.
167 2004; Nguyen and Zinner 2004). Once identified by their anomalous isotopic compositions,
168 presolar grains can be prepared by focused ion beam (FIB) methods and analyzed by
169 transmission electron microscopy (TEM). Such investigations of individual grains are now

170 providing remarkable insights regarding the ancient origins and evolution of stardust (Amari
171 2014; Zinner 2014; Nittler and Cielsa 2016).

172 At least 22 different IMA-approved mineral species and five other phases have been
173 confirmed as stellar minerals (Table 1). However, the varied grains in stardust, including several
174 amorphous or glassy phases, display a wide diversity of observed attributes, including distinctive
175 elemental and isotopic compositions, external morphologies, and microstructures that point to at
176 least three major paragenetic modes, resulting in a list of natural kinds of condensed stellar
177 phases significantly greater than the modest list of official mineral species. In this context, grains
178 with similar isotopic and structural attributes are assumed to have had similar histories, arising in
179 some cases from the same parent stellar environment. An important and as yet poorly
180 constrained aspect of stellar mineralogy is that the temperature-pressure-composition regimes of
181 dust-producing stars differ widely, both from star to star and spatially and temporally within the
182 evolving dynamic atmospheres of any given star. Consequently, suites of these grains will vary
183 significantly, depending on their specific peripatetic stellar histories. In some instances, presolar
184 mineral grains (especially suites of refractory inclusions) appear to represent relatively pristine
185 primary condensates—in essence pure fragments of a specific star. However, other grains may
186 have experienced subsequent reworking that significantly altered the mineral's elemental and
187 isotopic compositions and/or structural state, both within a dynamic stellar environment and
188 through subsequent nebular processing. As a result, stellar mineralogy, though limited to the
189 most refractory high-temperature phases of cosmically abundant elements, is richly varied in
190 ways that are only gradually coming to light.
191

This is a preprint, the final version is subject to change, of the American Mineralogist (MSA)
Cite as Authors (Year) Title. American Mineralogist, in press.
DOI: https://doi.org/10.2138/am-2020-7173

ON THE PARAGENESIS OF STELLAR MINERALS

Long before the emergence of our Solar System and its intriguing diversity of mineral-rich worlds, condensed crystalline and amorphous phases formed abundantly in the ejecta of supernovae and classical novae, as well as in the expanding, cooling gaseous envelopes of highly evolved stars (Mostefaoui and Hoppe 2004; Lodders and Amari 2005; Hynes et al. 2010; Davis 2011; Nittler and Ciesla 2016; Nittler et al. 2018b). Here we review stellar environments in which isotopes are synthesized and astrominerals emerge. In the following two sections we briefly summarize two key aspects of stardust: (1) the nucleosynthetic origins of mineral-forming elements, and (2) the three types of high-temperature stellar environments in which minerals most frequently condense. For detailed discussions of the stellar origins of astrominerals see reviews by Lodders and Amari (2005), Nittler and Dauphas (2006), Davis (2011), Zinner (2014), and Nittler and Ciesla (2016).

Stellar nucleosynthesis and the origins of mineral-forming elements: Minerals on Earth are known to incorporate almost 300 stable or long-lived isotopes of at least 72 chemical elements. Big-Bang Nucleosynthesis (BBN), by contrast, can account for significant quantities of only hydrogen, helium, and lithium (Bertulani 2013, and references therein), though trivial quantities of heavier elements, including carbon, nitrogen, and oxygen, also emerged from BBN (Iocca et al. 2008). Consequently, almost all mineral-forming elements other than hydrogen arose through processes of stellar nucleosynthesis (Burbidge et al. 1957; Cameron et al. 1957; Schatz 2010; Bertulani 2013), which began ~100 Ma after the Big Bang with the first generation of massive stars (Abel et al. 2002; Robertson et al. 2015; Bowman et al. 2018). A variety of nucleosynthetic mechanisms, each of which produces a distinctive pattern of elements and isotopes, contribute

significantly to suites of mineral-forming elements and their isotopes in stars (e.g., Truran and Heger 2003; Zinner 2014; Nittler and Ciesla 2016).

Nucleosynthesis in stars is inextricably linked to stellar evolution, which can be characterized as a competition between the inward force of gravitational contraction on the one hand, and the outward force of nuclear fusion reactions on the other. Gravitational compression within stars heats matter to the point where exothermic nuclear fusion reactions occur, providing energy to counteract collapse. When one nuclear fuel source is exhausted, depending on the mass and composition of the stellar core, gravity can cause core contraction until a new stage of fusion reactions commences. The formation of mineral-forming elements and isotopes is summarized below.

- *Hydrogen burning:* Most stellar nucleosynthesis, most of the time, involves "hydrogen burning"—the three-step fusion mechanism that transforms four protons into a ^{4}He nucleus (an alpha particle), with two protons and two neutrons. All stars spend most of their lives powered by hydrogen burning in their cores—the process that dominates stars on the main sequence of the Hertzsprung-Russell diagram (e.g., L. V. Jones 2009).
- *Helium burning and carbon nucleosynthesis*: As the alpha particle concentration increases in a star's core, "helium burning" commences, producing ^{12}C through the triple-alpha process (e.g., Carroll and Ostlie 2017)—a process characteristic of "red giant branch" (RGB) stars. In stars more massive than the Sun, ^{12}C catalyzes additional helium production from protons through the "CNO cycle" (e.g., Limongi and Chieffi 2012; Carroll and Ostlie 2017), while increasing the concentrations of ^{13}C and ^{15}N relative to

^{12}C and ^{14}N. However, these fusion reactions do not generate a significant suite of mineral-forming elements other than carbon.

- *Late-stage fusion processes—most elements to Fe:* Most synthesis of essential elements in stellar minerals occurs during late-stage fusion processes in stars that have left the main sequence. The details of what occurs after core He burning depend critically on the initial mass of the star. For stars less massive than about 8 times that of the Sun, the C-O core remains stable against gravity due to quantum mechanical "electron degeneracy" pressure, but H and He burning continue to produce energy in narrow shells outside the core. A star in this post-RGB stage is referred to as an "asymptotic giant branch" or AGB star, which produces copious amounts of dust that drives strong winds. An AGB star expels much of its dust-rich envelope into interstellar space, temporarily appearing as a spectacular "planetary nebula" before leaving behind its cooling core as a white dwarf star (Figure 2A). (Note that the misleadingly named "planetary" nebula is not related to planet formation, which occurs in a "solar nebula.")

The nuclear histories and fates of stars greater than ~8 solar masses are even more dramatic. Following He burning, massive stars continue the sequence of burning increasingly heavier fuels in their cores through the "alpha process" or "alpha ladder," by which alpha particles fuse initially with ^{12}C in a stepwise sequence: ^{12}C → ^{16}O → ^{20}Ne → ^{24}Mg → ^{28}Si, etc., to ^{56}Fe, thus producing several of the most abundant mineral-forming isotopes (e.g., L. V. Jones 2009). These and other fusion reactions, including myriad steps during carbon burning, neon burning, oxygen burning, and silicon burning, occur near the end of the lives of AGB stars significantly more massive than the Sun.

This increasingly rapid sequence of fusion reactions is responsible for much of the production of isotopes up to ^{60}Zn (e.g., Truran and Heger 2003; Carroll and Ostlie 2017).

- *Core collapse in Type II supernovae:* ^{56}Fe has the highest binding energy of any common nucleus; therefore, it cannot produce energy through fusion reactions and eventually the battle against gravity is lost. Consequently, when the core of a large star becomes enriched in ^{56}Fe, nuclear fusion reactions no longer exert an outward pressure and gravity takes over. The iron core collapses to form either a neutron star or a black hole and the outer layers are ejected in a spectacular Type II supernova explosion (Figure 2B). The extreme temperatures and pressures of gravitationally-induced core collapse result in a cascade of nuclear reactions, producing short-lived isotopes such as ^{26}Al, ^{44}Ti, and ^{49}V, which decay rapidly to stable ^{26}Mg, ^{44}Ca, and ^{49}Ti—diagnostic isotopes preserved in stellar minerals (Clayton 1975; Nittler et al. 1996; Timmes et al. 1996).
- *Slow neutron capture (s-process):* In spite of their importance in producing the major elements of stellar minerals, the fusion processes outlined above generate only about a third of Earth's mineral-forming chemical elements (Johnson 2019). Elements with atomic number greater than 30 arise primarily through neutron-capture processes in late-stage, evolved stars. Both the *s*-process and *r*-process (i.e., rapid neutron capture; see below) nucleosynthesis involve the addition of one neutron after another until a nucleus becomes unstable and undergoes beta decay, thus increasing atomic number by 1. The new element captures additional neutrons and the process repeats. Owing to the ~10-minute half-life of free neutrons, these neutron-capture scenarios must occur in specific stellar environments with intense neutron fluxes—conditions not met in main sequence

hydrogen-burning stars. Rather, *s*-process nucleosynthesis is thought to occur primarily in the helium-burning cores of certain red giant stars, as well as in low- to intermediate-mass asymptotic giant branch stars undergoing helium burning. Neutrons, which are initially captured on iron nuclei from previous generations of stars, lead to cascades of reactions that produce most of the stable elements heavier than iron (Käppeler 1999; Johnson 2019). In particular, as an Fe nucleus becomes neutron-rich, it undergoes beta decay and transforms to cobalt, the next element in the periodic table. The *s*-process continues, element by element, to Bi, with the relative abundances of resulting isotopes approximately inversely proportional to their neutron capture cross-sections (leading, for example, to the notable generation of Mo, Zr, Ru, Sr, Ba, W, and Pb). The *s*-process can thus produce diagnostic suites of trace and minor elements in AGB minerals.

- *Rapid neutron capture (r-process)*: Approximately 40 percent of elements heavier than iron, including all uranium and thorium atoms, arise from the rapid neutron capture process. Note that in the early history of the universe, before the emergence of the multi-generation iron-rich stars that fuel the *s*-process, the *r*-process must have dominated nucleosynthesis of heavy elements (e.g., Sneden et al. 2008). The *r*-process requires remarkable neutron fluxes, corresponding to free-neutron densities as high as 10 kg/cm^3—extreme conditions that point to the environments of neutron stars. Recent observations of a gravitational wave event (designated GW170817), coupled with intense electromagnetic radiation pulses in a wide range of wavelengths from host galaxy NGC4993, suggest that the *r*-process occurs in colliding neutron binary stars—energetic events dubbed "kilonovae" (Kasen et al. 2017; Coulter et al. 2017; Ghirlanda et al. 2019). An important diagnostic marker of the *r*-process is the anomalous abundance of the most

neutron-rich stable isotopes ("*r*-only isotopes," such as ^{134}Xe and ^{136}Xe) of elements heavier than iron. It is important to note that the distinctive isotopic attributes of presolar minerals have provided the first tangible evidence for the *s*-process, *r*-process, and other major nucleosynthetic mechanisms, which were long hypothesized (e.g., Burbidge et al. 1957; Cameron 1957) but not previously supported by observations (e.g., Nittler and Ciesla 2016).

- *Proton capture nucleosynthesis:* Some proton-rich isotopes are thought to form in very high-temperature environments (> 10^9 Kelvins) with high proton densities, for example during the accretion of hydrogen onto a neutron star (Bildsten 1998).
- *Cosmic-ray spallation*: Most lithium, beryllium, and boron nuclei form through the fragmentation of more massive nuclei—transformations triggered by cosmic-ray fluxes in at least three galactic environments. Intense spallation occurs during classic core-collapse supernova events (e.g., Clayton 1983), in contrast to much more gradual spallation as a consequence of exposure to the essentially isotropic galactic cosmic ray flux. A record of spallation-induced nucleosynthesis in proximity to the early active Sun is also preserved in the most ancient solar system materials (Caffee et al. 1987; Hohenberg et al. 1990; Feigelson et al. 2002; Sossi et al. 2017; Koop et al. 2018).

An intriguing aspect of nucleosynthesis is that the average composition of the universe evolves, from the initial 9:1 hydrogen-to-helium mixture of 13.8 billion years ago to the present state, when ~2 weight percent of H + He has been converted to heavier elements (Pagel 1997; Matteucci 2003; Johnson 2019). This evolving diversity and distribution of chemical elements has had a profound effect on the cosmic evolution of minerals, as well. In particular, the wide

This is a preprint, the final version is subject to change, of the American Mineralogist (MSA)
Cite as Authors (Year) Title. American Mineralogist, in press.
DOI: https://doi.org/10.2138/am-2020-7173

range of observed ratios of the isotopes of C, N, O, Si, and other elements in stellar minerals reflect a parent star's starting composition overlaid by its internal nucleosynthetic processes.

An example of this effect is provided by comparing the lower metallicity AGB stars in the Magellanic Clouds (a pair of nearby dwarf galaxies in the Local Cluster), with the more metal-rich AGB stars in the Milky Way. The atmospheres of evolved stars in the Magellanic Clouds are dominated by carbon-rich dust, in contrast to Milky Way stars that are much richer in SiC. That contrast arises because all AGB stars form and dredge up carbon, but silicon content depends on their initial metallicity (Sloan et al. 2016).

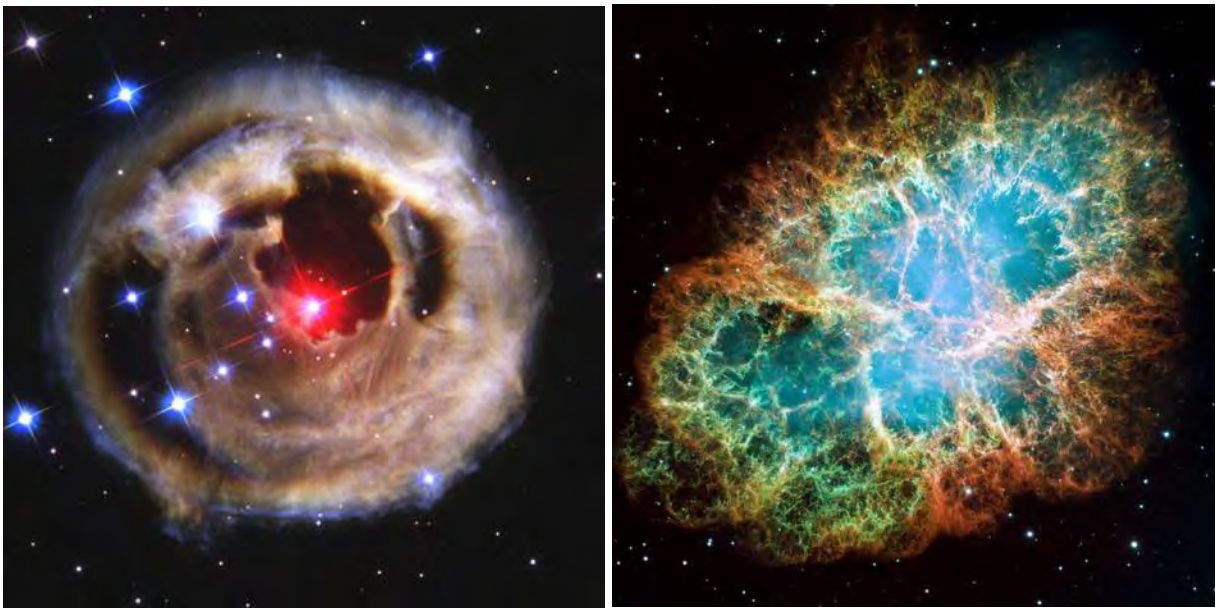

A **B**

Figure 2. Dust-forming stars. (Hubble Space Telescope images, courtesy of NASA).

A. Image of star V838 Monocerotis, a "planetary nebula" that formed from dust and gas surrounding an asymptotic giant branch (ABG) star.
B. Image of the Crab Nebula—the remnants of a supernova.

342 *On the variety of mineral-forming stars:* Three contrasting types of highly evolved stars—
343 AGB stars, Type II supernovae, and classical novae, are thought to be the primary producers of
344 dust in the universe and to have formed the majority of the refractory phases observed as
345 isotopically anomalous presolar grains in chondrite meteorites. Here we review these three major
346 types of mineral-producing stars.

347 Most stars for most of their lifetimes do not produce minerals. Like the Sun, the majority of
348 stars are now fusing hydrogen to form helium in their cores; these stars lie on the so-called
349 "Main Sequence" of the Hertzsprung-Russell diagram (e.g., Karttunen and Oja 2007; Carroll and
350 Ostlie 2017). Approximately 90 percent of stars visible in the night sky are in the midst of their
351 stable hydrogen-burning phase—extended intervals during which condensed phases are unlikely
352 to form.

353 For stars greater than about one-third of the Sun's mass, additional nucleosynthesis processes
354 eventually occur after an extended period of hydrogen burning—more than 9 billion years for the
355 Sun, but much shorter for more massive stars [e.g., an estimated ~30 million years for stars eight
356 times the mass of the Sun (Schröder and Connon Smith 2008; Peeples and Somerville 2013)].
357 Subsequent synthesis of elements heavier than helium (for example, the nucleosynthesis of
358 carbon by the triple-alpha process), coupled with convective overturn to bring these heavier
359 elements to a star's surface—a phenomenon known as "dredging"—produce the conditions by
360 which mineral-forming elements may enter a star's dynamic atmosphere and condense as
361 refractory phases. Consequently, stellar mineralogy primarily emerges from relatively late-stage
362 processes in the lifetimes of stars of sufficient mass.

363 Stars form minerals when stellar atmospheres sufficiently enriched in C, O, Si, and other
364 mineral-forming elements expand and cool below the condensation temperatures of refractory

phases. The range of environments in presumed mineral-forming stars varies significantly in several attributes, including mass, metallicity, composition, age, and the rapidity of the mineral-forming events. All of these characteristics significantly affect the production, attributes, and survival of stellar minerals and other condensates, but the two factors that most strongly influence the formation of minerals by stars are mass and metallicity. Stellar mass plays the major role in the production of elements heavier than helium. Consequently, stars with masses from slightly less than the Sun to many times the solar mass have the potential to produce minerals at some stages of their lifetimes. In general, more massive stars produce a wider range of elements by nucleosynthesis, they produce those elements more rapidly, and they are more efficient at dispersing those elements into the interstellar medium.

Superposed on the evolution of any individual star is its initial composition—the "metallicity," defined as the percent of a star's mass comprised of elements heavier than hydrogen and helium. The metallicity of distant stars is measured relative to the Sun, which had an estimated initial composition 4.5 billion years ago of ~71 weight percent hydrogen, ~27.5 weight percent helium, and ~1.5 weight percent "metal" (e.g., Johnson 2019). The earliest stars in the cosmos, represented by an ancient group of "Population III stars" (Tominga et al. 2007), formed from the abundant hydrogen and helium characteristic of Big Bang Nucleosynthesis and thus began their lives with metallicities less than a millionth that of the Sun—i.e., with essentially no mineral-forming elements (Frebel et al. 2009). Other stars that formed subsequently from the debris of earlier stellar generations display a range of metallicities, from significantly less than the Sun to more than twice the solar abundance of elements heavier than helium (Taylor 1996; Feltzing and Gonzales 2001; Peeples and Somerville 2013). As a general rule, stars with greater metallicity are more amenable to production of *s*-process elements from

neutron capture by iron, and they are more likely to host mineral-like condensates in their turbulent atmospheres.

The composition of stellar atmospheres may be further complicated by significant mass transfer, both large-scale mixing from the mergers of different galactic sources (Clayton 1997, 2003; Lugaro et al. 1999; see Nittler and Dauphas 2006, and references therein) and local mixing, for example from a companion binary star of different type (e.g., Nittler et al. 2008; Zega et al. 2014a). The consequent intimate connection between astrophysics and the earliest phases of cosmic mineral evolution is a gradually emerging, intensely fascinating facet of natural condensed materials science.

Three types of stars—AGB stars, Type II supernovae, and classical novae, each representing post hydrogen-burning stages of stellar evolution—have been implicated in the formation of most stellar minerals. It is important to note that these types of stars feature a complex and dynamic range of mineral-forming environments. Distributions of mineral-forming elements and their isotopic ratios reflect both the pressure-temperature-composition regime in which nucleosynthesis occurs and the dynamic convective (or explosive) processes that bring those elements to the cooler atmospheres where condensation can take place. These stars occur with a range of initial masses and metallicities, and they experience a succession of evolutionary phases, each of which may contribute in different ways to the inventory of stardust.

Asymptotic giant branch (AGB) stars. The largest producers of stardust are asymptotic giant branch (AGB) stars, which evolve from red giant stars between about 0.6 and 8 solar masses. AGB stars form spectacular planetary nebulas, which are a major source of mineral-rich dust in the galaxy (Figure 2A). Planetary nebulas form when AGB stars enter a late-stage of

411 nucleosynthesis characterized by fusion in a carbon- and oxygen-rich core, an inner shell of
412 helium burning, and a surrounding shell of hydrogen burning. An important characteristic of
413 AGB stars is a prolonged period of *s*-process nucleosynthesis, the mechanism by which existing
414 nuclei capture neutrons one at a time to increase atomic mass, trigger beta decay, and generate
415 new heavier isotopes and elements—notably Mo, Zr, Ru, Sr, Ba, W, and Pb. *S*-process
416 nucleosynthesis thus enriches some AGB stars in idiosyncratic isotopes and trace elements.

417 Several significant "dredge up" episodes of convective overturn bring C- and/or O-rich core
418 material to the surface, where these and other mineral-forming elements are introduced to the
419 stellar atmosphere. The "first dredge-up," which occurs after the main sequence as stars are
420 commencing their red giant phase, has a relatively minor effect on mineral-forming elements,
421 though it adds ^{13}C, ^{15}N, and ^{17}O from the CNO cycle and thus changes the isotope values of C,
422 N, and O significantly. The second dredge-up, which only occurs in stars greater than four times
423 the Sun's mass, leads to increased ^{14}N relative to ^{12}C and ^{16}O.

424 A sequence of "third dredge-up" (TDU) episodes, during which carbon and s-process
425 elements such as Mo and Zr are brought to the star's surface, occurs during the AGB phase of
426 stars less than ~8 solar masses. The significant transfer of ^{12}C to the surface during TDU
427 episodes may ultimately produce a star in which C/O > 1—an environment in which diamond,
428 graphite, and/or carbide grain formation is favored. Depending on the variable and evolving ratio
429 of C/O, which may range from C > O to O >> C, the dominant mineralogy will range from
430 carbon allotropes and silicon carbide to oxides and silicates. As the primary producers of carbon
431 in the universe, AGB stars are thought to be the source of most of the C-bearing presolar mineral

grains. Indeed, more than 95% of presolar SiC grains are attributed to AGB stars (Daulton et al. 2003; Davis 2011).

Though not fully understood, an additional hypothesized phase of an AGB star's evolution has been called "cool bottom processing" (CBP), which is thought to occur as significant mass convects from the outer stellar envelope into hot interior regions. There, additional nuclear fusion reactions may occur before mass is returned to the surface (Nollett et al. 2003; however, see Lugaro et al. 2017). Characteristic changes ascribed to CBP may include the rapid production of short-lived ^{26}Al (which decays to ^{26}Mg) and destruction of ^{18}O, leading to a significant decrease in ^{18}O/^{16}O. Furthermore, the significant destruction of ^{12}C by CBP may lead to C/O < 1, thus precluding carbide grain formation, while destruction of ^{15}N leads to increased ^{14}N/^{15}N. The distinctive isotopic compositions of some SiC grains may thus require such cool bottom processing (Alexander and Nittler 1999; Zinner et al. 2006).

In addition to this complex evolutionary sequence, some "born-again" AGB stars are thought to experience a late-stage surge of helium burning that leads to a pulse of ^{13}C and other *s*-process, neutron-rich isotopes (Herwig et al. 2011; Fujiya et al. 2013). This distinctive isotopic mix matches some of the observed compositions of a scarce population of ^{13}C -rich silicon carbide grains.

Finally, enigmatic J-type carbon-rich stars (Abia and Isern 2000) are characterized by C > O and extreme enrichment in ^{13}C (1 < ^{12}C /^{13}C < 10, compared to solar values ~90), as well as enrichment of ^{14}N relative to ^{15}N. J stars, which contrast to the more abundant ^{12}C-rich N-type stars (also known as "C-rich AGB stars"), account for as many as 15% of carbon-rich stars

(Morgan et al. 2003). Their origins are not well understood, but their unique compositions appear to be reflected in some presolar grains, for example a distinctive population of "AB-type" silicon carbide grains (Liu et al. 2017a).

Supernovae: Most presolar mineral grains have isotopic compositions that conform to mixtures that are plausibly derived from AGB stars. However, a small fraction of anomalous grains, notably those with extreme concentrations of neutron-rich isotopes, demand alternative origin hypotheses. In particular, stars more massive than approximately 8 times the Sun are relatively short lived (< 30 My; Karakas and Lattanzio 2014) and end in catastrophic core-collapse events called Type II supernovae ("SN-II", Figure 2B). Following a short and intense period of core-collapse nucleosynthesis, including brief "neutron bursts" that may produce a suite of heavy element isotopes distinct from the *s*- or *r*-processes (Meyer et al. 2000; Rauscher et al. 2002), SN-II events eject a significant fraction of their mass into the interstellar environment, with consequent jumbling of isotopes from different stellar layers as the cooling, expanding, turbulent atmosphere produces a variety of presolar minerals (Nittler et al. 1996, 2008; Travaglio et al. 1999; Hoppe et al. 2000). Shock waves associated with SN-II explosions have also been implicated in the formation and/or alteration of some presolar grains, notably nanodiamonds (Stroud et al. 2011). Diagnostic features of Type II supernovae include elevated $^{18}O/^{16}O$, as well as the production of a distinctive suite of isotopes, notably ^{26}Al, ^{44}Ti, and ^{49}V, which decay to stable ^{26}Mg, ^{44}Ca, and ^{49}Ti, respectively. Analyses of short-lived isotopes in supernova-derived SiC grains suggest that dust formation commences more than 2 years after, and continues for at least 10 years following, the explosion (Liu et al. 2018).

Additional mineral condensation may occur as a consequence of Type Ia supernovae, which are an end stage for some white dwarf stars—the collapsed remnants of a main sequence star up to ~8 solar masses. White dwarf stars have exhausted their helium-burning phase, but they lack the critical mass (the Chandrasekhar limit; Chandrasekhar 1931) to trigger a core-collapse (SN-II) supernova. However, if that limit is eventually exceeded through mass transfer from a binary companion star, then collapse is accompanied by explosive hydrogen burning and rapid consumption of a significant fraction of carbon and oxygen to yield ejecta concentrated in heavier elements (Khokhlov et al. 1993; Mazzali et al. 2007). Type Ia supernova nucleosynthesis probably accounts for only a small fraction of observed presolar grains, and few if any examples have been confirmed. Nevertheless, recent investigations of ^{54}Cr-rich grains by Nittler et al. (2018a) may best be ascribed to SN-Ia origins.

Other varieties of exploding/colliding stars may also play as yet unconfirmed minor roles in the formation of stellar minerals. In addition to "kilonovae," which are colliding binary neutron stars that may facilitate abundant *r*-process nucleosynthesis (see above; Kasen et al. 2017; Coulter et al. 2017; Ghirlanda et al. 2019), "electron-capture supernovae" are another putative stellar source of presolar grains with anomalous excesses of neutron-rich ^{48}Ca, ^{50}Ti, ^{54}Cr, and ^{60}Fe (Jones et al. 2019a, 2019b).

Novae: A "nova" is a transient event, during which a star's brightness suddenly increases many orders of magnitude and then gradual dims over weeks or months. All novae occur in binary systems with one white dwarf star. The most common type of nova, and the one most closely tied to the creation of stardust, is the so-called "classical nova." If the white dwarf star

497 and its companion (typically a main sequence or red giant star) are close enough, significant
498 transfer hydrogen-rich material can occur. The white dwarf's newly accreted hydrogen
499 atmosphere is heated to extreme temperatures, resulting in thermonuclear ignition and runaway
500 fusion, with the associated production of CNO-cycle isotopes ^{13}C, ^{15}N, and ^{17}O (e.g., Prialnik
501 2001). Expulsion of this atmosphere may be accompanied by the condensation of carbon- and
502 oxygen-rich phases, including amorphous carbon, moissanite, oxides, and silicates (Gyngard et
503 al. 2010a; Leitner et al. 2012a; Nittler and Ciesla 2016; Iliadis et al. 2018). Classic novae are
504 significantly less energetic than supernovae and they produce correspondingly less ejecta.
505 However, they make up for some of this difference in stardust production because they occur
506 much more frequently than supernovae.
507
508 *Pressure-temperature regimes of mineral-forming stars*: Pressures and temperatures within
509 stellar atmospheres (Figure 1B) are generally coupled through adiabatic cooling during
510 expansion, though they can be modified by extreme turbulence, with accompanying mixing and
511 shockwave alteration. Given these complex environments, pressure-temperature ranges of the
512 mineral-forming zones of stellar atmospheres are not always well known, though the occurrences
513 of specific mineral species and mineral associations provide some constraints. The maximum
514 possible temperature for formation of a stellar mineral is the >2000 K condensation temperature
515 of diamond in a carbon-rich atmosphere, though actual formation temperatures in low-pressure
516 stellar atmospheres are likely much lower (and evidence for stellar diamond is as yet ambiguous;
517 Dai et al. 2002; Verchovsky et al. 2006; Stroud et al. 2011; Heck et al. 2014; Lewis et al. 2018).
518 Soker and Harpaz (1999) documented AGB-sourced graphite grains with TiC cores, which limits
519 both temperature ($T < 2200$ K) and pressure [$P < 7 \times 10^{-4}$ atm; see also Croat et al. (2005) for

similar analyses based on ZrC and MoC inclusions]. Surveys of moissanite polytypes by Daulton and coworkers (Daulton et al. 2002, 2003) found that the lowest-temperature cubic (3C) form is dominant, which constrains temperature to a range from ~1500 to 1700 K.

Stellar oxide and silicate minerals form at temperatures similar to or lower than those of the observed carbon allotropes and carbides. Corundum and hibonite are the most refractory oxides, with formation temperatures estimated to exceed 1700 K (Ebel 2006 and references therein). By contrast, Zega et al. (2014a) documented the occurrence of pristine stellar oxide spinel grains that imply lower-temperature regimes, as $MgAl_2O_4$ condenses at 1161 K at 10^{-6} atm, and 1221 K at 10^{-3} atm.

A few rare nanoscale presolar grains point to significantly lower temperatures of formation. For example, Haenecour et al. (2016) describe an 80-nanometer-diameter iron sulfide grain as an inclusion in a presumed Type II supernova graphite (though origins in a low-metallicity AGB star could not be ruled out). Lodders (2003) estimates the highest condensation temperature for an iron sulfide to be troilite, FeS (~ 700 K at 10^{-4} atm). If the grain described by Haenecour et al. (2016) is a primary condensate, then it must have formed in a relatively cool regime and was subsequently transported to a much hotter region, where the graphite could precipitate around it. Sarangi and Cherchneff (2015) suggest that supernova ejecta can feature clumpiness and compositional heterogeneities that might support this scenario. However, Lodders (personal communications) suggests an equally plausible alternative scenario by which troilite formed from the "sulfurization" of a grain of presolar iron metal through secondary gas/solid reactions that occurred in reduced AGB winds (Lauretta et al. 1998).

Similarly, reports of stellar magnetite grains (estimated condensation at ~400 K at 10^{-4} atm) by Zega et al. (2015) have been explained by gradual oxidation (10^4 to 10^6 years) of primary native iron grains that condensed at much higher temperatures (Yoneda and Grossman 1995; Hong and Fegley 1998; Lodders 2003).

Formation pressures of stellar minerals are constrained in part by the observed sequence of condensation. For example, stellar graphite has not been found to incorporate moissanite (SiC) inclusions—an observation that places a lower pressure bound for carbon-rich stars, as SiC condenses before graphite only at pressures greater than 3×10^{-5} atm (Bernatowicz et al. 1996). Several observations also point to transient events that may raise local pressures to significantly greater than 10^{-3} atmospheres in some stellar environments. For example, the observed sizes of the largest AGB-derived presolar grains (> 1 micrometer), including moissanite (Bernatowicz et al. 2006) and corundum (Takigawa et al. 2018), imply sustained exposure to regions of higher pressure, which in turn suggests that the pressure environments surrounding AGB stars are not radially symmetric. Mass outflows from such stars are likely influenced by jets and clumps, as well as by periodic shocks in the atmosphere above the photosphere. These events enhance local density and thus promote grain growth (Bernatowicz et al. 1996; Chigai et al. 2002; Gobrecht et al. 2016). In addition, stacking disorder observed for several minerals in TEM studies (Stroud et al. 2011; Zega et al. 2014a), as well as surface irregularities on otherwise subhedral crystals (Takigawa et al. 2018), could point to grain-to-grain impact-induced strain in stellar atmospheres. Finally, the shock waves of supernovae have been implicated in the formation of some presolar nanodiamonds (Stroud et al. 2011), as well as the possible transformation of $MgSiO_3$ enstatite to the high-pressure bridgmanite polymorph (Vollmer et al. 2007).

563

564 *The application of cluster analysis to stellar minerals:* A central theme of the evolutionary
565 approach to mineral classification is that many IMA mineral species emerge multiple times
566 during the evolution of stars, planets, and moons. Each new paragenetic process is likely to
567 impart a distinctive suite of attributes to minerals as they form; therefore, we classify each
568 unique combination of mineral species and paragenetic mode as a distinct natural kind.

569 Two types of information contribute to the recognition of mineral natural kinds. In the
570 proposed evolutionary system of mineralogy, we link mineral species to distinctive mineral-
571 forming environments—major paragenetic modes. Thus, moissanite formed in the explosive
572 regime of a Type II supernova ("*SN-II moissanite*") is different from moissanite formed in the
573 evolving atmosphere of an AGB star ("*AGB moissanite*") or in a classic nova explosion ("*CN*
574 *moissanite*"). Additional mineral-forming stellar environments may be confidently documented
575 in the future, at which time the classification system could easily be expanded.

576 Extending this approach, the opportunity exists to further subdivide minerals based on
577 distinctive combinations or "clusters" of attributes, including trace and minor elements, isotopic
578 ratios, solid and fluid inclusions, grain size and morphology, structural defects, and other
579 diagnostic characteristics. Tabulations of attributes of analyzed mineral specimens, for example
580 the Presolar Grain Database that now incorporates information on ~20,000 moissanite grains
581 (Hynes and Gyngard 2009; see "presolar.physics.wustl.edu" accessed 24 Jan 2019), presents the
582 opportunity to examine clusters of minerals based on multiple attributes in ever greater detail.
583 Thus, for example, stellar moissanite grains have been subdivided into as many as 12 groups
584 based primarily on ranges of Si and C isotopes (e.g., Davis 2011; Zinner 2014). Several of these
585 groups are ascribed to AGB stars of differing mass, metallicity, and/or age—aspects of a star that

586 are reflected in evolving element and isotope ratios. Cluster analysis thus has the potential to
587 reveal a range of SiC subsets that have implication for understanding stellar evolution (Boyd
588 1991, 1999; Bailey 1994; Millikan 1999; Everitt 2011; Hazen 2019). However, for the purposes
589 of this evolutionary system of mineralogy, origins in the atmosphere of an AGB star—whatever
590 the mass, metallicity, or dredge-up stage—is considered to be one paragenetic mode. Similarly,
591 stardust formation through Type II supernovae explosions, in spite of varied shells and stages of
592 mineral formation in the evolving object, is also treated as one paragenetic mode.
593

SYSTEMATIC EVOLUTIONARY MINERALOGY: PART I—STELLAR MINERALOGY

At least 24 different crystalline and three amorphous condensed phases, associated with 41 natural kinds, have been identified as stellar minerals (e.g., Lodders and Amari 2005; Davis 2011; Zinner 2014), as detailed in Table 1. The following section summarizes stellar mineralogy based on stardust analyzed since the first discoveries of 1987 (Lewis et al. 1987; Bernatowicz et al. 1987; Zinner et al. 1987), and lists all confirmed or likely species of stellar minerals of which we are aware as of 10 October 2019. Table 1 also lists 14 as yet unconfirmed stellar minerals, including native elements, nitrides, silicides, phosphides, and oxides, that have been reported as nanoscale inclusions but have not yet been fully described or independently confirmed.

This field is evolving rapidly, both in terms of the variety of stellar mineral species identified and the ranges of distinctive chemical and physical properties displayed by those minerals. For example, Lodders and Amari (2005; their Table 9) catalog more than 30 IMA-approved mineral species that might occur in stellar atmospheres on the basis of thermodynamic equilibrium condensation sequences of the most refractory phases of 17 cosmically abundant elements, including Na, Mn, Ni, P, Cl, and K, for which no stellar condensed phases have yet been confirmed. Consequently, we expect that the list of condensed phases known to form in the atmospheres of stars will expand significantly in the coming years.

A note regarding nomenclature: Minerals are arranged first by chemical class (i.e., Native Elements; Sulfides; Oxides; etc.), as employed in the revolutionary third edition of James Dwight Dana's *System of Mineralogy* (J. D. Dana 1850; see also Hazen 1984) and subsequently widely adopted and expanded (e.g., Edward S. Dana and Ford 1947; James D. Dana et al. 1973; Gaines et al. 1997). Secondary headings indicate IMA-approved mineral species (i.e., "diamond"

617 or "corundum") or, in the case of non-crystalline phases, an appropriate compositional name
618 (e.g., "amorphous Al_2O_3" or "silicate glass").

619 The evolutionary system of mineralogy emphasizes paragenetic modes of minerals in addition
620 to their chemical compositions and atomic structures. Therefore, we adopt a binomial
621 nomenclature for each suspected natural kind of mineral in stardust (e.g., "SN-II diamond" or
622 "AGB chromite"). The case of stellar mineralogy is especially revealing in this regard. All
623 minerals formed in stellar environments are characterized by significantly non-solar major and
624 trace isotopic compositions—attributes that clearly differentiate these minerals from their
625 terrestrial or solar nebular counterparts. The sometimes extreme isotopic deviations from solar
626 averages, as well as idiosyncratic suites of trace and minor elements, often point to a specific
627 type of host star. Such diagnostic element and isotope signatures suggest that presolar minerals,
628 though often examples of relatively common terrestrial mineral species, represent distinctively
629 non-terrestrial natural kinds.

630 An added complexity when dealing with stardust mineralogy is the occurrence of
631 compositionally homogeneous domains, subgrains, or inclusions only a few nanometers in
632 diameter that are encased in larger mineral grains. For example, it is difficult to know whether
633 reports of isolated concentrations of Fe-Ni-Si atoms (Hynes 2010) constitute valid condensed
634 silicide phases. In instances where such localized chemical concentrations have been observed
635 but no diagnostic electron diffraction or other structural information has been obtained, we
636 record "Other possible phases" under the appropriate compositional group.

637

638

639 **NATIVE ELEMENTS**

Allotropes of carbon, including diamond, graphite, and varieties of non-crystalline C, are abundant presolar phases (Davis 2011). These and other carbon-bearing phases were among the earliest stellar minerals to be recognized, both because of their extreme isotopic anomalies and their relative ease of concentration through acid dissolution.

At least three forms of iron, alloyed variously with Ni, Ru, Os, and other metallic elements, have been confirmed as "refractory metal nuggets," which occur as inclusions in stellar graphite (Croat et al. 2003, 2008, 2013; Hynes et al. 2010). In some alloys Ni or Ru may be locally greater than Fe. In addition, nano-inclusions of native Os with minor Mo, Ru, and Fe have been reported as inclusions in SN-II graphite (Croat et al. 2005, 2013).

Diamond (C): Diamond was suggested by Hazen et al. (2008) to be the first mineral in the cosmos, presumably formed by vapor deposition as the carbon-bearing atmospheres of energetic stars expanded and cooled significantly below the 4400 K maximum condensation temperature of diamond. In parallel to that idea, diamond was the first presolar mineral to be positively identified (Lewis et al. 1987), and it remains the most abundant known presolar phase, both in terms of weight percent (~1400 ppm in CM chondrites) and numbers of grains (Davis 2011). Based on microstructural studies, for example by Daulton et al. (1996), the source of these nanodiamonds is likely vapor deposition. However, in spite of these discoveries, an ancient stellar (as opposed to solar nebular) source for meteoritic presolar nanodiamonds has not been unambiguously verified (Nuth and Allen 1992; Ozima and Mochizuki 1993; Richter et al. 1998; Dai et al. 2002; Stroud et al. 2011). In the words of Zinner (2014), "Although diamond is the most abundant presolar grain species (~1400 ppm), … it remains the least understood."

662 The principal difficulty in characterizing presolar diamond has been their diminutive size,
663 typically less than 10 nm diameter, with an average size of 2 to 3 nm diameter, corresponding to
664 fewer than 2000 carbon atoms. As a result, most analytical studies have of necessity measured
665 average compositions of millions of grains—averages that, in general, do not deviate
666 significantly from the observed solar $^{12}C/^{13}C \sim 90$ or $^{14}N/^{15}N \sim 249$ (Russell et al. 1991, 1996;
667 Daulton et al. 1996; Dai et al. 2002). [Note that throughout this contribution we use the
668 somewhat quirky isotope ratio conventions employed in most astromineralogy publications;
669 namely, $^{12}C/^{13}C$, $^{14}N/^{15}N$, $^{17}O/^{16}O$, $^{18}O/^{16}O$, $^{29}Si/^{28}Si$, and $^{30}Si/^{28}Si$ (as opposed, for
670 example, to delta notation), because of the extreme deviations from solar averages (e.g., Davis
671 2011; Zinner 2014).] Until recently it has been impossible to characterize individual diamond
672 grains that might bear the distinctive isotopic signatures of stars (Heck et al. 2014; Lewis et al.
673 2018).

674 Two studies point to plausible stellar sources for some presolar diamonds. Verchovsky et al.
675 (2006) successfully isolated a slightly larger size fraction of crystallites—the largest 1 percent of
676 grains that collectively yield isotopically light carbon, heavy nitrogen, and noble gas signatures
677 characteristic of some AGB stars. However, Stroud et al. (2011) found the co-occurrence of a
678 "glassy carbon" fraction in these residues, calling into question whether the AGB isotopic
679 anomalies are associated with diamond, the amorphous phase, or both.

680 Additional evidence for populations of stellar diamonds comes from Lewis et al. (2018), who
681 employed NanoSIMS with a minimized high-resolution 50-nm beam diameter to examine tens of
682 thousands of discrete small volumes, each with approximately 1000 nanodiamonds per
683 observation. They suggest that if stellar diamonds with large isotopic anomalies are present in
684 the sample, then the Gaussian statistical distribution of observed $^{12}C/^{13}C$ should display a

685 significant broadening compared to similar measurements on a homogeneous diamond
686 population. Lewis and coworkers found that the average carbon isotopic value was close to solar,
687 in agreement with prior studies, but they also documented significant broadening, which they
688 attributed to multiple isotopic values, including both ^{13}C-enriched and depleted grains,
689 presumably from multiple stellar sources. Nevertheless, the likely occurrence of amorphous
690 carbon in all diamond residues (Stroud et al. 2011) makes unambiguous recognition of stellar
691 diamond problematic.

692 With these uncertainties in mind, we provisionally list two kinds of stellar diamond.

693

694 *AGB diamond:* Nanometer-scale diamond with isotopically light carbon (e.g., high ^{12}C/^{13}C),
695 heavy nitrogen (low ^{14}N/^{15}N), and noble gas signatures characteristic of AGB stars (Verchovsky
696 et al. 2006; Lewis et al. 2018).

697

698 *SN-II diamond:* Nanometer-scale diamond with low ^{12}C/^{13}C, possibly associated with
699 isotopically anomalous xenon isotopes (Lewis et al. 1987; Clayton et al. 1995; Lewis et al.
700 2018).

701

702 **Graphite (C):** Grains of stellar graphite were among the first presolar minerals to be discovered,
703 initially based on anomalous neon isotopes (Amari et al. 1990), and they have received intense
704 subsequent study (Amari et al. 1994, 1995a, 1995b, 2004; Bernatowicz et al. 1996, 2006; Croat
705 et al. 2003, 2005, 2008; Stadermann et al. 2005; Davis 2011; Groopman et al. 2012; Zinner 2014
706 and references therein; Groopman and Nittler 2018). Presolar graphite constitutes ~10 ppm by

707 weight of CM chondrite meteorites, with sizes up to 20-micrometers in diameter (Zinner et al.
708 1995). The relative abundance of stellar graphite is reflected in the Presolar Grain Database,
709 which records 2200 analyzed grains (Hynes and Gyngard 2009; see "presolar.physics.wustl.edu"
710 accessed 24 Jan 2019).

711 The morphologies of stellar graphite grains are varied, with one distinctive population of
712 grains having cores of randomly oriented graphene sheets surrounded by well-graphitized
713 "onion-like" concentric layers (Fraundorf and Wackenhut 2002; Zinner 2014; Figure 3A). Other
714 "cauliflower" type grains, by contrast, form as aggregates of smaller crystallites (Bernatowicz et
715 al. 1996; Hoppe et al. 1995; Figure 3B). Most of these stellar graphite grains have been extracted
716 from the widely available Murchison and Orgueil carbonaceous meteorites. These samples have
717 been further divided into density fractions—aliquots that reveal intriguing differences in size and
718 isotopic attributes of two populations described as HD (higher density) and LD (lower density).
719 The carbon isotope ratios of stellar graphite vary widely: $2 < {}^{12}C/{}^{13}C < 7500$ (Hynes and
720 Gyngard 2009), with most grains isotopically lighter than the solar average of ~90. Furthermore,
721 the HD fraction of grains is on average smaller and of greater ${}^{12}C/{}^{13}C$ than the LD fraction.
722 Identification of different stellar origins depends additionally on isotopic ratios of minor O, N,
723 and Si impurities, as well as trace amounts of diagnostic *r*-process and *s*-process elements. We
724 list three types of stellar graphite, originating in three contrasting stellar environments, as
725 distinguished by their chemical and isotopic anomalies, coupled with their physical properties
726 and morphologies (e.g., Davis 2011; Zinner 2014).
727
728

This is a preprint, the final version is subject to change, of the American Mineralogist (MSA)
Cite as Authors (Year) Title. American Mineralogist, in press.
DOI: https://doi.org/10.2138/am-2020-7173

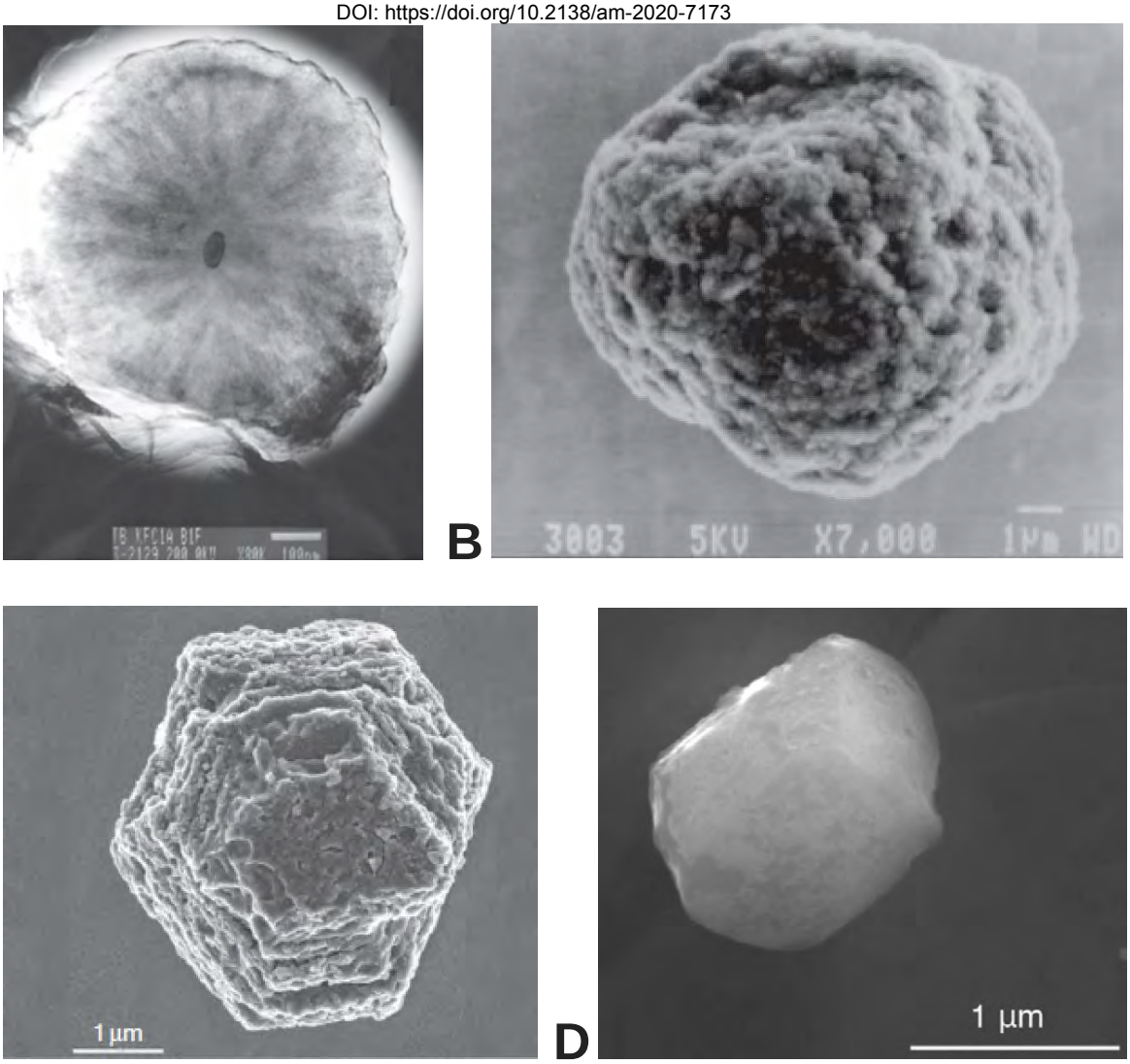

Figure 3. Electron microscope images of stellar minerals. (A) Cross-section of a 1-micron diameter "onion" AGB graphite with central khamrabaevite (TiC) inclusion (Zinner 2014); (B) 13-micron diameter "cauliflower" SN-II graphite grain—a composite of smaller crystallites (Zinner 2014); (C) 4.5-micron diameter euhedral "mainstream" AGB moissanite (SiC) crystal (Zinner 2014); (D) 1.4-micron diameter euhedral AGB corundum (Al_2O_3) crystal (Takigawa et al. 2018).

740 *AGB graphite*: Approximately 30% of stellar graphite grains, the great majority of which are
741 from the higher density (HD) population, have high $^{12}C/^{13}C$ relative to solar abundances and
742 display enrichment in characteristic *s*-process elements Zr, Mo, and Ti, which form carbide
743 inclusions up to 200 nanometers in diameter (Amari et al. 1994, 1995b, 1995c, 2006;
744 Bernatowicz et al. 1996; Croat et al. 2005; Heck et al. 2009a; Meier et al. 2012). AGB graphite
745 grains typically display platy or onion-like morphologies and are, on average, smaller than other
746 kinds (Croat et al. 2008). They display a range of crystallinity, as revealed by electron
747 microscopy (Bernatowicz et al. 2006) and Raman spectroscopy (Wopenka et al. 2011a).

748 A small fraction of AGB graphite grains display extremely low $^{12}C/^{13}C$ values relative to
749 solar, coupled with Ca and Ti isotopic anomalies. The most likely sources are enigmatic carbon-
750 rich born-again AGB stars, or J stars (Jadhav et al. 2008, 2013; Nittler and Ciesla 2016). We
751 suggest that the paragenetic mode of these grains is the same as that of other AGB star grains,
752 i.e., gradual condensation from the gas phase. However, cluster analysis may demonstrate that
753 these grains point to the existence of multiple varieties of AGB graphite.

754

755 *SN-II graphite:* An estimated 60% of stellar graphite grains, including the majority of lower
756 density (LD) population grains (Zinner et al. 2006), display compositional characteristics of
757 Type II supernovae, with low $^{14}N/^{15}N$, high $^{18}O/^{16}O$, and remnants of ^{26}Mg, ^{44}Ca, ^{49}Ti, and
758 other diagnostic trace isotopes (Nittler et al. 1996; Stadermann et al. 2005; Jadhav et al. 2013;
759 Zinner 2014, and references therein). These grains are typically irregularly crystallized with
760 "cauliflower" morphology, often with TiC cores and sometimes numerous (up to hundreds) of
761 TiC inclusions from 30 to 230 nanometers in diameter (Amari et al. 1995b; Soker and Harpez

762 1999; Croat et al. 2008), as well as distinctive inclusions of Fe-Ni metal and/or Os-rich regions
763 (Stadermann et al. 2005; Groopman et al. 2012).
764
765 *CN graphite:* A small population of graphite grains has very low $^{12}C/^{13}C$ (< 10) and high
766 $^{30}Si/^{28}Si$, as well as neon isotope anomalies, which collectively point to a possible origin in
767 classical novae (Amari et al. 2001c; Jadhav et al. 2008; Heck et al. 2009a; Haenecour et al.
768 2016). Cluster analysis of stellar graphite grains (in progress) may clarify the extent to which
769 these samples represent a discrete population with a different paragenetic mode.
770
771 **Amorphous Carbon (C):** A low-density fraction of presolar carbon occurs in amorphous and/or
772 structurally disordered states, possibly representing several distinct types of non-crystalline C.
773 For example, Stroud et al. (2011) report disordered "glassy" carbon with *sp*2 bonding—a
774 population of grains that displays distinctive Raman spectra (Wopenka et al. 2011b). However,
775 until more definitive structural and compositional information is available, we catalog only one
776 kind of amorphous carbon.
777
778 *Stellar amorphous C:* Non-crystalline carbon with anomalous $^{12}C/^{13}C$.
779
780 **Refractory Metal Nuggets (Fe,Ni,Ru,Cr,Mo,Os,Ir):** Refractory metal alloys, incorporating
781 two or more of Fe, Ni, Ru, Cr, Mo, and Os, represent intriguing minor phases in stardust. At least
782 three different groups of Fe-bearing alloys have been identified as inclusions in SN-II graphite
783 (Bernatowicz et al. 1996; Croat et al. 2003, 2005, 2008, 2010, 2013; Stadermann et al. 2005;

Gyngard et al. 2018). Croat et al. (2003, 2005, 2008) and Hynes (2010) characterized both native iron (the alpha-iron alloy of Fe:Ni, sometimes referred to as "kamacite"; space group *Im3m*) and taenite (the gamma-iron alloy of Fe-Ni; space group *Fm3m*) by ion probe and electron microscopy. In addition, Fe combines with Ni, Ru, Os, and Mo in metal inclusions in graphite, presumably in space group $P6_3/mmc$ (Croat et al. 2008; Rubin and Ma 2017).

The variable compositions of stellar iron alloys present a classification challenge. Consider the case of the Fe-Ni alloy taenite, which is observed to vary from Fe >> Ni to Ni > Fe in a continuous solid solution. IMA protocols would assign different mineral names to the iron- and nickel-rich end members of this solid solution. However, in the evolutionary system of mineralogy we lump all members of a continuous solid solution that form under similar conditions as a single natural kind. Thus, even though Ni may approach 60 atom percent in some taenite inclusions (thus approximating in composition the IMA-approved mineral species awaruite), we lump all of these inclusions into *SN-II taenite*.

The case of the $P6_3/mmc$ alloy of Fe-Ni-Mo-Cr-W-Ru-Os-Ir is more difficult to resolve. These nano-inclusions in graphite, which may represent the earliest condensates in some C-rich stars, display extensive solid solutions, with some individual inclusions dominated by Fe, Ru, or Os. Croat et al. (2013) point to immiscible regions, for example between Fe-Ni-rich and Ru-rich compositions. The case of osmium, with ~50-nanometer inclusions with Os > 70 atom percent, would seem to demand that native Os be considered a valid stellar mineral. The case of ruthenium is less clear-cut. Most grains have Fe >> Ru, but a few grains have Ru > Fe (up to $Ru_{77}Fe_{23}$), suggesting an extensive Fe-Ru solid solution, but with a possible immiscibility region (Croat et al. 2013). Given that uncertainty, we include native ruthenium as a stellar

806 mineral. However, if additional data on the compositional range of metallic inclusions in SN-II
807 graphite reveal a continuous solid solution among Fe, Ni, Ru, Os, and other elements, then we
808 may in the future ascribe most or all of these "refractory metal nuggets" to a single natural kind.
809
810 *SN-II iron:* The alpha-iron alloy [(Fe,Ni); space group *Im3m*], sometimes called "kamacite"
811 occurs both as isolated inclusions and epitaxially attached to TiC inclusions in SN-II graphite
812 (Croat et al. 2003). These Fe-rich grains, extracted from the Murchison meteorite, contain 0 to 24
813 atom percent Ni.
814
815 *SN-II taenite:* Taenite [(Fe,Ni), space group *Fm3m*] occurs as nano-inclusions attached
816 through epitaxial growth to TiC inclusions in SN-II graphite from the Murchison meteorite
817 (Croat et al. 2003). The majority of grains have Fe > Ni, though a few grains have up to 60 atom
818 percent Ni.
819
820 *SN-II ruthenium:* Croat et al. (2005) describe nano-inclusions (> 20 nanometers diameter) of
821 Fe-Ru alloys in SN-II graphite, mostly with Fe > Ru but some of which have Ru >> Fe (ranging
822 to as high as $Ru_{77}Fe_{23}$). In addition, Croat et al. (2013) report a 21-nanometer-diameter Ru-
823 dominant refractory metal inclusion of composition ($Ru_{29}Mo_{24}Fe_{17}Os_{13}Ir_{13}$ $Ni_2W_1Cr_1$)—a
824 composition that underscores the difficulty of ascribing many such nuggets to a single element
825 end-member. Note that the hexagonal unit-cell dimensions of this grain (a = 2.80 Å; c = 4.44 Å)
826 are consistent with the $P6_3/mmc$ space group of native ruthenium.
827

828 *SN-II osmium:* Croat et al. (2005) report a single 50-nanometer-diameter Os-rich inclusion
829 ($Os_{79}Mo_{10}Ru_9Fe_2$) in a SN-II graphite grain. Croat et al. (2013) describe a grain of similar
830 composition ($Os_{74}Ru_9W_6Mo_4Fe_3Ir_2$), with hexagonal symmetry (a = 2.77 Å; c = 4.48 Å),
831 consistent with the *P6₃/mmc* space group of elemental osmium. These unusual grains do not fall
832 close to the Fe-Ni-Ru composition space of many other stellar alloy inclusions; therefore, we
833 recognize osmium as a distinct stellar mineral. The sequence of Os condensing prior to its
834 inclusion in graphite points to formation in a supernova environment.
835
836
837 **CARBIDES**
838 Grains of stellar carbides, primarily moissanite (SiC), but also khamrabaevite (TiC) in some
839 cases significantly enriched in V, Mo, Zr, and/or Ru, are among the most abundant and well-
840 studied presolar grains (Davidson et al. 2014; Zinner 2014). Almost all carbide grains found in
841 meteorites are thought to arise from condensation in stellar atmospheres, in contrast, for
842 example, to oxides and silicates, most of which bear the Solar System's isotopic ratios and are
843 thus thought to be condensates from the solar nebula. The majority of these isotopically
844 anomalous carbide phases form in the chemically reduced atmospheres of carbon-rich AGB
845 stars.
846
847 **Moissanite (SiC):** Interstellar silicon carbide was first recognized as a component of stars from
848 distinctive IR emission spectra of the dust-rich atmosphere of carbon stars (Treffers and Cohen
849 1974; Forrest et al. 1975). Subsequent discovery of isotopically anomalous moissanite grains in

the insoluble residues of CM meteorites (Zinner et al. 1987; Lewis et al. 1990, 1994) established SiC as the second known stardust mineral. Moissanite, though less abundant than presumed presolar diamonds, averages ~30 ppm in CM chondrites (Davis 2011; Davidson et al. 2014), with reported concentrations as high as 160 ppm in some meteorites (Leitner et al. 2012b; see Zinner 2014)].

Moissanite forms the largest known stellar mineral grains, with some crystals greater than 20 microns in diameter (Gyngard et al. 2018), though most grains are less than a micron in diameter (Zinner et al. 2007; Gyngard et al. 2009; Heck et al. 2009b; Hoppe et al. 2010; Davis 2011; Figure 3C). Consequently, SiC has received the most detailed study of any stellar mineral, with more than 17,300 measured grains recorded in the Presolar Grain Database (Hynes and Gyngard 2009; see "presolar.physics.wustl.edu" accessed 24 Jan 2019).

The isotopic ratios of carbon, silicon, and nitrogen (the latter a ubiquitous impurity in stellar SiC), as well as varied concentrations of trace elements and isotopes of characteristic *s*-process elements (e.g., Ti, Zr, and Mo) and extinct radionuclides (notably short-lived ^{26}Al, ^{44}Ti, and ^{49}V recognized by their decay products ^{26}Mg, ^{44}Ca, and ^{49}Ti), have been used to differentiate moissanite into as many as seven varieties (Davis 2011), representing both AGB stars and explosive environments of novae and supernovae (Table 1; Figure 4). In addition, rare anomalous individual grains point to additional possible origins or evolutionary pathways for moissanite grains in stellar atmospheres that are not yet fully understood (Leitner et al. 2012b; Nguyen et al. 2016). This diversity reflects not only the stability of SiC in a variety of carbon-rich stellar environments, but also the benefits (and complexities) arising from broad surveys of large numbers of presolar grains.

872 It should be noted that an evolving nomenclature for types of stellar moissanite has already
873 gained some traction in the astromineralogy community. Approximately 9 in 10 stellar SiC
874 grains bear the distinctive isotopic signatures of AGB stars—characteristics of so-called
875 "mainstream" stellar SiC (e.g., Zinner 2014). The first SiC grain to be discovered with a
876 markedly different isotopic composition, presumably formed in a Type II supernova, was called
877 "Type X" (Amari et al. 1992; Nittler et al. 1996; Hoppe et al. 2000). Subsequent distinctive finds
878 of presolar SiC were called types Y and Z (Alexander 1993; Hoppe et al. 1994, 1997; Amari et
879 al. 2001a; Nittler and Alexander 2003), followed by A, B, and C. Types A and B were later
880 merged into "Type AB," though Liu et al. (2017c) subsequently proposed a split into AB1 and
881 AB2 based on nitrogen isotopes. In addition, Liu et al. (2016) suggested splitting C into C1 and
882 C2 based on carbon isotopes, while Type X is sometimes subdivided into X0, X1, and X2 (Lin et
883 al. 2010). It is not yet possible to unambiguously assign every stellar SiC grain to one category,
884 much less to one stellar paragenesis.

885 In this study, we recognize three major paragenetic processes that produce the great majority
886 of stellar moissanite—AGB stars, Type II supernovae, and classical novae. In addition, cluster
887 analysis studies of presolar SiC grains are now in progress to provide a quantitative basis for
888 distinct subdivisions of stellar moissanite.

889 An important characteristic of moissanite is its diverse array of stacking polytypes, of which
890 more than 200 have been documented in synthetic samples (Kelly et al. 2005; Cheung 2006).
891 Presolar moissanite grains are found in two principal structural polytypes, most commonly in the
892 lowest-temperature cubic (3C) form, with a smaller fraction of the hexagonal (2H) polytype
893 (Daulton et al. 2002, 2003; Bernatowicz et al. 1987, 2003; Alexander et al. 1990; Amari et al.

1990; 1994, 2001a, 2001b, 2001c; Liu et al. 2017b), though a few grains with higher-order polytypes have been reported (Liu et al. 2017b; Gyngard et al. 2018).

Hints regarding the pressure of formation of stellar moissanite are provided by the absence of SiC inclusions in graphite, indicating that graphite precipitates first. Such a condensation sequence requires that pressures in the stellar atmosphere are less than 3×10^{-5} (Bernatowicz et al. 1996), at which pressure the condensation temperature of SiC falls significantly below 2000 K.

As with presolar graphite, some moissanite grains incorporate inclusions of other refractory phases, including rare examples of graphite, Ti(N,C), (Mg,Al)N, and Fe-Ni metal (Zinner 2014; Gyngard et al. 2018).

AGB moissanite: Representing ~90% of all stellar SiC grains, mainstream AGB moissanite is characterized by the distinctive combination of low $^{12}C/^{13}C$, high $^{14}N/^{15}N$, and abundant *s*-process trace elements, including Ti, Zr, and Mo (Nittler et al. 1996). Unlike polycrystalline SiC from Type II supernovae, AGB moissanite grains are typically single crystals (Stroud et al. 2004a; Hynes et al. 2010). Several authors suggest that the distinctive isotopic signatures of these abundant SiC stellar grains point to mixing of several galactic sources (Clayton 1997, 2003; Alexander and Nittler 1999; Lugaro et al. 1999).

Several moissanite grains (a few percent of presolar SiC), dubbed "Y" type, are presumed to come from AGB stars with ~50% solar metallicity (Hoppe et al. 1994). These grains have the unusual combination of high $^{12}C/^{13}C$ and high $^{14}N/^{15}N$ (Amari et al. 2001a; Nguyen et al. 2018), possibly with excesses of *s*-process Ti and Mo isotopes (Larry Nittler, personal

916 communications). In addition, a few percent of stellar SiC grains, called "Z" grains, are ascribed
917 to AGB stars with ~25% solar metallicity and have low $^{12}C/^{13}C$, high $^{14}N/^{15}N$, low $^{29}Si/^{28}Si$,
918 and high $^{30}Si/^{28}Si$, in combination with excess *s*-process ^{50}Ti and ^{96}Mo. These attributes are
919 thought to indicate low-mass stars with low metallicity (Hoppe et al. 1997; Nguyen et al. 2018).
920 Note that a continuum may exist from Z- to Y- to mainstream-type ABG moissanite; further
921 investigation by cluster analysis is thus warranted.

922 Additional subtypes of moissanite can be confidently ascribed to origins through condensation
923 in the atmosphere of a late-stage AGB star. So-called "AB-type" moissanite is characterized by
924 the distinctive combination of very low $^{12}C/^{13}C$ (< 10) and a wide range of $^{14}N/^{15}N$ (from
925 significantly greater to significantly less than solar), without significant enrichment in *s*-process
926 trace elements—attributes that point to a carbon-rich J star or born-again AGB star (Hoppe et al.
927 1995; Huss et al. 1997; Amari et al. 2001b; Nittler and Alexander 2003; Liu et al. 2017a, 2017c;
928 Nguyen et al. 2018). Indeed, cluster analysis of these grains may reveal two distinct sources
929 (Amari et al. 2001b), with born-again AGB grains characterized by anomalous ^{32}S, a byproduct
930 of ^{32}Si decay (Fujiya et al. 2013). Note that Liu et al. (2017c) suggests that AB moissanite
931 should be divided into two subgroups—those with $^{14}N/^{15}N$ < solar (proposed to derive from
932 Type II supernovae) and those with $^{14}N/^{15}N$ > solar (probably from J stars).

933

934 *SN-II moissanite:* Two distinct populations of stellar SiC, most of which are aggregates of
935 nanocrystals (a consequence of relatively rapid crystallization), have been ascribed to different
936 Type II supernova processes. C-type moissanite, representing only about one in a thousand

937 stellar SiC grains, is characterized by low $^{14}N/^{15}N$, as well as significant excesses of ^{29}Si and
938 ^{30}Si relative to ^{28}Si (Amari et al. 1999; Croat et al. 2010). Significant ^{26}Mg and ^{44}Ca reveal the
939 production of short-lived radioactive ^{26}Al and ^{44}Ti (Gyngard et al. 2010b). Note that Liu et al.
940 (2016) further divided C moissanite into C1 and C2 types, based on differences in $^{12}C/^{13}C$.

941 Fewer than 2% of stellar moissanite grains have been identified as "X"-type, with diagnostic
942 isotopic signatures of Type II supernovae. All X-type silicon carbide grains display low ^{14}N
943 $/^{15}N$, $^{29}Si/^{28}Si$, and $^{30}Si/^{28}Si$, and significant ^{26}Mg, ^{44}Ca, and ^{49}Ti (Liu et al. 2018). Grains of
944 X moissanite are also distinguished by their polycrystalline habit, with crystallites typically from
945 10 to 200 nanometers diameter.

946 Note that Lin et al. (2010) subdivide these grains into three distinct groups; the division of
947 X0, X1, and X2 moissanite is based primarily on $^{29}Si/^{30}Si$, with high, average, and low values
948 relative to solar average, respectively. However, Zinner (2014) lumps all X-type moissanite
949 grains into a single group and it seems plausible that cluster analysis of "X"-type SiC grains will
950 reveal a continuum among these grains rather than three distinct natural kinds. Consequently, we
951 group all X-type moissanite grains together, and suggest that cluster analysis of X-type stellar
952 SiC is warranted.

953

954 *CN moissanite:* Approximately one in a thousand moissanite grains has very low $^{12}C/^{13}C$ and
955 $^{14}N/^{15}N$, very high $^{30}Si/^{28}Si$, and neon isotope anomalies that point to possible origins in
956 classical novae (Amari et al. 2001c; José and Hernandez 2007; Liu et al. 2016)—characteristics

957 that match those of nova graphite. Note that these grains have also been designated "putative
958 nova grains" or "PNG" moissanite. Further studies employing cluster analysis will help to
959 resolve whether these grains represent a population characterized by a distinct paragenetic mode.
960
961 **Khamrabaevite (TiC):** Nanograins of titanium carbide up to 200 nanometers in diameter have
962 been found in the cores and as inclusions in many presolar graphite grains (Figure 3A; Soker and
963 Harpez 1999; Croat et al. 2005, 2011; Stadermann et al. 2005; Bernatowicz et al. 2006;
964 Groopman et al. 2012). Most of these grains appear to predate graphite formation, having been
965 swept up during graphite crystallization and, in some instances serving as nucleation sites for
966 graphite.

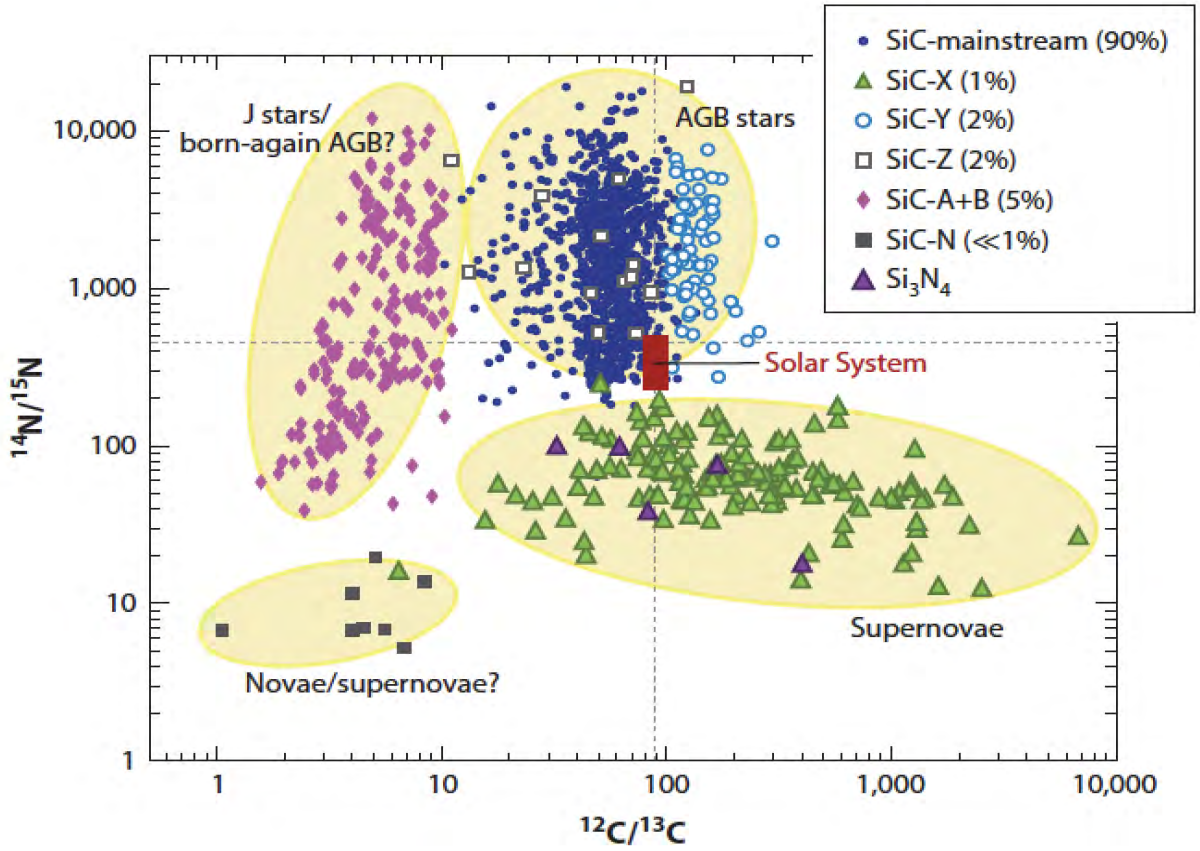

967
968 Figure 4. Isotope ratios for carbon and nitrogen in presolar moissanite (SiC) and nierite (Si_3N_4) reveal
969 clustering that corresponds to several distinct natural kinds of stellar minerals, formed near different kinds

of stars. Courtesy of Zinner (2014). Future multi-dimensional cluster analysis and visualization of these data coupled with Si isotopic and trace element measurements have the potential to reveal more definitive differentiations of the natural kinds of stellar SiC.

AGB khamrabaevite: TiC subgrains in AGB graphite are typically enriched in *s*-process elements, including V, Zr, Mo, and Ru. Presolar graphite grains with internal TiC seeds constrain both $1.0 < C/O < 1.2$ and formation conditions ($P < 7 \times 10^{-4}$ atm) (Soker and Harpez 1999).

SN-II khamrabaevite: Titanium carbide nano-crystals are common in the cores of SN-II graphite grains. These TiC grains often display significant V for Ti substitution, but not substitution by Zr, Ru, or Mo, which arise from the *s*-process in AGB stars (Croat et al. 2003, 2011; Groopman et al. 2012).

AGB (Mo,Zr)C: Bernatowicz et al. (1996) report a variety of carbide inclusions in AGB graphite, most commonly TiC but also Ti-Mo-Zr carbides, some of which are nearly pure (Mo,Zr)C. Bernatowicz et al. (1996) suggest a crystallization sequence upon cooling of ZrC first (at T ~ 1800 K), followed by MoC and TiC. Note that neither molybdenum nor zirconium carbides are yet IMA-approved mineral species.

Cohenite (Fe_3C): Bernatowicz et al. (1999) reported grains of the iron carbide cohenite (with orthorhombic symmetry) as inclusions in a SN-II graphite.

SN-II cohenite: Nanograins as inclusions in SN-II graphite.

994 **Iron Carbide [$(Fe,Cr)_7C_3$]:** Croat et al. (2005) report a single grain of hexagonal iron
995 carbide [metal composition ($Fe_{73}Cr_{21}Ti_6$)] as an inclusion in an "onion" AGB graphite. The
996 hexagonal unit-cell parameters, a = 6.95 Å and c = 4.5 Å, match a known synthetic phase
997 (Fe_7C_3; space group $P6_3/mc$). Note that this iron carbide is not yet an IMA-approved mineral
998 species.
999
1000 **Other Possible Stellar Carbides:** Some stellar TiC grains display local concentrations of Mo,
1001 Zr, and Ru-rich carbides (Bernatowicz et al. 1996; Croat et al. 2008), though these regions are
1002 not obviously separate inclusions of distinct phases. Similarly, Croat et al. (2011) describe Al-
1003 rich regions in TiC subgrains in SN-II graphite; they suggest that cubic (a = 4.2 Å) Ti_3AlC might
1004 be present.
1005
1006
1007 **SILICIDES [UNCONFIRMED]**
1008 A wide variety of nano-scale inclusions, subgrains, and/or local element concentrations have
1009 been reported in stellar moissanite and graphite. While it is not yet proven that these
1010 compositional regions are discrete mineral phases, potential stellar minerals include two iron-
1011 nickel silicides, possibly $(Fe,Ni)_2Si$, and/or $(Fe,Ni)_3Si$, as inclusions in SN-II (X-type)
1012 moissanite (Hynes 2010; Hynes et al. 2010). Neither the composition nor structure type was
1013 determined; therefore, stellar silicide is listed here as an unconfirmed astromineral.
1014
1015 **PHOSPHIDES [UNCONFIRMED]**

Lodders and Amari (2005) list schreibersite (Fe_3P) as a stellar condensate in their table of "expected and observed major element condensates." They suggest conditions of formation as ~1250 K at 10^{-4} atm; however, to our knowledge schreibersite has not yet been observed as a stellar mineral.

NITRIDES

Nitrogen, among the most abundant "metal" elements in stars, is a ubiquitous minor element in presolar moissanite, though the only confirmed stellar grains of refractory nitrogen minerals are the silicon nitride, nierite (Si_3N_4).

Nierite (Si_3N_4): Nierite is formed in the ejecta of core-collapse supernovae (Nittler et al. 1995; Hoppe et al. 1996; Lin et al. 2010). The few documented grains of stellar nierite, representing ~2 ppb of the Murchison CM chondrite, display uniform excesses of ^{15}N and ^{28}Si relative to solar values, as well as Ti isotopic anomalies that point to likely origins in Type II supernovae. The Presolar Grain Database, which records 41 analyzed nierite grains (Hynes and Gyngard 2009; see "presolar.physics.wustl.edu" accessed 24 Jan 2019), documents distinctive ranges of nitrogen isotopes ($18 < {}^{14}N/{}^{15}N < 190$, compared to 249 for the solar average) and low $^{30}Si/^{28}Si$.

SN-II nierite: Characterized by low $^{14}N/^{15}N$ and $^{30}Si/^{28}Si$ relative to solar averages.

Other Possible Stellar Nitrides: Reports of nanoscale concentrations, inclusions, or subgrains in stellar X-type moissanite include Ti(N,C) and (Mg,Al)N (Groopman and Nittler 2018; Gyngard et al. 2018), as well as an aluminum nitride, possibly AlN (Stroud and Bernatowicz 2005; Hynes et al. 2010). Further chemical and structural characterization will be required before assigning mineral names to these minute features.

SULFIDES

Rare stellar sulfide grains of oldhamite (CaS) and iron sulfide, most likely troilite (FeS), have been reported as nanoscale inclusions in graphite and moissanite grains (Hynes 2010; Hynes et al. 2011; Haenecour et al. 2016). These unambiguously stellar inclusions are characterized by anomalous S isotopes, in host grains with anomalous C isotopes.

Oldhamite (CaS): Oldhamite is calculated to be the highest temperature sulfide to condense in the atmosphere of a carbon-rich star (~1300 K at 10^{-4} atm; Lodders and Amari 2005, their Figure 1). The rarity of oldhamite presolar grains is likely a consequence of two factors: (1) the relatively low abundances of sulfur and calcium in stellar atmospheres of carbon stars, and (2) the solubility of oldhamite in water, which is often used in the preparation of meteorite mineral separates and polished sections.

AGB oldhamite: Hynes (2010) and Hynes et al. (2011) describe 7 anhedral inclusions of oldhamite with diameters from 16 to 40 nanometers. These subgrains occur as epitaxially aligned inclusions in AGB moissanite (ascribed to "AB"-type, possibly from a J star) grains.

Troilite [?] (FeS): Of special note is a report by Haenecour et al. (2016), who describe a presolar iron sulfide inclusion (80 nanometers diameter) in a 300-nanometer diameter graphite of suspected Type II supernova origins, though an AGB source cannot be ruled out. This observation is surprising, as the highest-temperature iron sulfide, troilite, condenses at a relatively low temperature (~700 K at 10^{-4} atm; Lodders 2003), compared to other confirmed presolar phases. However, the anomalously low $^{33}S/^{32}S$ and $^{34}S/^{32}S$ relative to solar abundances, coupled with the carbon isotope ratio of the graphite (characterized by $^{12}C/^{13}C >$ 200), point unambiguously to a stellar origin. Haenecour et al. (2016) suggest that the graphite grain and troilite inclusion originated in a Type II supernova, with the graphite and troilite condensing in different shells of the ejecta—a scenario consistent with models of supernova heterogeneities (Sarangi and Cherchneff 2015). However, they do not rule out the possibility of an origin in a ~3 solar mass, low-metallicity AGB star.

Given the low condensation temperature of troilite, Lodders (personal communication) suggests "sulfurization" of a stellar iron grain as a plausible alternative explanation. If so, then the troilite grain formed by secondary gas/solid reactions that occurred in reduced AGB winds—a process discussed by Lauretta et al. (1998).

SN-II (?) troilite: Nano-inclusion in graphite, characterized by anomalously negative delta^{33}S and delta^{34}S (Haenecour et al. 2016). Note that an AGB origin cannot be ruled out.

Other Possible Sulfides

Lodders and Amari (2005) list niningerite (MgS) as a stellar condensate in their table of "expected and observed major element condensates." They suggest conditions of formation as ~1050 K at 10^{-4} atm; however, to our knowledge niningerite has not yet been observed as a stellar mineral.

OXIDES

Suites of refractory oxide and silicate minerals have long been recognized as constituents of the dusty atmospheres of aging oxygen-rich stars and supernovae, based on astronomical observations of characteristic mid-infrared absorption features (Gillett et al. 1968; Stein et al. 1969; Woolf and Ney 1969; Onaka et al. 1989; Little-Marenin and Little 1990; Sloan and Price 1998; Speck et al. 2000; DePew et al. 2006), with notable advances in resolution and sensitivity following the successful launch of orbiting infrared telescopes (Neugebauer et al. 1984; Waters et al. 1996; Messenger et al. 2003; Nguyen and Zinner 2004; Rieke 2009; Jiang et al. 2013). Nevertheless, the isolation and characterization of oxides and silicates from primitive meteorites has proven challenging. Unlike the acid-insoluble carbon allotropes and carbides, which form a distinctive population of unambiguously stellar minerals, the rare, diminutive grains of stellar oxides and silicates are difficult to distinguish from the ubiquitous background of similar nebular condensates.

Following the fortuitous discovery of a stellar corundum grain with extreme enrichments in ^{17}O coupled with enhanced ^{26}Mg—an unambiguous signature of the decay of short-lived ^{26}Al and a likely consequence of its AGB origins (Hutcheon et al. 1994)—rapid progress was made by the application of automated methods to detect individual oxide and silicate grains with

anomalous isotopic values (Huss et al. 1994; Nittler et al. 1994, 1997, 2008; Choi et al. 1998; Nguyen et al. 2007; Takigawa et al. 2014, 2018; Figure 5). Corundum and amorphous Al_2O_3 dominate the inventory of stellar oxides, with modest numbers of oxide spinel and hibonite grains, as well as minor titanium oxide. The stellar oxide content of meteorites varies widely, with primitive carbonaceous chondrites holding the highest amounts—up to 55 ppm reported by Nguyen et al. (2007).

While efforts to characterize the diversity of stellar oxide and silicate phases are still in progress, several broad groups of these astrominerals have been classified based primarily on oxygen isotope ratios relative to solar averages. Approximately 70% of grains, labeled "Group 1" by Nittler et al. (1997), carry high $^{17}O/^{16}O$ and average or slightly low $^{18}O/^{16}O$—values that point to nucleosynthesis in typical oxygen-rich red giant and AGB stars during and after the first dredge up phase. Variations in stellar mass and initial metallicity play a significant role in the values of $^{17}O/^{16}O$ and $^{18}O/^{16}O$ (e.g., Timmes et al. 1995).

A smaller population of "Group 2" grains, ~15% of all oxides and silicates, display the high $^{17}O/^{16}O$ characteristic of AGB stars, but very low $^{18}O/^{16}O$—a feature initially thought to arise from cool-bottom processing (CBP) from relatively small (< 2 solar mass) AGB stars. Note, however, that Lugaro et al. (2017) suggest a similar isotopic signature might arise from a > 4-solar mass AGB star, based on a revised experimental determination of the proton-capture rate of ^{17}O (Bruno et al. 2016). By contrast, AGB stars of low mass and low metallicity produce "Group 3" grains (5% of all oxide and silicate samples) that display light oxygen isotopes, with both low $^{17}O/^{16}O$ and low $^{18}O/^{16}O$ relative to solar averages.

The origins of "Group 4" grains (perhaps 10% of all stellar oxides and silicates), with significant excesses of ^{18}O relative to ^{16}O and a range of $^{17}O/^{16}O$, as well as elevated ^{26}Mg coupled with ^{28}Mg depletions, remain a matter of debate. Both AGB stars with high metallicity and low mass and Type II supernovae with a complex mixing history have been invoked (Nittler et al. 1997; Choi et al. 1998; Nguyen and Messenger 2014; Zinner 2014). Finally, rare (less than 1%) "N-type" oxide and silicate grains are thought to arise from classical novae and are characterized by significantly elevated $^{17}O/^{16}O$, while $^{18}O/^{16}O$ is low (Nittler et al. 2008, 2011; Gyngard et al. 2010c, 2011; Nguyen and Messenger 2014).

In conformity with our proposed evolutionary classification system of minerals, we recognize three distinct paragenetic modes for stellar oxide and silicate grains: AGB stars (including Group 1, 2, 3, and perhaps some Group 4 grains), Type II supernovae (including some Group 4 grains), and classic novae (N-type grains).

This is a preprint, the final version is subject to change, of the American Mineralogist (MSA)
Cite as Authors (Year) Title. American Mineralogist, in press.
DOI: https://doi.org/10.2138/am-2020-7173

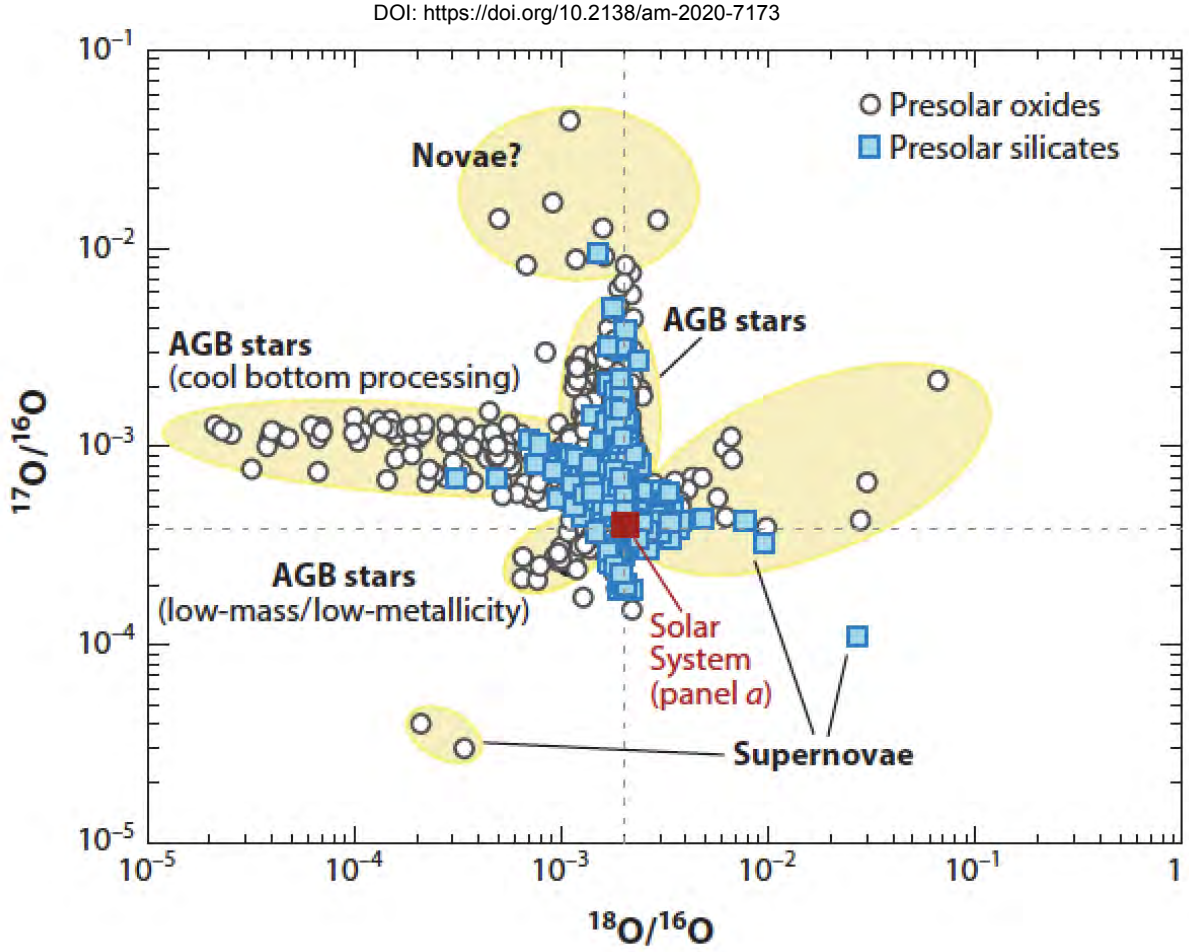

Figure 5. Oxygen isotopes in presolar oxides and silicates display extreme isotopic anomalies relative to solar averages. Clustering of these data points to a variety of stellar environments. Courtesy of Nittler et al (2008) and Zinner (2014).

Corundum (Al_2O_3): The occurrence of stellar corundum was suspected on the basis of a sharp infrared absorption feature at ~13 micrometers in the spectra of oxygen-rich AGB stars (Onaka et al. 1989; Speck et al. 2000; Takigawa et al. 2015). Corundum condenses at temperatures as high as 1700 K, and is thought to be the first phase to crystallize in the atmospheres of these stars (Grossman 1972; Salpeter 1977). Grains of stellar corundum were first identified in acid residues of meteorites by measurements of oxygen isotope anomalies

(Hutcheon et al. 1994; Nittler et al. 1997; Choi et al. 1998; Zinner et al. 2011; Takigawa et al. 2014, 2018). Corundum (alpha-Al_2O_3) and amorphous aluminum oxide are now known to be common constituents of presolar grains.

A matter of debate has been whether corundum can precipitate directly in its crystalline form in stellar atmospheres, or whether the crystalline form arises later from annealing of amorphous Al_2O_3. This issue was resolved by Takigawa et al. (2018), who describe a single 1.4-micron subhedral grain that represents a primary stellar condensate, formed in the atmosphere of a low- or intermediate-mass AGB star based on its characteristic isotopic signature: elevated ^{17}O (in this case enriched by a factor of ~3) and lower ^{18}O (depleted by a factor of ~25) relative to solar abundances (Figure 3D). The principal impurity in this grain was magnesium, enriched in ^{26}Mg as a consequence of the rapid decay of short-lived ^{26}Al from *s*-process nucleosynthesis. The relatively large size of this corundum grain, furthermore, suggests that it grew for several years in the extended atmosphere of its parent star. Such "large" grains are particularly subject to radiation pressure and have been invoked in triggering of dust-driven winds from AGB stars (Höfner 2008).

The more than 250 corundum grains tabulated in the Presolar Grain Database (Hynes and Gyngard 2009; see "presolar.physics.wustl.edu" accessed 24 Jan 2019) span the several groups of stellar oxides and silicates proposed by Nittler et al. (1997). Therefore, we recognize three different natural kinds of corundum from stars. It should be noted, however, that relatively few Al_2O_3 grains have been examined by electron diffraction; therefore, the crystallinity of many

grains remains uncertain. For example, of two grains studied by Stroud et al. (2004b), one was found to be corundum and the other amorphous Al_2O_3.

AGB corundum: The majority of presolar corundum grains carry the Group 1 isotopic signatures of AGB stars from 1 to < 3 solar masses, including elevated $^{17}O/^{16}O$ and normal or slightly low $^{18}O/^{16}O$ (Hutcheon et al. 1994; Nittler et al. 1997; Choi et al. 1998; Takigawa et al. 2014). In addition, approximately one in 6 stellar corundum grains displays elevated $^{17}O/^{16}O$ and very low $^{18}O/^{16}O$ characteristic of Group 2 late-stage cool-bottom processing in AGB stars (Davis 2011; Takigawa et al. 2014). Some grains also incorporate significant ^{26}Mg, a consequence of short-lived ^{26}Al. Takigawa et al. (2018) describe a euhedral Group 2 AGB corundum grain, 1.4 micrometers in diameter, that suggests extended growth of a pristine crystal in the stellar atmosphere. Finally, a small population of Group 3 stellar corundum grains has both low $^{17}O/^{16}O$ and low $^{18}O/^{16}O$—features ascribed to AGB stars of relatively low mass and low metallicity (Nittler et al. 2008).

SN-II corundum: Approximately one in 10 stellar corundum grains has low $^{17}O/^{16}O$ and low $^{18}O/^{16}O$, similar to Group 3 AGB corundum, but they also incorporate significant ^{26}Mg, ^{44}Ca, and ^{49}Ti, which point to origins in a Type II supernova (Choi et al. 1998; Nittler et al. 2008).

CNova corundum: Fewer than one percent of stellar corundum grains have oxygen isotope signatures associated with origins in classical novae: very high $^{17}O/^{16}O$ combined with low $^{18}O/^{16}O$ (Nittler et al. 2008).

Amorphous Al_2O_3: Amorphous Al_2O_3, which was verified on the basis of electron diffraction by Stroud et al. (2004b), arises from rapid cooling of Al-O rich zones in an AGB stellar atmosphere. Takigawa et al. (2018) suggest that the amorphous form could subsequently anneal to corundum.

AGB amorphous Al_2O_3: Origins of amorphous Al_2O_3 in an O-rich AGB star was inferred from anomalously elevated $^{17}O/^{16}O$, as well as $^{26}Mg/^{24}Mg$.

Eskolaite (Cr_2O_3): Croat et al. (2008) describe two SN-II graphite grains with 50-nanometer diameter inclusions of chromium oxide and trigonal unit-cell parameters matching those of eskolaite. Additional nano-inclusions rich in Cr-oxide display cubic unit-cell parameters, perhaps corresponding to CrO.

SN-II eskolaite: Occurs as nanoscale inclusions in SN-II graphite (Croat et al. 2008).

Titanium Oxide (TiO_2): Nittler et al. (2008) identified four grains of TiO_2 with elevated ^{17}O, thus pointing to origins in an AGB star, with subsequent work by Bose et al. (2010a) and

Zega et al. (2011). Thus far, no electron diffraction data are available on the polymorph of AGB TiO_2 (L. Nittler, personal communications). Croat et al. (2011) performed electron diffraction experiments on 52 TiO_2 inclusions in SN-II graphite and employed electron diffraction to confirm that specimens possessed the tetragonal rutile structure. Groopman and Nittler (2018) subsequently employed Ti-XANES to identify a presolar rutile inclusion in a graphite grain of presumed supernova origins, based on its high $^{12}C/^{13}C$ and high $^{18}O/^{16}O$ relative to solar abundances.

AGB TiO_2: Characterized by high $^{17}O/^{16}O$ (Nittler et al. 2008; Bose et al. 2010a; Zega et al. 2011); the polymorph is not yet resolved.

SN-II rutile: Inclusions in in SN-II graphite with elevated $^{12}C/^{13}C$ and $^{18}O/^{16}O$ (Groopman and Nittler 2018). TEM analyses reveals tetragonal grains with rutile unit-cell parameters (Croat et al. 2011).

Magnetite (Fe_3O_4). Croat et al. (2008) reported magnetite inclusions in stellar graphite. A single crystal of stellar magnetite (maximum dimension ~750 nanometers) was subsequently described by Zega et al. (2015), who measured elevated $^{17}O/^{16}O$ relative to solar abundances. They postulate that the grain formed by oxidation of an iron grain in the O-rich atmosphere of a solar metallicity AGB star (~2 stellar mass) during the first dredge up phase over time scales of 10^4 to 10^6 years. If so, then AGB magnetite would represent one of only three plausible

1228 secondary stellar minerals (in contrast to a primary condensate), the others being troilite (FeS;
1229 Haenecour et al. 2016) and shock-produced $MgSiO_3$ silicate perovskite (Vollmer et al. 2007).
1230
1231 *AGB magnetite:* Magnetite with elevated $^{17}O/^{16}O$ relative to solar abundances; likely formed
1232 by secondary gas/solid oxidation reactions of stellar iron.
1233
1234 **Spinel ($MgAl_2O_4$):** Stellar oxide spinel grains were initially recognized as presolar grains
1235 because of their anomalous oxygen isotope values—notably enrichment in ^{17}O and depletion in
1236 ^{18}O relative to solar averages (Nittler et al. 1994; Choi et al. 1998). Gyngard et al. (2010c)
1237 subsequently analyzed 38 spinel grains from the Murray CM2 meteorite. The majority have
1238 isotope anomalies consistent with AGB origins, but one grain with extreme enrichments in ^{17}O,
1239 ^{25}Mg, and ^{26}Mg is thought to have formed in a supernova environment.
1240 Zega et al. (2014a) described automated analyses of the acid-resistant fraction of several
1241 chondrite meteorites, in which they identified 37 oxide spinel grains. The majority of these
1242 grains were close to Mg-Al-spinel, but 5 grains displayed compositions in the Fe-Cr-chromite
1243 field (see below). From this suite of samples, they selected 4 grains, each up to 0.5 microns in
1244 maximum diameter, for detailed study. All of the 37 spinel grains identified display isotopic
1245 anomalies consistent with a presolar origin, notably ^{17}O enrichment consistent with origins in an
1246 AGB star somewhat more massive than the Sun and with approximately solar metallicity. Zega
1247 et al. (2014a) estimated the host star's mass to be 1.2 to 1.4 times than the Sun; note, however,
1248 that revised experimental measurements of nuclear reaction rates, for example the ^{17}O's proton-

capture rate (Bruno et al. 2016), may affect estimates of AGB stellar masses (Lugaro et al. 2017). Three of these grains are Mg-Al spinel with minor Fe and Cr; one with minor Ca as well; for example, $(Mg_{0.98},Fe_{0.01})(Al_{1.94}Cr_{0.06})O_4$. Pure Mg-Al spinel condenses at 1161 K at 10^{-6} atm and 1221 K at 10^{-3} atm, respectively. Note that stacking disorder observed in TEM studies could point to grain-to-grain impact-induced strain in the stellar atmosphere. Thus, while high pressures do not appear to play any significant role in presolar grain formation, transient events may influence their microstructures.

AGB spinel: The majority of stellar spinel samples are typical of Group 1 grains, displaying the high $^{17}O/^{16}O$ characteristic of AGB stars (Choi et al. 1998; Gyngard et al. 2010c; Zega et al. 2014a).

SN-II spinel: Nittler et al. (2008) and Gyngard et al. (2010c) describe Group 4 oxide spinel grains with high $^{18}O/^{16}O$, low ^{25}Mg, and high ^{26}Mg—characteristics that are ascribed to a Type II supernova origin.

CNova spinel: A single grain reported by Gyngard et al. (2010c) has extreme enrichments in ^{17}O, ^{25}Mg, and ^{26}Mg, likely condensed from classic nova ejecta.

Chromite ($Fe^{2+}Cr_2O_4$): Five grains studied by Nittler et al. (2005) and Zega et al. (2014a) are Fe-Cr-rich chromite. One of the grains is a composite with an average composition $[(Fe_{0.67}Mg_{0.31}Ni_{0.02})(Cr_{1.58}Al_{0.21}Mg_{0.06}Ti_{0.13})O_4]$, close to chromite composition.

AGB chromite: Zega et al. (2014a) describe 5 chromite grains with high $^{17}O/^{16}O$ and low $^{18}O/^{16}O$ relative to solar averages.

Hibonite ($CaAl_{12}O_{16}$): Prior to 1999, the refractory calcium aluminate hibonite [ideally $CaAl_{12}O_{19}$, but given misleadingly by IMA as $(Ca,Ce)(Al,Ti,Mg)_{12}O_{19}$] was assumed by most researchers to be exclusively a primary condensate in the solar nebula. Hibonite is a significant component of calcium aluminum inclusions (CAIs) from chondrite meteorites and specimens from several carbonaceous chondrite meteorites have been studied intensively (Zinner et al. 1986; Fahey et al. 1987; Hinton et al. 1988; Ireland 1988, 1990; Choi et al. 1999; Nittler et al. 2008; Zega et al. 2011; Han et al. 2015). Experimental evidence suggests that corundum and hibonite are among the earliest oxide condensates in a solar nebula, with reported condensation temperatures ranging from 1730 to 1780 K (Wood and Hashimoto 1993; Yoneda and Grossman 1995; Ebel and Grossman 2000; see Ebel 2006 for an overview)—relationships that will be examined in Part II of this series. However, the report by Choi et al. (1999) of two meteoritic hibonite grains with high high$^{17}O/^{16}O$ and high ^{26}Mg confirmed the AGB origins of a small fraction of the smallest hibonite grains in chondrites. Subsequent analyses by Nittler et al. (2008) and Zega et al. (2011), including hibonite grains with compositions in the $Ca(Mg,Ti,Al)_{12}O_{19}$

1289 field, point to origins in both AGB stars and Type II supernovae. In addition, Nittler et al. (2011)
1290 described a Group 3 hibonite grain with significant depletions in both ^{17}O and ^{18}O relative to
1291 solar averages, as well as low $^{25}Mg/^{24}Mg$—an unusual combination not easily ascribed to any
1292 one stellar origin.
1293
1294 *AGB hibonite:* The majority of stellar hibonite specimens are typical Group 1 grains,
1295 characterized by high $^{17}O/^{16}O$, average to low $^{18}O/^{16}O$, and high ^{26}Mg and ^{41}K—the latter
1296 from ^{41}Ca decay (Choi et al. 1999; Nittler et al. 2008; Zega et al. 2011). In addition, one unusual
1297 Group 3 hibonite grain displays significant depletions in both ^{17}O and ^{18}O relative to solar
1298 averages, as well as low $^{25}Mg/^{24}Mg$ (Nittler et al. 2011).
1299
1300 *SN-II hibonite:* A few Group 4 stellar hibonite grains display high $^{18}O/^{16}O$, as well as
1301 elevated ^{26}Mg and ^{41}K (Nittler et al. 2008; Zega et al. 2011), characteristic of core-collapse
1302 supernovae.
1303
1304 **Other Possible Oxide Phases:** Additional potential stellar oxide phases include unidentified
1305 iron oxides (Floss et al. 2008; Bose et al. 2010b); a cubic chromium oxide, possibly CrO (Croat
1306 et al. 2008); as well as possible Ca-Al oxide and Mg-Cr oxide grains (Nittler et al. 2008), though
1307 no definitive identifications of these phases are yet forthcoming. In addition, Stroud et al.
1308 (2004b) report evidence for a non-corundum hexagonal polymorph of Al_2O_3.

SILICATES

Amorphous silicate phases have been recognized as an important, if not dominant, component of the atmospheric dust produced by oxygen-rich evolved AGB stars, based on detection of distinctive infrared features (Woolf and Ney 1969; Treffers and Cohen 1974; T.W. Jones and Merrill 1976; Speck et al. 2000; McAdam et al. 2018). Higher resolution studies by Waters et al. (1996) using the Infrared Space Observatory confirmed the presence of crystalline silicates, as well—work that has been amplified by measurements with subsequent orbiting infrared observatories (e.g., Jiang et al. 2013).

The first unambiguously stellar silicate grains were discovered in interplanetary dust particles (Messenger et al. 2003), with subsequent identification in both polished sections of meteorites (Mostefaoui and Hoppe 2004; Nagashima et al. 2004; Nguyen and Zinner 2004) and Antarctic micrometeorites (Yada et al. 2008). Numerous subsequent publications (Zinner 2014 and references therein) record more than 250 meteoritic silicate grains with extreme isotopic anomalies that formed in the atmospheres of stars. These investigations suggest that stellar silicate grains, though typically less than 1 micron in diameter and with many grains smaller than 100 nanometers diameter, represent the most abundant group of stellar minerals—up to a few hundred ppm in primitive chondrite meteorites, compared to ~30 ppm for stellar moissanite (Zinner 2014, his Figure 17; Nittler et al. 2018b). Most stellar silicate grains appear to have AGB origins, though at least one supernova olivine grain with excess ^{18}O and depleted ^{17}O has been identified (Messenger et al. 2005).

A significant challenge in the systematic classification of stellar silicates is their diminutive scale, which makes chemical and structural analysis difficult. Major element analysis of Mg, Fe,

and Si reveal a number of grains with pyroxene or olivine stoichiometry, with significant iron content in all measurements (possibly a consequence of subsequent alteration). However, more than half of analyzed grains appear to be nonstoichiometric and may represent amorphous silicates (Floss and Stadermann 2009, 2012; Vollmer et al. 2009; Bose et al. 2010a; Nguyen et al. 2010; Kemper et al. 2011; see Zinner 2014, his Figure 18). The complexity of some stellar oxide and silicate grains is represented by a zoned AGB (Group 1) grain with an Al-Ca-Ti oxide core and Mg-Ca-silicate mantle (Leitner et al. 2018), as well as other composite oxide-silicate grains (Vollmer 2013; Nguyen et al. 2016; Nittler et al. 2018b). As the identification and characterization of stellar silicates is still in its infancy, we recognize olivine and enstatite as the only two confirmed IMA-approved species.

Forsterite (Mg_2SiO_4): Based on astronomical observations, Mg-rich olivine is the most common stellar crystalline silicate, estimated to exceed the quantity of pyroxene by a factor between 2 and 3 (Kemper et al. 2004; O. C. Jones et al. 2012). Most confirmed presolar olivine grains display characteristics of AGB stars, though distinctive SN-II grains have also been observed (Zinner 2014). Note that a significant fraction of stellar forsterite may be subsequently lost through amorphization by shock and/or irradiation (Brucato et al. 2004).

AGB forsterite: Mostefaoui and Hoppe (2004) described three forsterite grains with elevated ^{17}O, typical of AGB stars. Additional reports of stellar AGB olivine include Busemann et al. (2009), Vollmer et al. (2009), Zega et al. (2014b; notably Ca-bearing), Nguyen and Messenger (2016), and Nittler et al. (2018b).

This is a preprint, the final version is subject to change, of the American Mineralogist (MSA)
Cite as Authors (Year) Title. American Mineralogist, in press.
DOI: https://doi.org/10.2138/am-2020-7173

SN-II forsterite: Messenger et al. (2005) describe a single grain of olivine with high $^{18}O/^{16}O$ and low $^{17}O/^{16}O$, characteristic of supernova origins.

Enstatite ($MgSiO_3$): Magnesium silicate pyroxene is the second important crystalline stellar silicate phase, based on both astronomical observations and analyses of isotopically anomalous presolar silicate grains (Mostefaoui and Hoppe 2004; Zinner 2014). Note that while enstatite may condense directly, Carrez et al. (2002b) suggested that enstatite could also crystallize from amorphous silicate under the influence of electron radiation in a circumstellar environment.

AGB enstatite: Mostefaoui and Hoppe (2004) described four pyroxene grains with the characteristic elevated $^{17}O/^{16}O$ of ABG origins. Subsequent studies have documented dozens of additional examples, a few of which have been confirmed by TEM analyses to have the pyroxene structure, though most identifications of "enstatite" are based on bulk compositions with (Mg + Fe) ~ Si (Floss and Stademann 2009, 2012; Bose et al. 2010a; Vollmer et al. 2013; Nguyen et al. 2016; see also Zinner 2014, his Figure 18).

SN-II enstatite: One pyroxene grain examined by Mostefaoui and Hoppe (2004) displayed normal $^{17}O/^{16}O$ and extremely elevated $^{18}O/^{16}O$, thought to result from Type II supernovae.

Bridgmanite ($MgSiO_3$): Of special interest is a grain of bridgmanite, the high-pressure, perovskite-structured polymorph of $MgSiO_3$, which possibly formed as the result of a high-

velocity impact of a stellar shock wave on enstatite (Vollmer et al. 2007). If so, then stellar bridgmanite represents a secondary alteration phase. The grain possesses high $^{17}O/^{16}O$ and low $^{18}O/^{16}O$, perhaps reflecting an origin in a low-mass, solar metallicity AGB star during and after the first dredge up phase.

AGB bridgmanite: High-pressure $MgSiO_3$ polymorph, perhaps the consequence of shock alteration of AGB enstatite.

Amorphous Silicate: More than half of studied presolar silicate grains are amorphous (Kemper et al. 2004; Messenger et al. 2003; Zinner 2014), and most of those are non-stoichiometric phases with compositions intermediate to those of forsterite and enstatite (e.g., Zinner 2014, his Figure 18). The great majority of these grains display the elevated $^{17}O/^{16}O$ associated with AGB stars. Note, however, that Kemper et al. (2004) suggest that Type II supernovae may be a significant additional source of amorphous silicates. Amorphous silicates may condense directly in the stellar atmosphere, or they may occur as a result of subsequent irradiation and/or shocks in the circumstellar/interstellar medium (A.P. Jones et al. 1994; Demyk et al. 2000; Carrez et al. 2002a; Brucato et al. 2004; A.P. Jones 2007).

AGB amorphous Mg-Fe silicate: Amorphous Mg-Fe silicate compositions with elevated $^{17}O/^{16}O$.

This is a preprint, the final version is subject to change, of the American Mineralogist (MSA)
Cite as Authors (Year) Title. American Mineralogist, in press.
DOI: https://doi.org/10.2138/am-2020-7173

NETWORK GRAPH OF STELLAR MINERALS

Network graphs provide a useful method to visualize relationships among varied minerals and their attributes (Morrison et al. 2017). Figure 6 displays a bipartite force-directed network graph of stellar minerals, in which 27 phases—22 IMA approved mineral species, two additional crystalline phases not yet recognized by IMA (MoC and Fe_7C_3), plus three amorphous condensed phases (C, Al_2O_3, and silicate)—are represented by diamond-shaped nodes. These mineral nodes are linked to three types of stars (AGB, SN-II, and CNova) represented by star-shaped nodes. Compositional information is conveyed by mineral node colors: black (C-bearing), green (not C or O), blue (contains O, but not Si), and red (contains Si + O).

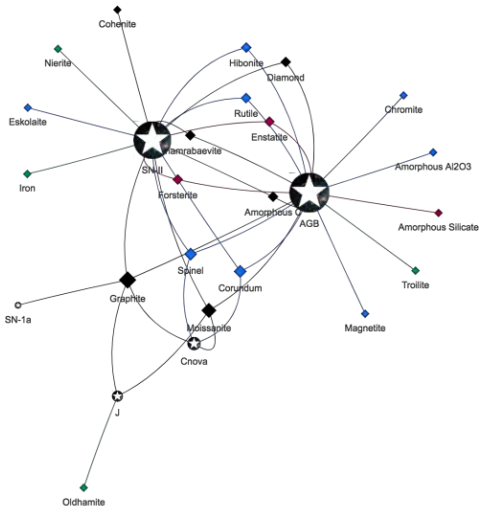

Figure 6. Bipartite force-directed network graph (Morrison et al. 2017) of stellar minerals linked to their host stars. Diamond-shaped nodes represent condensed crystalline and amorphous phases [black (C-bearing), green (not C or O), blue (contains O, but not Si), and red (contains Si + O)], whereas star-shaped nodes represent three types of host stars—asymptotic giant branch stars

(AGB), Type II supernovae (SN-II), and classical novae (CNova). The sizes of nodes correspond to the number of links to other nodes. [Courtesy of Anirudh Prabhu, RPI]

This visual representation of all confirmed stellar minerals underscores several important trends. First, all of these stellar phases (and the great majority of confirmed stellar mineral grains) are formed in the atmospheres of AGB stars (17 phases) and/or Type II supernovae (19 phases). Furthermore, 23 types of condensed stellar phases are only known from these sources. By contrast, only four minerals are confidently ascribed to classical novae: graphite, moissanite, corundum, and spinel. Both ABG stars and Type II supernovae produce a wide compositional range of grains, including native elements, carbides, oxides, and silicates.

Graphite, moissanite, corundum, and spinel are the only phases thus far identified from all three of these stellar hosts. This uneven distribution of stellar minerals among types of stars in part reflects the prodigious production of stardust in ABG planetary nebulas and Type II supernovae.

This is a preprint, the final version is subject to change, of the American Mineralogist (MSA)
Cite as Authors (Year) Title. American Mineralogist, in press.
DOI: https://doi.org/10.2138/am-2020-7173

TRACE AND MINOR ELEMENTS IN STELLAR MINERALS

The 27 phases represented by the known inventory of stellar minerals incorporate only 11 different abundant chemical elements and 6 minor elements as essential constituents (Figure 1). An important unanswered question relates to the scores of other chemical elements that are not represented as significant constituents during the pre-solar phase of mineral evolution. All of these elements must be present in stardust particles, but where do they reside? One possible answer lies in the proposal of Lodders and Amari (2005; Table 9), who suggested that a number of refractory minerals may await discovery as stellar minerals. Among their proposed condensates are gehlenite ($Ca_2Al_2SiO_7$), grossite ($CaAl_4O_7$), anorthite ($CaAl_2Si_2O_8$), perovskite ($CaTiO_3$), iron silicide (FeSi), and aluminum nitride (AlN), as well as phases of S [niningerite (MgS), daubréelite ($FeCr_2S_4$), alabandite (Mn,Fe)S], P [schreibersite $(Fe,Ni)_3P$], Na [albite ($NaAlSi_3O_4$)], K [orthoclase ($KAlSi_3O_4$)], and Cl {sodalite [$Na_4(AlSiO_4)_3Cl$]}.

However, for a variety of less abundant elements at least three additional structural roles have likely occurred. A few elements are close proxies for common constituents of the ur-minerals, and thus were easily incorporated into the adaptable lattices of these earliest minerals (Table 1). For example, gallium substitutes for aluminum, cobalt for iron, and manganese for calcium and/or iron. This propensity for some rarer elements to follow their chemically similar but more abundant neighbors may result in a relative paucity of mineral species for many of these elements (e.g., Christy 2015; Hazen et al. 2015).

A second possibility is that rarer elements are "swept up" during crystallization and thus are incorporated as defect sites in crystals. Nitrogen and boron, for example are common defect

elements in diamond, while N and Ti are ubiquitous in stellar moissanite. The range of possible single-atom defects in crystals is at present poorly constrained but deserves further study.

The third likely locus for trace and minor elements in pre-solar minerals is grain boundary regions in complex polycrystalline and/or amorphous composite stellar grains. Structural and compositional details of grain boundaries are lacking. In particular, it is not known the extent to which these regions are amorphous versus nano-crystalline. It is plausible that some moderately rare "minerals" form as local concentrations with dozens to hundreds of unit cells—"phases" that may be revealed as atomic-scale-resolution microscopy becomes more widely applied to mineral systems (e.g., Ma et al. 2013, 2017; Rubin and Ma 2017).

This is a preprint, the final version is subject to change, of the American Mineralogist (MSA)
Cite as Authors (Year) Title. American Mineralogist, in press.
DOI: https://doi.org/10.2138/am-2020-7173

IMPLICATIONS

The fascinating discipline of stellar mineralogy holds two important lessons for the field of mineralogy. First, a rigorous, quantitative methodology is needed to identify discrete natural kinds of minerals. In the case of astrominerals, we need to adopt and modify data-driven methodologies that rely on the richness of idiosyncratic, diagnostic attributes of presolar grains: trace and minor elements, ratios of isotopes, structural defects, inclusions, external morphologies, and other attributes that derive from their specific paragenetic histories and that distinguish them from other populations. We suggest that multi-dimensional analysis based on natural kind clustering of large, reliable, open-access data resources will reveal quantitative discriminants that place our systematic classification of stellar minerals on a secure footing. For example, we are now expanding the Presolar Grain Database (Hynes and Gyngard 2009; see "presolar.physics.wustl.edu") to investigate more than 20,000 stellar moissanite grain analyses based on $^{12}C/^{13}C$, $^{14}N/^{15}N$, $^{30}Si/^{28}Si$, $^{29}Si/^{28}Si$, and such trace isotopes as ^{26}Mg, ^{44}Ca, and ^{49}Ti. Preliminary cluster analysis reveals several discrete populations; however, an important caveat relates to the degree of separation or "distance" both within and between different presumed clusters of stellar mineral grains. We hope to determine whether clusters based on attributes of stardust grains are non-overlapping in multi-dimensional composition space, as opposed to possessing variations that arise from continuous ranges of attributes in complex temperature-pressure-composition space. In either eventuality, cluster analysis will enhance our understanding of the dynamic, evolving sources of stardust.

Secondly, these varied, ancient condensed stellar phases underscore the need for an evolutionary system of mineralogy, which complements the existing IMA protocols based on idealized end-member compositions and crystal structures. Stellar minerals represent at least 22

IMA-approved mineral species, but their remarkable isotopic and morphological idiosyncrasies point to more than 40 "natural kinds" that are quite distinct from their more familiar terrestrial counterparts. Minerals that condensed from the atmospheres of stars are fundamentally distinct in chemistry, isotopic composition, morphology, and associations from more recent terrestrial examples of the same IMA-approved species. Stellar mineralogy also embraces the most ancient of a growing inventory of condensed non-crystalline phases that are important in all eras of the mineral evolution of Earth and other planets, but have received scant attention in the systematic consideration of evolving planetary systems.

For more than 13 billion years, the stardust of the earliest stage of mineral evolution has enriched the interstellar medium, comprising a significant fraction of the molecular clouds and nebulas where new generations of stars, and their diverse retinue mineral-rich planets and moons, are born. In the process, new minerals, including ices and other low-temperature condensates, expanded the cosmic mineralogical inventory. These far-flung interstellar processes were prelude to the condensation and/or low-pressure melting in the solar nebula of a growing inventory of minerals—phases that are preserved as chondrules, refractory inclusions, and the matrix of chondrite meteorites. That phase of mineral evolution will be the subject of the second contribution in this series.

In this and subsequent contributions, the guiding principal of the evolutionary system of mineralogy is that each mineral sample is a rich storehouse of information. Each specimen possesses myriad physical and chemical attributes that point to its origin and subsequent alteration pathways through space and time. We thus embrace the inherent "messiness" of nature—the complexities that reveal the evolution of stars, planets, minerals, and life.

This is a preprint, the final version is subject to change, of the American Mineralogist (MSA)
Cite as Authors (Year) Title. American Mineralogist, in press.
DOI: https://doi.org/10.2138/am-2020-7173

ACKNOWLEDGMENTS

Throughout the preparation of this paper we have benefitted from the generous advice and deep expertise of Larry R. Nittler, a pioneer in astromineralogy, who was an early reviewer of this contribution and a constant adviser during its revisions. We are grateful to Anirudh Prabhu for providing the network diagram of the Evolutionary System of stellar mineralogy. Denton Ebel and an anonymous reviewer offered thoughtful comments and suggestions that have greatly improved this study. In addition, we thank Conel O.M'D. Alexander, Asmaa Boujibar, Carol Cleland, Robert T. Downs, Olivier Gagné, Pierre Haenecour, Peter Heaney, Samantha Howell, Sergey Krivovichev, Chao Liu, Katharina Lodders, Michael Walter, and Shuang Zhang for thoughtful discussions and comments.

This publication is a contribution to the Deep Carbon Observatory. Studies of mineral evolution and mineral ecology are supported by the Deep Carbon Observatory, the Alfred P. Sloan Foundation, the W. M. Keck Foundation, the John Templeton Foundation, the NASA Astrobiology Institute, a private foundation, and the Carnegie Institution for Science. Any opinions, findings, or recommendations expressed herein are those of the authors and do not necessarily reflect the views of the National Aeronautics and Space Administration.

REFERENCES

Abel, T., Bryan, G.L., and Norman, M.L. (2002) The formation of the first stars in the universe. Science, 295, 93-98.

Abia, C. and Isern, J. (2000) The chemical composition of carbon stars. II. The J-type stars. The Astrophysical Journal, 536, 438-449.

Alexander, C.M.O'D. (1993) Presolar SiC in chondrites: How variable and how many sources? Geochemica et Cosmochimica Acta, 57, 2869-2888.

Alexander, C.M.O'D. and Nittler, L.R. (1999) The galactic evolution of Si, Ti, and O isotopic ratios. The Astrophysical Journal, 519, 222-235.

Alexander, C.M.O'D., Swan, P., and Walker, R.M. (1990) In situ measurement of interstellar silicon carbide in two CM chondrite meteorites. Nature, 348, 715-717.

Amari, S. (2014) Recent progress in presolar grain research. Mass Spectrometry, 3, 6 pp. doi: 10.5702/massspectrometry.S0042

Amari, S., Anders, E., Virag, A., and Zinner, E. (1990) Interstellar graphite in meteorites. Nature, 345, 238-240.

Amari, S., Hoppe, P., Zinner, E., and Lewis, R.S. (1992) Interstellar SiC with unusualk isotopic compositions: Grains from a supernova? The Astrophysical Journal, 394, L43-L46.

Amari, S., Lewis, R.S., and Anders, E. (1994) Interstellar grains in meteorites: I. Isolation of SiC, graphite, and diamond; size distributions of SiC and graphite. Geochimica et Cosmochimica Acta, 58, 459-470.

1548 Amari, S., Zinner, E., and Lewis, R.S. (1995a) Large ^{18}O excesses in circumstellar graphite
1549 grains from Murchison meteorite: Indication of a massive-star origin. The Astrophysical
1550 Journal Letters, 447, L147-L150.
1551 Amari, S., Lewis, R.S., and Anders, E. (1995b) Interstellar grains in meteorites: III. Graphite and
1552 its noble gases. Geochimica et Cosmochimica Acta, 59, 1411-1426.
1553 Amari, S., Hoppe, P., Zinner, E., and Lewis, R.S. (1995c) Trace-element concentrations in single
1554 circumstellar silicon carbide grains from the Murchison meteorite. Meteoritics, 30, 679-693.
1555 Amari, S., Zinner, E., and Lewis, R.S. (1999) A singular presolar SiC grain with extreme ^{29}Si
1556 and ^{30}Si excesses. The Astrophysical Journal, 517, L59–L62.
1557 Amari, S., Nittler, L.R., Zinner, E, Gallino, R., Lugaro, M., and Lewis, R.S. (2001a) Presolar SiC
1558 grains of type Y: Origin from low metallicity asymptotic giant branch stars. The
1559 Astrophysical Journal, 546, 248-266.
1560 Amari, S., Nittler, L.R., Zinner, E., Lodders, K., and Lewis, R.S. (2001b) Presolar SiC grains of
1561 Type A and B: Their isotopic compositions and stellar origins. The Astrophysical Journal,
1562 559, 463-483.
1563 Amari, S., Gao, X., Nittler, L.R., Zinner, E., José, J., Hernandez, H., and Lewis, R.S. (2001c)
1564 Presolar grains from novae. The Astrophysical Journal, 551, 1065–1072.
1565 Amari, S., Zinner, E., and Lewis, R.S. (2004) Comparison study of presolar graphite separates
1566 KE3 and KFA1 from the Murchison meteorite. Lunar and Planetary Science, 35, #2103.
1567 Amari, S., Gallino, R., and Pignatari, M. (2006) Presolar graphite from the Murchison meteorite:
1568 Noble gases revisited. Lunar and Planetary Science, 37, #2409.

1569 Bailey, K.D. (1994) Typologies and Taxonomies: An Introduction to Classification Techniques.
1570 Studies in Quantitative Applications in the Social Sciences, 102. New York: SAGE
1571 Publications.

1572 Bernatowicz, T.J., Fraundorf, G., Ming, T., Anders, E., Wopenka, B., Zinner, E., and Fraundorf,
1573 P. (1987) Evidence for interstellar SiC in the Murray carbonaceous chondrite. Nature, 330,
1574 728-730.

1575 Bernatowicz, T.J., Cowsik, R., Gibbons, P., Loddeers, K., Fegley, B., Amari, S., and Lewis, R.
1576 (1996) Constraints on stellar grain formation from presolar graphite in the Murchison
1577 meteorite. The Astrophysical Journal, 472, 760-782.

1578 Bernatowicz, T.J., Bradley, J., Amari, S., Messenger, S., and Lewis, R. (1999) New kinds of
1579 massive star condensates in a presolar graphite from Murchison. Lunar and Planetary Science
1580 Conference, 30, #1392.

1581 Bernatowicz, T.J., Messenger, S., Pravdivtseva, O., Swan, P., and Walker, R.M. (2003) Pristine
1582 presolar silicon carbide. Geochimica et Cosmochimica Acta, 67, 4679-4691.

1583 Bernatowicz, T.J., Croat, T.K., and Daulton, T.L. (2006) Origin and evolution of carbonaceous
1584 grains in stellar environments. In D.S. Lauretta and H.Y. McSween Jr. (eds.), Meteorites and
1585 the Early Solar System II. Tucson: University of Arizona Press, pp.109-126.

1586 Bertulani, C.A. (2013) Nuclei in the Cosmos. Singapore: World Scientific.

1587 Bildsten, L. (1998) Thermonuclear burning on rapidly accreting neutron stars. In R.Buccheri, J.
1588 van Paradijs, and M.A. Alpar [Editors], The Many Faces of Neutron Stars. Dordrecht,
1589 Germany: Kluwer, pp. 419B.

1590 Bose, M., Floss, C., and Stadermann, F.J. (2010a) An investigation into the origin of Fe-rich
1591 presolar silicates in Acfer 094. The Astrophysical Journal, 714, 1624–1636.

1592 Bose, M., Zhao, X., Floss, C., Stadermann, F.J., and Lin, Y. (2010b) Stardust material in the
1593 paired enstatite chondrites: SAH 97096 and SAH 97159. Proceedings of Science, (NIC-XI)
1594 138
1595 Boulanger, F., Joblin, C., Jones, A., Madden, S., and Tielens, A.G.G.M. (2009) Infrared
1596 spectroscopy of interstellar dust. European Astronomical Society Publications Series, 35, 33-
1597 56.
1598 Bowman, J.D., Rogers, A.E.E., Monsalve, R.A., Mozdzen, T.J., and Mahesh, N. (2018) An
1599 absorption profile centred at 78 megahertz in the sky-averaged spectrum. Nature, 555, 67-70.
1600 Boyd, R. (1991) Realism, anti-foundationalism and the enthusiasm for natural kinds.
1601 Philosophical Studies, 61, 127-148.
1602 Boyd, R. (1999) Homeostasis, species, and higher taxa. In R. Wilson [Editor], Species: New
1603 Interdisciplinary Essays. Cambridge, Massachusetts: Cambridge University Press, pp. 141-
1604 186.
1605 Brucato, J.R., Strazzulla, G., Baratta, G, and Colangeli, L. (2004) Forsterite amorphisation by ion
1606 irradiation: Monitoring by infrared spectroscopy. Astronomy & Astrophysics, 413, 395-401.
1607 Bruno, C.G., Scott, D.A., Aliotta, M., Fortmicola, A., Best, A., and 30 others (2016) Improved
1608 direct measurement of the 65 keV resonance strength in the ^{17}O(p,alpha)^{14}N reaction at
1609 LUNA. Physical Review Letters, 117, 142502.
1610 Burbidge, E.M., Burbidge, G.R., Fowler, W.A., and Hoyle, F. (1957) Synthesis of the elements
1611 in stars. Review of Modern Physics, 29, 547-650.
1612 Burke, E.A.J. (2006) The end of CNMMN and CCM—Long live the CNMNC! Elements, 2,
1613 388.

1614 Busemann, H., Nguyen, A.N., Cody, G.D., Hoppe, P., Kilcoyne, A.L.D., Stroud, R.M., Zega, T.,
1615 and Nittler, L.R. (2009) Ultra-primitive interplanetary dust particles from the comet
1616 26P/Grigg-Skjellerup dust strean collection. Earth and Planetary Science Letters, 288, 44-57.
1617 Caffee, M.W., Hohenberg, C.M., Swindle, T.D., and Goswami, J.N. (1987) Evidence in
1618 meteorites for an active early sun. The Astrophysical Journal Letters, 313, L31-L35.
1619 Cameron, A.G.W. (1957) Nuclear reactions in stars and nucleogenesis. Publications of the
1620 Astronomical Society of the Pacific, 69, 201-222.
1621 Carrez, P., Demyk, K., Cordier, P., Gengembre, L., Grimblot, J., D'Hendecourt, L., Jones, A.P.,
1622 and Leroux, H. (2002a) Low-energy helium ion irradiation-induced amorphization and
1623 chemical changes in olivine: Insights for silicate dust evolution in the interstellar medium.
1624 Meteoritics & Planetary Science, 37, 1599-1614.
1625 Carrez, P., Demyk, K., Leroux, H., Cordier, P., Jones, A.P., and D'Hendecourt, L. (2002b) Low-
1626 temperature crystallisation of $MgSiO_3$ glasses under electron irradiation: Possible implications
1627 for silicate dust evolution in circumstellar environments. Meteoritics & Planetary Science, 37,
1628 1615-1622.
1629 Carroll, B.W. and Ostlie, D.A. (2017) An Introduction to Modern Astrophysics: Edition 2.
1630 Cambridge, UK: Cambridge University Press.
1631 Chandrasekhar, S. (1931) The maximum mass of ideal white dwarfs. The Astrophysical Journal,
1632 74, 81-82.
1633 Cheung, R. (2006) Silicon Carbide Microelectromechanical Systems for Harsh Environments.
1634 London: Imperial College Press.

1635 Chigai, T., Yamamoto, T, and Kozasa, T. (2002) Heterogeneous condensation of presolar
1636 titanium carbide core-graphite mantle spherules. Meteoritics and Planetary Science, 37, 1937-
1637 1951.
1638 Choi, B.-G., Huss, G.R., Wasserburg, G.J., and Gallino, R. (1998) Presolar corundum and spinel
1639 in ordinary chondrites: Origins from AGB stars and a supernova. Science, 282, 1284-1289.
1640 Choi, B.-G., Wasserburg, G.J., and Huss, G.R. (1999) Circumstellar hibonite and corundum and
1641 nucleosynthesis in asymptotic giant branch stars. The Astrophysical Journal, 522, L133–
1642 L136.
1643 Christy, A.G. (2015) Causes of anomalous mineralogical diversity in the Periodic Table.
1644 Mineralogical Magazine, 79, 33-49.
1645 Clayton, D.D. (1975) Extinct radioactivities: Trapped residuals of presolar grains. The
1646 Astrophysical Journal, 199, 765.
1647 Clayton, D.D. (1978) Precondensed matter: Key to the early solar system. Moon and Planets, 19,
1648 109-137.
1649 Clayton, D.D. (1983) Principles of Stellar Evolution and Nucleosynthesis. Chicago: University
1650 of Chicago Press.
1651 Clayton, D.D. (1997) Placing the sun and mainstream SiC particles in galactic chemodynamic
1652 evolution. The Astrophysical Journal, 484, L67-L70.
1653 Clayton, D.D. (2003) Presolar galactic merger spawned the SiC mainstream. The Astrophysical
1654 Journal, 598, 313-324.
1655 Clayton, D.D. and Ward, R.A. (1978) S-process studies: Xenon and krypton isotopic
1656 abundances. The Astrophysical Journal, 224, 1000-1006.

1657 Clayton, D.D. and Nittler, L.R. (2004) Astrophysics with presolar stardust. Annual Reviews of
1658 Astronomy and Astrophysics, 42, 39-78.
1659 Clayton, D.D., Meyer, B.S., Sanderson, C.I., Russell, S.S., and Pillinger, C.T. (1995) Carbon and
1660 nitrogen isotopes in type II supernova diamonds. The Astrophysical Journal, 447, 894-905.
1661 Coulter, D.A., Foley, R.J., Kilpatrick, C.D., Drout, M.R., Piro, A.L., Shappee, B.J., Siebert,
1662 M.R., Simon, J.D., Ulloa, N., Kasen, D., Madore, B.F., Murguia-Berthier, A., Pan, Y.-C.,
1663 Prochaska, J.X., Ramirez-Ruiz, E., Rest, A., and Rojas-Bravo, C. (2017) Swope Supernova
1664 Survey 2017a (SSS17a), the optical counterpart to a gravitational wave source. Science, 358,
1665 1556-1558.
1666 Croat, T.K., Bernatowicz, T., Amari, S., Messenger, S., and Stadermann, F.J. (2003) Structural,
1667 chemical and isotopic microanalytical investigations of graphite from supernovae.
1668 Geochimica et Cosmochimica Acta, 67, 4705-4725.
1669 Croat, T.K., Stadermann, F.J., and Bernatowicz, T.J. (2005) Presolar graphite from AGB stars:
1670 Microsctructure and s-process enrichment. The Astrophysical Journal, 631, 976-987.
1671 Croat, T.K., Stadermann, F.J., and Bernatowicz, T.J. (2008) Correlated isotopic and
1672 microstructural studies of turbostratic presolar graphites from the Murchison meteorite.
1673 Meteoritics and Planetary Science, 43, 1497-1516.
1674 Croat, T.K., Stadermann, F.J., and Bernatowicz, T.J. (2010) Unusual ^{29,30}Si-rich SiCs of
1675 massive star origin found within graphites from the Murchison meteorite. The Astronomical
1676 Journal, 139, 2159-2169.
1677 Croat, T.K., Jadhav, M., Lebsack, E., and Bernatowicz, T.J. (2011) TiC and rutile within a
1678 supernova graphite. Meteoritics & Planetary Science, 46, A51.

1679 Croat, T.K., Berg, T., Bernatowicz, T.J., and Jadhav, M. (2013) Refractory metal nuggets within
1680 presolar graphite: First condensates from a circumstellar environment. Meteoritics &
1681 Planetary Science, 48, 686–699.
1682 Dai, Z.R., Bradely, J.P., Joswiak, D.J., Brownlee, D.E., Hill, H.G.M., and Genge, M.J. (2002)
1683 Possible in situ formation of meteoritic nanodiamonds in the early solar system. Nature, 418,
1684 157-159.
1685 Dana, E.S. and Ford, W.E. (1947) Dana's Textbook of Mineralogy, 4th Edition. New York: John
1686 Wiley & Sons.
1687 Dana, J.D. (1850) A System of Mineralogy, Comprising the Most Recent Discoveries, Including
1688 Full Descriptions of Species and their Localities, Chemical Analyses and Formulas, Tables
1689 for the Determination of Minerals, and a Treatise on Mathematical Crystallography and the
1690 Drafting of Figures of Crystals. Third Edition, Rewritten, Rearranged, and Enlarged. New
1691 York and London: George P. Putnam.
1692 Dana, J.D., Dana, E.S., Palache, C., Berman, H., and Frondel, C. (1973) Dana's System of
1693 Mineralogy, 7th Edition, Complete in 3 Volumes. New York: John Wiley & Sons.
1694 Daulton, T.L., Eisenhour, D.D., Bernatowicz, T.J., Lewis, R.S., and Buseck, P.R. (1996) Genesis
1695 of presolar diamonds: Comparative high-resolution transmission electron microscopy study of
1696 meteoritic and terrestrial nano-diamonds. Geochimica et Cosmochimica Acta, 60, 4853-4872.
1697 Daulton, T.L., Bernatowicz, T.J., Lewis, R.S., Messenger, S., Stadermann, F.J., and Amari, S.
1698 (2002) Polytype distribution in circumstellar silicon carbide. Science, 296, 1852-1855.
1699 Daulton, T.L., Bernatowicz, T.J., Lewis, R.S., Messenger, S., Stadermann, F.J., and Amari, S.
1700 (2003) Polytype distribution in circumstellar silicon carbide: Microstructural characterization
1701 by transmission electron microscopy. Geochimica et Cosmochimica Acta, 67, 4743-4767.

1702 Davidson, J., Busemann, H., Nittler, L.R., Alexander, C.M.O'D., Orthous-Daunay, F.-R.,
1703 Franchi, I.A., and Hoppe, P. (2014) Abundances of presolar silicon carbide grains in primitive
1704 meteorites determined by nanoSIMS. Geochimica et Cosmochimica Acta, 139, 248-266.
1705 Davis, A.M. (2011) Stardust in meteorites. Proceedings of the National Academy of Sciences
1706 USA, 108, 19142-19146.
1707 Davis, A.M. (2014) Meteorites and Cosmochemical Processes: Treatise on Geochemistry,
1708 Volume 1. Oxford: Elsevier-Pergamon. Second Edition.
1709 Demyk, K., Dartois, E., Wiesemeyer, H., Jones, A.P., and d'Hendecourt, L. (2000) Structure and
1710 chemical composition of the silicate dust around OH/IR stars. Astronomy & Astrophysics,
1711 364, 170-178.
1712 DePew, K., Speck, A., and Dijkstra, C. (2006) Astromineralogy of the 13 micrometer feature in
1713 the spectra of oxygen-rich asymptotic giant branch stars. I. corundum and spinel. The
1714 Astrophysical Journal, 640, 971-981.
1715 Dermott, S.F. and Liou, J.C. (1994) Detection of asteroidal dust particles from known families in
1716 near-Earth orbits. In M. Zolensky, T. Wilson, F. Rietmeijer, and G. Flynn (eds.), Analysis of
1717 Interplanetary Dust. Ndew York: American Institute of Physics, pp.13-22.
1718 Ebel, D.S. (2006) Condensation of rocky materials in astrophysical environments. In D.S.
1719 Lauretta and H.Y. McSween Jr. (Editors), Meteorites and the Early Solar System II. Tucson:
1720 University of Arizona Press, pp.253-277.
1721 Ebel, D.S. and Grossman, L. (2000) Condensation in dust-rich systems. Geochimica et
1722 Cosmochimica Acta, 65, 469-477.
1723 Everitt, B. (2011) Cluster Analysis. Chichester, United Kingdom: Wiley.

Fahey, A.J., Goswami, J.N., McKeegan, K.D., and Zinner, E. (1987) ^{26}Al, ^{244}Pu , ^{50}Ti, REE and trace element abundances in hibonite grains from CM and CV meteorites. Geochimica et Cosmochimica Acta, 51, 329-350.

Feigelson, E.D., Broos, P., Gaffney, J.A. III, Garmire, G., Hillenbrand, L.A., Pravdo, S.H., Townsley, L., and Tsuboi, Y. (2002) X-ray emitting young stars in the Orion Nebula. The Astrophysical Journal, 574, 258-292.

Feltzing, S. and Gonzales, G. (2001) The nature of super-metal-rich stars. Detailed abundance analysis of 8 super metal-rich star candidates. Astronomy and Astrophysics, 367, 253-265.

Floss, C. and Stadermann, F. (2009) Auger Nanoprobe analysis of presolar ferromagnesian silicate grains from primitive CR chondrites QUE 99177 and MET 00426. Geochimica et Cosmochimica Acta, 73, 2415–2440.

Floss, C. and Stadermann, F.J. (2012) Presolar silicate and oxide abundances and compositions in the ungrouped carbonaceous chondrite Adelaide and the K chondrite Kakangari: The effects of secondary processing. Meteoritics & Planetary Science, 47, 992–1009.

Floss, C., Stadermann, F.J., and Bose, M. (2008) Circumstellar Fe oxide from the Acfer 094 carbonaceous chondrite. The Astrophysical Journal, 672, 1266–1271.

Forrest, W.J., Gillett, F.C., and Stein, W.A. (1975) Circumstellar grains and the intrinsic polarization of starlight. The Astrophysical Journal, 195, 423-440.

Fraundorf, P. and Wackenhut, M. (2002) The core structure of presolar graphite onions. The Astrophysical Journal Letters, 578, L153-L156.

Frebel, A., Johnson, J.L., and Bromm, V. (2009) The minimum stellar metallicity observable in the Galaxy. Monthly Notices of the Royal Astronomical Society, 392, L50-L54.

1746 Fujiya, W., Hoppe, P., Zinner, E., Pignatari, M., and Herwig, F. (2013) Evidence for radiogeneic
1747 sulfur-32 in type AB presolar silicon carbide grains? The Astrophysical Journal Letters, 776,
1748 L29 (6 pp).
1749 Gaines, R.V., Skinner, H.C.W., Foord, E.E., Mason, B., and Rosenzweig, A. (1997) Dana's New
1750 Mineralogy: The System of Mineralogy of James Dwight Dana and Edward Salisbury Dana,
1751 8th edition. New York: John Wiley and Sons.
1752 Ghirlanda, G., Salafia, O.S., Paragi, Z., Giroletti, M., and 32 others (2019) Compact radio
1753 emission indicates a structured jet was produced by a binary neutron star merger. Science,
1754 363, 968-971.
1755 Gillett, F.C., Low, F.J., and Stein, W.A. (1968) Stellar spectra from 2.8 to 14 microns. The
1756 Astrophysical Journal, 154, 677.
1757 Gobrecht, D., Cherchneff, I., Sarang, A., Piene, J.M.C., and Bromley, S.T. (2016) Dust
1758 formation in the oxygen-rich AGB star 1K Tauri. Astronomy & Astrophysics, 585, Article
1759 A6, 15 p.
1760 Grew, E.S., Dymek, R.F., De Hoog, J.C.M., Harley, S.L., Boak, J.M., Hazen, R.M., and Yates,
1761 M.G. (2015) Boron isotopes in tourmaline from the 3.7-3.8 Ga Isua Belt, Greenland: Sources
1762 for boron in Eoarchean continental crust and seawater. *Geochimica et Cosmochimica Acta*,
1763 **163**, 156-177.
1764 Groopman, E. and Nittler, L.R. (2018) Correlated XANES, TEM, and NanoSIMS of presolar
1765 graphite grains. Geochimica et Cosmochimica Acta, 221, 219-236.
1766 Groopman, E., Bernatowicz, T., and Zinner, E. (2012) C, N, and O isotopic heterogeneities in
1767 low-density supernova graphite grains from Orgueil. The Astrophysical Journal Letters, 754,
1768 L8 (6 pp).

1769 Grossman, L. (1972) Condensation in the primitive solar nebula. Geochimica et Cosmochimica
1770 Acta, 36, 597-619.
1771 Gyngard, F., Amari, S., Zinner, E., and Ott, U. (2009) Interstellar exposure age of large presolar
1772 SiC grains from the Murchison meteorite. The Astrophysical Journal, 694, 359-366.
1773 Gyngard, F., Zinner, E., Nittler, L.R., Morgand, A., Stadermann, F.J., and Hynes, K.M. (2010a)
1774 Automated nanoSIMS measurements of spinel stardust from the Murray meteorite. The
1775 Astrophysical Journal, 717, 107-120.
1776 Gyngard, F., Nittler, L.R., and Zinner, E. (2010b) Presolar SiC grains of Type C. Meteoritics &
1777 Planetary Sciences, 45, A72.
1778 Gyngard, F., Zinner, E., Nittler, L.R., Morgand, A., Stadermann, F.J., and Hynes, K.M. (2010c)
1779 Automated NanoSIMS measurements of spinel stardust from the Murray meteorite. The
1780 Astrophysical Journal, 717, 107–120.
1781 Gyngard, F., Nittler, L.R., Zinner, E., José, J., and Cristallo, S. (2011) New reaction rates and
1782 implications for nova nucleosynthesis and presolar grains. Lunar and Planetary Science, 42,
1783 #2675.
1784 Gyngard, F., Jadhav, M., Nittler, L.R., Stroud, R.M., and Zinner, E. (2018) Bonanza: An
1785 extremely large dust grain from a supernova. Geochimica et Cosmochimica Acta, 221, 60-86.
1786 Haenecour. P., Floss, C., Jose, J., Amari, S., Lodders, K., Jadhav, M., Wang, A., and Gyngard, F.
1787 (2016) Coordinated analysis of two graphite grains from the CO3.0 LAP031117 meteorite:
1788 First identification of a CO nova graphite and a presolar iron sulfide subgrain. The
1789 Astrophysical Journal, 825, 88 (9 pp).

Han, J., Brearley, A.J., and Keller, L.P. (2015) Microstructural evidence for a disequilibrium condensation origin for hibonite-spinel inclusions in the ALHA77307 CO3.0 chondrite. Meteoritics & Planetary Science, 50, 2121-2136.

Hazen, R.M. (1984) Mineralogy: A historical review. Journal of Geological Education, 32, 288-298.

Hazen, R.M. (2019) An evolutionary system of mineralogy: Proposal for a classification of planetary materials based on natural kind clustering. American Mineralogist, 104, 810-816.

Hazen, R.M., Papineau, D., Bleeker, W., Downs, R.T., Ferry, J.M., McCoy, T.L., Sverjensky, D.A., and Yang, H. (2008) Mineral evolution. American Mineralogist, 93, 1693-1720.

Hazen, R.M., Hystad, G., Downs, R.T., Golden, J.J., Pires, A.J., and Grew, E.S. (2015) Earth's "missing" minerals. American Mineralogist, 100, 2344-2347.

Heck, P.R., Amari, S., Hoppe, P., Baur, H., Lewis, R.S., and Wieler, R. (2009a) Ne isotopes in individual presolar graphite grains from the Murchison meteorite together with He, C, O, Mg-Al isotopic analyses as tracers of their origins. The Astrophysical Journal, 701, 1415-1425.

Heck, P.R., Gyngard, F., Ott, U., Meier, M.M.M., Ávila, J.N., Amari, S., Zinner, E.K., Lewis, R., Baur, H., and Wieler, R. (2009b) Interstellar residence times of presolar SiC dust grains from the Murchison carbonaceous chondrite. The Astrophysical Journal, 698, 1155-1173.

Heck, P.R., Stadermann, F.J., Isheim, D., Auciello, O., Daulton, T.L., Davis, A.M., Elam, J.W., Floss, C., Hiller, J., Larson, D.J., Lewis, J.B., Mane, A., Pellin, M.J., Savina, M.R., Seidman, D.N., and Stephan, T. (2014) Atom-probe analyses of nanodiamonds from Allende. Meteoritics & Planetary Science, 49, 453-467.

Herwig, F., Pignatari, M., Woodward, P.R., Porter, D.H., Rockefeller, G., Fryer, C.L., Bennett, M., and Hirschi, R. (2011) Convective-reactive proton-^{12}C combustion in Sakurai's object

(V4334 Sagittarii and implications for the evolution and yields from the first generations of stars. The Astrophysical Journal, 727, 89-111.

Hinton, R.W., Davis, A.M., Scatena-Wachel, D.E., Grossman, L., and Draus, R.J. (1988) A chemical and isotopic study of hibonite-rich refractory inclusions in primitive meteorites. Geochimica et Cosmochimica Acta, 52, 2573-2598.

Hodge, P.W. (1961) Sampling dust from the stratosphere. Smithsonian Contributions to Astrophysics, 5, 145-152.

Höfner, S. (2008) Winds of M-type AGB stars driven by micron-sized grains. Astronomy & Astrophysics, 491, L1-L4.

Hohenberg, C.M., Nichols, R.H. Jr., Olinger, C.T., and Goswami, J.N. (1990) Cosmogenic neon from individual grains of CM meteorites: Extremely long pre-compaction exposure histories or an enhanced early particle flux. Geochimica et Cosmochimica Acta, 54, 2133-2140.

Hong, Y. and Fegley, B. Jr. (1998) Experimental studies of magnetite formation in the solar system. Meteoritics & Planetary Science, 33, 1101-1112.

Hoppe, P., Amari, S., Zinner, E., Ireland, T., and Lewis, R.S. (1994) Carbon, nitrogen, magnesium, silicon, and titanium isotopic compositions of single interstellar silicon carbide grains from the Murchison meteorite. The Astrophysical Journal, 430, 870-890.

Hoppe, P., Amari, S., Zinner, E., and Lewis, R.S. (1995) Isotopic compositions of C, N, O, Mg, and Si, trace element abundances, and morphologies of single circumstellar graphite grains in four density fractions from the Murchison meteorite. Geochimica et Cosmochimica Acta, 59, 4029-4056.

1834 Hoppe, P., Strebel, R., Eberhardt, P., Amari, S., and Lewis, R.S. (1996) Small SiC grains and a
1835 nitride grain of circumstellar origin from the Murchison carbonaceous chondrite. Geochimica
1836 et Cosmochimica Acta, 60, 883-907.
1837 Hoppe, P., Annen, P., Strebel, R., Eberhardt, P., Gallino, R., Lugaro, M., Amari, S., and Lewis,
1838 R.S. (1997) Meteoritic silicon carbide grains with unusual Si-isotopic compositions: Evidence
1839 for an origin in low-mass, low-metallicity asymptotic giant branch stars. The Astrophysical
1840 Journal, 546, 248-266.
1841 Hoppe, P., Strebel, R., Eberhardt, P., Amari, S., and Lewis, R.S. (2000) Isotopic properties of
1842 silicon carbide X grains from the Murchison meteorite in the size range 0.5-1.5 microns.
1843 Meteoritics & Planetary Sciences, 35, 1157-1176.
1844 Hoppe, P., Leitner, J., Gröner, E., Marhas, K.K., Meyer, B.S., and Amari, S. (2010) NanoSIMS
1845 isotopic analysis of small presolar SiC grains: New insights into supernova nucleosynthesis,
1846 chemistry, and dust formation. The Astrophysical Journal, 719, 1370-1384.
1847 Huss, G.R., Fahey, A.J., Galilino, R., and Wasserburg, G.J. (1994) Oxygen isotopes in
1848 circumstellar Al_2O_3 grains from meteorites and stellar nucleosynthesis. The Astrophysical
1849 Journal Letters, 430, L81-L84
1850 Huss, G.R., Hutcheon, I.D., and Wasserburg, G.J. (1997) Isotopic systematics of presolar silicon
1851 carbide from the Orgueil (CI) carbonaceous chondrite: Implications for solar system
1852 formation and stellar nucleosynthesis. Geochimica et Cosmochimica Acta, 61, 5117–5148.
1853 Hutcheon, I.D., Huss, G.R., Fahey, A.J., and Wasserburg, G.J. (1994) Extreme ^{26}Mg and ^{17}O
1854 enrichments in an Orgueil corundum: Identification of a presolar oxide grain. The
1855 Astrophysical Journal Letters, 425, L97-L100.

1856 Hynes, K.M. (2010) Microanalytical Investigations of Presolar SiC Grains as Probes of
1857 Condensation Conditions in Astrophysical Environments. Ph.D. Thesis, Washington
1858 University, St. Louis, Missouri.
1859 Hynes, K.M., and Gyngard, F. (2009) The presolar grain database. Lunar and Planetary Science
1860 Conference, 42, #1595.
1861 Hynes, K.M., Croat, T.K., Amari, S., Mertz, A.F., and Bernatowicz, T.J. (2010) Structural and
1862 isotopic microanalysis of presolar SiC from supernovae. Meteoritics & Planetary Sciences,
1863 45, 596-614.
1864 Hynes, K.M., Amari, S., Bernatowicz, T.J., Lebsack, E., Gyngard, F., and Nittler, L.R. (2011)
1865 Combined TEM and NanoSIMS analysis of subgrains in a SiC AB grain. Lunar and Planetary
1866 Science, 42, #2332.
1867 Iliadis, C., Downen, L.N., Jose, J., Nittler, L.R., and Starrfield, S. (2018) On presolar stardust
1868 grains from CO classical novae. The Astrophysical Journal, 855, 76 (14 pp).
1869 Iocco, F., Mangano, G., Miele, G., Pisanti, O., and Serpico, P.D. (2008) Primordial
1870 nucleosynthesis: from precision cosmology to fundamental physics. Physics Reports, 472, 1-
1871 76.
1872 Ireland, T.R. (1988) Correlated morphological, chemical, and isotopic characteristics of
1873 hibonites from the Murchison carbonaceous chondrite. Geochimica et Cosmochimica Acta,
1874 52, 2827-2839.
1875 Ireland, T.R. (1990) Presolar isotopic and chemical signatures in hibonite-bearing refractory
1876 inclusions from the Murchison carbonaceous chondrite. Geochimica et Cosmochimica Acta,
1877 54, 3219-3237.

1878 Jadhav, M., Amari, S., Marhas, K.K., Zinner, E., Maruoka, T., and Gallino, R. (2008) New
1879 stellar sources for high-density, presolar graphite grains. The Astrophysical Journal, 682,
1880 1479–1485.
1881 Jadhav, M., Zinner, E., Amari, S., Maruoka, T., Marhas, K.K., and Gallino, R. (2013) Multi-
1882 element isotopic analyses of presolar graphite grains from Orgueil. Geochimica et
1883 Cosmochimica Acta, 113, 193–224.
1884 Jiang, B.W., Zhang, K., Li, A., and Lisse, C.M. (2013) Crystalline silicates in evolved stars. I.
1885 Spitzer/infrared spectrograph spectroscopy of IRAS 16456-3542, 18354-0638, and
1886 23239+5754. The Astrophysical Journal, 765, 72 (7 pp).
1887 Johnson, J.A. (2019) Populating the periodic table: nucleosynthesis of the elements. Science,
1888 363, 474-478.
1889 Jones, A.P. (2007) The mineralogy of cosmic dust: astromineralogy. European Journal of
1890 Mineralogy, 19, 771-782.
1891 Jones, A.P., Tielens, A.G.G.M., Hollenbach, D.J., and McKee, C.F. (1994) Grain destruction in
1892 shocks in the interstellar medium. The Astrophysical Journal, 433, 797-810.
1893 Jones, L.V. (2009) Stars and Galaxies. Santa Barbara, California: ABC-CLIO.
1894 Jones, O.C., Kemper, F. Sargent, B.A., McDonald, I., Gielen, C., Woods, P.M., Sloan, G.C.,
1895 Boyer, M.L., Zijlstra, A.A., Clayton, G.C., Kraemer, K.E., Srinivasan, S., and Ruffle, P.M.E.
1896 (2012) On the metallicity dependence of crystalline silicates in oxygen-rich asymptotic giant
1897 branch stars and red supergiants. Monthly Notices of the Royal Astronomical Society, 427,
1898 3209-3229.
1899 Jones, S., Côte, B., Röpke, F.K., and Wanajo, S. (2019a) A new model for electron-capture
1900 supernovae in galactic chemical evolution. The Astrophysical Journal, 882, 170-179.

Jones, S., Röpke, F.K., Freyer, C., Ruiter, A.J., Seitenzahl, I.R., Nittler, L.R., Ohlmann, S.T., Reifarth, R., Pignatari, M., and Belczynski, K. (2019b) Remnants and ejecta of thermonuclear electron-capture supernovae: Constraining oxygen-neon deflagrations in high-density white dwarfs. Astronomy & Astrophysics, 622, A74 (22 p.).

Jones, T.W. and Merrill, K.M. (1976) Model dust envelopes around late-type stars. The Astrophysical Journal, 209, 509-524.

José, J. and Hernandez, M. (2007) The origin of presolar nova grains. Meteoritics & Planetary Science, 42, 1135–1143.

Käppeler, F. (1999) The origin of the heavy elements: the *s* process. Progress in Particle and Nuclear Physics, 43, 419-483.

Karakas, A.I. and Lattanzio, J.C. (2014) The Dawes Review 2: Nucleosynthesis and the stellar yields of low and intermediate-mass single stars. Publications of the Astronomical Society of Australia, 31, e030.

Karttunen, H. and Oja, H. (2007) Fundamental Astronomy, 5th edition. New York: Springer.

Kasen, D., Metzger, B., Barnes, J., Quataert, E., and Ramirez-Ruiz, E. (2017) Origin of the heavy elements in binary neutron star mergers from a gravitational-wave event. Nature, 551, 80–84.

Kelly, J.F., Fisher, G.R., and Barnes, P. (2005) Correlation between layer thickness and periodicity of long polytypes in silicon carbide. Materials Research Bulletin, 40, 249-255.

Kemper, F., Vriend, W.J., and Tielens, A.G.G.M. (2004) The absence of crystalline silicates in the diffuse interstellar medium. The Astrophysical Journal, 609, 826-837.

Kemper, F., Markwick, A.J., and Woods, P.M. (2011) The crystalline fraction of interstellar silicates in starburst galaxies. Monthly Notices of the Royal Astronimcal Society, 413, 1192-1199.

Khokhlov, A. Müller, E., and Höflich, P. (1993) Light curves of Type 1a supernova models with different explosion mechanisms. Astronomy and Astrophysics, 270, 223-248.

Kööp, L., Heck, P.R., Busemann, H., Davis, A.M., Greer, J., Maden, C., Meier, M.M.M., and Wieler, R. (2018) High early solar activity inferred from helium and neon excesses in the oldest meteorite inclusions. Nature Astronomy, 2, 709-713.

Lauretta, D.S., Lodders, K., and Fegley, B. Jr. (1998) Kamacite sulfurization in the solar nebula. Meteoritics & Planetary Science, 33, 821-834.

Leitner, J., Vollmer, C., Hoppe, P., and Zipfel, J. (2012a) Characterization of presolar material in the CR chondrite Northwest Africa 852. The Astrophysical Journal, 745, 38–52.

Leitner, J., Kodolányi, J., Hoppe, P., and Floss, C. (2012b) Laboratory analysis of presolar silicate stardust from a nova. The Astrophysical Journal Letters, 754, L41.

Leitner, J., Hoppe, P., Floss, C., Hillion, F., and Henkel, T. (2018) Correlated nanoscale characterization of a unique complex oxygen-rich stardust grain: Implications for circumstellar dust formation. Geochimica et Cosmochimica Acta, 221, 255-274.

Lewis, R.S., Ming, T., Wacker, J.F., Anders, E., and Steel, E. (1987) Interstellar diamonds in meteorites. Nature, 339, 117-121.

Lewis, R.S., Amari, S., and Anders, E. (1990) Meteoritic silicon carbide: Pristine material from carbon stars. Nature, 348, 293-298.

Lewis, R.S., Amari, S., and Anders, E. (1994) Interstellar grains in metorites: II. SiC and its noble gases. Geochimica et Cosmochimica Acta, 58, 471-494.

1945 Lewis, J.B., Floss, C., and Gyngard, F. (2018) Origin of nanodiamonds from Allende constrained
1946 by statistical analysis of C isotopes from small clusters of acid residue by NanoSIMS.
1947 Geochimica et Cosmochimica Acta, 221, 237-254.

1948 Limongi, M. and Chieffi, A. (2012) Evolution, explosion, and nucleosynthesis of core-collapse
1949 supernovae. The Astrophysical Journal Supplement Series, 199, 38-46.

1950 Lin, Y., Gyngard, F., Zinner, E. (2010) Isotopic analysis of supernova SiC and Si_3N_4 grains
1951 from the Qingzhen (EH3) chondrite. The Astrophysical Journal, 709, 1157-1173.

1952 Little-Marenin, I.R. and Little, S.J. (1990) Emission features in IRAS low-resolution spectra of
1953 MS,S and SC stars. The Astrophysical Journal, 333, 305-315.

1954 Liu, N., Nittler, L.R., Alexander, C.M.O'D., Wang, J., Pignatari, M., José, J., and Nguyen, A.N.
1955 (2016) Stellar origins of extremely ^{13}C- and ^{15}N-enriched presolar SiC grains: Novae or
1956 supernovae? The Astrophysical Journal, 820, 140 (14 pp).

1957 Liu, N., Stephan, T., Boehnke, P., Nittler, L.R., Alexander, C.M.O'D., Wang, J., Davis, A.M.,
1958 Trappitsch, R., and Pellin, M.J. (2017a) J-type carbon stars: A dominant source of ^{14}N-rich
1959 presolar SiC grains of type AB. The Astrophysical Journal Letters, 844, L12.

1960 Liu, N., Steele, A., Nittler, L.R., Stroud, R.M, De Gregorio, B.T., Alexander, C.M.O'D., and
1961 Wang, J. (2017b) Coordinated EDX and micro-Raman analysis of presolar silicon carbide: A
1962 novel, nondestructive method to identify rare subgroup SiC. Meteoritics & Planetary Science,
1963 52, 1-20.

1964 Liu, N., Nittler, L.R., Pignatari, M., Alexander, C.M.O'D., and Wang, J. (2017c) Stellar origin of
1965 ^{15}N-rich presolar SiC grains of Type AB: Supernovae with explosive hydrogen burning.
1966 Astrophysical Journal Letters, 842, L1.

1967 Liu, N., Nittler, L.R., Alexander, C.M.O'D., and Wang, J. (2018) Late formation of silicon
1968 carbide in type II supernovae. Science Advances, 4, eaao1054.
1969 Lodders, K. (2003) Solar system abundance and condensation temperatures of the elements. The
1970 Astrophysical Journal, 591, 1220-1247.
1971 Lodders, K., and Amari, S. (2005) Presolar grains from meteorites: Remnants from the early
1972 times of the solar system. Chemie der Erde, 65, 93-166.
1973 Lugaro, M. (2005) Stardust from Meteorites: An Introduction to Presolar Grains. New York:
1974 World Scientific.
1975 Lugaro, M., Zinner, E., Gallino, R., ands Amari, S. (1999) Isotopic ratios in mainstream presolar
1976 SiC grains revisited. The Astrophysical Journal, 527, 369-394.
1977 Lugaro, M., Karakas, A.I., Bruno, C.G., Aliotta, M., Nittler, L.R., and 32 others (2017) Origin of
1978 meteoritic stardust unveiled by a revised proton-capture rate of ^{17}O. Nature Astronomy, 1,
1979 0027.
1980 Matteucci, F. (2003) The Chemical Evolution of the Galaxy. Dordrecht, Germany: Kluwer
1981 Academic.
1982 Mazzali, P.A., Röpke, F.K., Benetti, S., and Hillebrandt, W. (2007) A common explosion
1983 mechanism for type 1a supernovae. Science, 315, 825-828.
1984 McAdam, M.M., Sunshine, J.M., Howard, K.T., Alexander, C.M.O'D., McCoy, T.J., and Bus,
1985 S.J. (2018) Spectral evidence for amorphous silicates in least-processed CO meteorites and
1986 their parent bodies. Icarus, 306, 32-49.
1987 Ma, C., Krot, A.N., and Bizzarro, M. (2013) Discovery of dmisteinbergite (hexagonal
1988 $CaAl_2Si_2O_8$) in the Allende meteorite: A new member of refractory silicates formed in the
1989 solar nebula. American Mineralogist, 98, 1368-1371.

Ma, C., Krot, A.N., and Nagashima, K. (2017) Addibischoffite, $CaAl_6Al_6O_{20}$, a new calcium aluminate mineral from the Acfer 214 CH carbonaceous chondrite: A new refractory phase from the solar nebula. American Mineralogist, 102, 1556-1560.

McKeegan, K.D., Aleon, J., Bradley, J., Brownlee, D., Busemann, H., Butterworth, A., Chaussidon, M., Fallon, S., and 39 others (2006) Isotopic compositions of cometary matter returned by Stardust. Science, 314, 1724-1728.

Meier, M.M.M., Heck, P.R., Amari, S., Baur, H., and Wieler, R. (2012) Graphite grains in supernova ejecta – Insights from a noble gas study of 91 individual KFC1 presolar graphite grains from the Murchison meteorite. Geochimica et Cosmochimica Acta, 76, 147–160.

Messenger, S. (2002) Opportunities for the stratospheric collection of dust from short-period comets. Meteoritics & Planetary Science, 37, 1491-1505.

Messenger, S., Keller, L.P., Stadermann, F.J., Walker, R.M., and Zinner, E. (2003) Samples of stars beyond the solar system: Silicate grains in interplanetary dust. Science, 300, 105-108.

Messenger, S., Keller, L.P., and Lauretta, D.S. (2005) Supernova olivine from cometary dust. Science, 309, 737–741.

Meyer, B.S., Clayton, D.D., and The, L.-S. (2000) Molybdenum and zirconium isotopes from a supernova neutron burst. The Astrophysical Journal, 540, L49–L52.

Millikan, R.G. (1999) Historical kinds and the special sciences. Philosophical Studies, 95, 45-65.

Mills, S.J., Hatert, F., Nickel, E.H., and Ferrais, G. (2009) The standardization of mineral group hierarchies: Application to recent nomenclature proposals. European Journal of Mineralogy, 21, 1073-1080.

Morgan, D.H., Cannon, R.D., Hatzidimitriou, D., and Croke, B.F.W. (2003) J-type carbon stars in the Large Magellanic Cloud. Monthly Notices of the Royal Astronomical Society, 341, 534-550.

Morrison S.M., Liu C., Eleish A., Prabhu A., Li C., Ralph J., Downs, R.T., Golden, J.J., Fox P., and Hazen, R.M. (2017) Network Analysis of Mineralogical Systems. American Mineralogist, 102, 1588-1596.

Mostefouai, S. and Hoppe, P. (2004) Discovery of abundant in situ silicate and spinel grains from red giant stars in a primitive meteorite. The Astrophysical Journal, 613, L149-L152.

Nagashima, K., Krot, A.N., and Yurimoto, H. (2004) Stardust silicates from primitive meteorites, Nature, 428, 921-924.

Neugebauer, G., Habing, H.J., van Duinen, R., Aumann, H.H., et al. (1984) The Infrared Astronomical Satellite (IRAS) mission. The Astrophysical Journal, Part 2, 278, L1-L6.

Nguyen, A.N. and Messenger, S. (2014) Resolving the stellar sources of isotopically rare presolar silicate grains through Mg and Fe isotopic analysis. The Astrophysical Journal, 784, 149 (15 pp).

Nguyen, A.N. and Zinner, E. (2004) Discovery of ancient silicate stardust in a meteorite. Science, 303, 1496-1499.

Nguyen, A.N., Stadermann, F.J., Zinner, E., Srtroud, R.M., Alexander, C.M.O.'D., and Nittler, L.R. (2007) Characterization of presolar silicate and oxide grains in primitive carbonaceous chondrites. The Astrophysical Journal, 656, 1223-1240.

Nguyen, A.N., Nittler, L.R., Stadermann, F.J., Stroud, R.M., and Alexander, C.M.O'D. (2010) Coordinated analyses of presolar grains in the Allan Hills 77307 and Queen Elizabeth Range 99177 meteorites. The Astrophysical Journal, 719, 166–189.

2034 Nguyen, A.N., Keller, L.P., and Messenger, S. (2016) Mineralogy of presolar silicate and oxide
2035 grains of diverse stellar origins. The Astrophysical Journal, 818, 51 (17 pp).
2036 Nguyen, A.N., Nittler, L.R., Alexander, C.M.O'D., and Hoppe, P. (2018) Titanium isotopic
2037 compositions of rare presolar SiC grain types from the Murchison meteorite. Geochimica
2038 et Cosmochimica Acta, 221, 162-181.
2039 Nittler, L.R. and Alexander, C.O.M'D. (2003) Automated isotopic measurements of micron-
2040 sized dust: Application to meteoritic presolar silicon carbide. Geochimica et Cosmochimica
2041 Acta, 67, 4961–4980.
2042 Nittler, L.R., and Ciesla, F. (2016) Astrophysics with extraterrestrial materials. Annual Reviews
2043 of Astronomy and Astrophysics, 54, 53-93.
2044 Nittler, L.R. and Dauphas, N. (2006) Meteorites and the chemical evolution of the Milky Way.
2045 In D.S. Lauretta and H.Y. McSween Jr. [Editors], Meteorites and the Early Solar System II,
2046 Tucson: University of Arizona Press, pp.127-146.
2047 Nittler, L.R., Alexander, C.O.M'D., Gao, X., Walker, R.M., and Zinner, E. (1994) Interstellar
2048 oxide grains from the Tieschitz ordinary chondrite. Nature, 370, 443-446.
2049 Nittler, L.R., Hoppe, P., Alexander, C.O.M'D., Amari, S., Eberhardt, P., Gao, X., Lewis, R.S.,
2050 Strebel, R., Walker, R.M., and Zinner, E. (1995) Silicon nitride from supernovae. The
2051 Astrophysical Journal, 453, L25-L28.
2052 Nittler, L.R., Amari, S., Zinner, E., Woosley, S.E., and Lewis, R.S. (1996) Extinct ^{44}Ti in
2053 presolar graphite and SiC: Proof of a supernova origin. The Astrophysical Journal Letters,
2054 462, L31-L34.

2055 Nittler, L.R., Alexander, C.O.M'D., Gao, X., Walker, R.M., and Zinner, E. (1997) Stellar
2056 sapphires: The properties and origins of presolar Al_2O_3 in meteorites. The Astrophysical
2057 Journal, 483, 475-495.
2058 Nittler, L.R., Alexander, C.M.O'D., Stadermann, F.J., and Zinner, E.K. (2005) Presolar chromite
2059 in Orgueil. Meteoritics & Planetary Science, 40, A114.
2060 Nittler, L.R., Alexander, C.O.M'D., Gallino, R., Hoppe, P., Nguyen, A.N., Stadermann, F.J., and
2061 Zinner, E.K. (2008) Aluminum-, calcium-, and titanium-rich oxide stardust in ordinary
2062 chondrite meteorites. The Astrophysical Journal, 682, 1450-1478.
2063 Nittler, L.R., Gyngard, F., Zinner, E., and Stroud, R.M. (2011) Mg and Ca isotopic anomalies in
2064 presolar oxides: Large anomalies in a group 3 hibonite grain. Lunar and Planetary Science,
2065 42, #1872.
2066 Nittler, L.R., Alexander, C.M.O'D., Liu, N., and Wang, J. (2018a) Extremely ^{54}Cr- and ^{50}Ti-
2067 rich presolar oxide grains in a primitive meteorite: Formation in rare types of supernovae and
2068 implications for the astrophysical context of Solar System birth. The Astrophysical Journal
2069 Letters, 856, L24 (7 pp).
2070 Nittler, L.R., Alexander, C.M.O'D., Davidson, J., Riebe, M.E.I., Stroud, R.M., and Wang, J.
2071 (2018b) High abundances of presolar grains and 15N-rich organic matter in CO3.0 chondrite
2072 Dominion Range 08006. Geochimica et Cosmochimica Acta, 226, 107-131.
2073 Nollett, K.M., Busso, M., and Wasserburg, G.J. (2003) Cool bottom processing on the thermally
2074 pulsing asymptotic giant branch and the isotopic composition of circumstellar dust grains. The
2075 Astrophysical Journal, 582, 1036-1058.
2076 Nuth, J.A. III, and Allen, J.E. Jr. (1992) Supernovae as sources of interstellar diamonds.
2077 Astrophysics and Space Science, 196, 117-123.

Onaka, T., de Jong, T., and Willems, F.J. (1989) A study of M Mira variables based on IRAS LRS observations. I – dust formation in the circumstellar shell. Astronomy & Astrophysics, 18, 169-179.

Ozima, M. and Mochizuki, K. (1993) Origin of nanodiamonds in primitive chondrites: (1) Theory. Meteoritics, 28, 416-417.

Pagel, B.E.J. (1997) Nucleosynthesis and Chemical Evolution of Galaxies. Cambridge, UK: Cambridge University Press.

Peeples, M.S. and Somerville, R.S. (2013) An empirical prediction for stellar metallicity distributions in nearby galaxies. Monthly Notices of the Royal Astronomical Society, 428, 1766-1773.

Prialnik, D. (2001) Novae. In P. Murdin [Editor], Encyclopedia of Astronomy and Astrophysics. Washington, DC: Institute of Physics Publishing, pp. 1846-1856.

Rauscher, T., Heger, A., Hoffman, R.D., and Woosley, S.E. (2002) Nucleosynthesis in massive stars with improved nuclear and stellar physics. The Astrophysical Journal, 576, 323–348.

Rieke, G.H. (2009) History of infrared telescopes and astronomy. Experimental Astronomy, 25, 125-141.

Richter, S., Ort, U., and Begemann, F. (1998) Tellurium in pre-solar diamonds as an indicator of rapid separation of supernova ejecta. Nature, 391, 261-263.

Robertson, B.E., Ellis, R.S., Furlanetto, S.R., and Dunlop, J.S. (2015) Cosmic reionization and early star-forming galaxies: A joint analysis of new constraints from Planck and the Hubble Space Telescope. The Astrophysical Journal, 802, L19-L23.

Rolfs, C.E. and Rodney, W.S. (2005) Cauldrons in the Cosmos: Nuclear Astrophysics. Chicago: University of Chicago Press.

2101 Rubin, A.E. and Ma, C. (2017) Meteoritic minerals and their origins. Chemie der Erde, 77, 325-
2102 385.
2103 Russell, S.S., Arden, J.W., and Pillinger, C.T. (1991) Evidence for multiple sources of diamond
2104 from primitive chondrites. Science, 254, 1188-1191.
2105 Russell, S.S., Arden, J.W., and Pillinger, C.T. (1996) A carbon and nitrogen isotope study of
2106 diamond from primitive chondrites. Meteoritics & Planetary Science, 31, 343-355.
2107 Salpeter, E.E. (1977) Formation and destruction of dust grains. Annual Review of Astronomy
2108 and Astrophysics, 15, 267-293.
2109 Santana, C. (2019) Mineral misbehavior: why mineralogists don't deal in natural kinds. Frontiers
2110 of Chemistry, https//doi.org/10.1007/s10698-019-09338-3.
2111 Sarangi, A. and Cherchneff, I. (2015) Condensation of dust in the ejecta of Type II supernovae.
2112 Astronomy & Astrophysics, 575, A95 (20 pp).
2113 Schatz, H. (2013) The evolution of elements and isotopes. Elements, 6, 13-17.
2114 Schertl, H.-P., Mills, S.J., and Maresch, W.V. (2018) A Compendium of IMA-Approved Mineral
2115 Nomenclature. Melbourne, Australia: International Mineralogical Association.
2116 Schröder, K.-P. and Connon Smith, R. (2008) Distant future of the Sun and Earth revisited.
2117 Monthly Notices of the Royal Astronomical Society, 386, 155-163.
2118 Sloan, G.C. and Price, S.D. (1998) The infrared spectral classification of oxygen-rich dust shells.
2119 The Astrophysical Journal Supplement Series, 119, 141-158.
2120 Sloan, G.C., Kraemer, K.E., McDonald, I., Groenewegen, M.A.T., Wood, P.R., Zijlstra, A.A.,
2121 Lagadec, E., Boyer, M.L., Kemper, F., Matsuura, M., Sahai, R., Sargent, B.A., Srinivasan, S.,
2122 van Loon, J.T., and Volk, K. (2016) The infrared spectral properties of Magellanic carbon
2123 stars. The Astrophysical Journal, 826, 44 (19 pp).

2124 Sneden, C., Cowan, J.J., and Gallino, R. (2008) Neutron-capture elements in the early galaxy.
2125 Annual Review of Astronomy and Astrophysics, 46, 241-288.
2126 Soker, N. and Harpaz, A. (1999) Stellar structure and mass loss on the upper asymptotic giant
2127 branch. Monthly Notices of the Royal Astronomical Society, 310, 1158-1164.
2128 Sossi, P.A., Moynier, F., Chaussidon, M., Villeneuve, J., Kato, C., and Gounelle (2017) Early
2129 solar system irradiation quantified by linked vanadium and beryllium isotope variations in
2130 meteorites. Nature Astronomy, 1, article 55.
2131 Speck, A.K., Barlow, M.J., Sylvester, R.J., and Hofmeister, A.M. (2000) Dust features in the 10-
2132 micrometer infrared spectra of oxygen-rich evolved stars. Astronomy & Astrophysics, 146,
2133 437-464.
2134 Stadermann, F.J., Croat, T.K., Bernatowiicz, T.J., Amario, S., Messenger, S., Walker, R.M., and
2135 Zinner, E. (2005) Supernova graphite in the NanoSIMS: Carbon, oxygen and titanium
2136 isotopic compositions of a spherule and its TiC sub-components. Geochimica et
2137 Cosmochimica Acta, 69, 177-188.
2138 Stadermann, F.J., Hoppe, P., Floss, C., Heck, P.R., Hörz, F., Huth, J., Kearsley, A.T., Leitner, J.,
2139 Marhas, K.K., McKeegan, K.D., and Stephan, T. (2008) Stardust in Stardust—The C, N, and
2140 O isotopic compositions of Wild 2 cometary matter in Al foil impacts. Meteoritics &
2141 Planetary Science, 43, 299-313.
2142 Stein, W.A., Gaustad, J.E., Gillett, F.C., and Knacke, R.F. (1969) The spectrum of Cygnus from
2143 7.5 to 14 microns. The Astrophysical Journal, 155, L177-L179.
2144 Stroud, R. M. and Bernatowicz, T. J. (2005) Surface and internal structure of pristine presolar
2145 silicon carbide. Lunar and Planetary Science Conference, 36, #2010.

2146 Stroud, R.M., Nittler, L.R., and Hoppe, P. (2004a) Microstructures and isotopic compositions of
2147 two SiC X grains. Meteoritics & Planetary Science, 39, A101.

2148 Stroud, R.M., Nittler, L.R., and Alexander, C.M.O'D. (2004b) Polymorphism in presolar Al_2O_3:
2149 Grains from asymptotic giant branch stars. Science, 305, 1455-1457.

2150 Stroud, R.M., Chisholm, M.F., Heck, P.R., Alexander, C.M.O'D., and Nittler, L.R. (2011)
2151 Supernova shock-wave-induced co-formation of glassy carbon and nanodiamond. The
2152 Astrophysical Journal, 738, L27 (5 pp).

2153 Takigawa, A., Tachibana, S., Huss, G.R., Nagashima, K., Makide, K., Krot, A.N., and Nagahara,
2154 H. (2014) Morphology and crystal structures of solar and presolar Al_2O_3 in unequilibrated
2155 ordinary chindrites. Geochimica et Cosmochimica Acta, 124, 309-327.

2156 Takigawa, A., Tachibana, S., Nagahara, H., and Ozawa, K. (2015) Evaporation and condensation
2157 kinetics of corundum: The origin of the 13-micrometer feature of oxygen-rich AGB stars. The
2158 Astrophysical Journal Supplement Series, 218, (16 pp). doi: 10.1088/0067-0049/218/1/2

2159 Takigawa, A., Stroud, R.M., Nittler, L.R., Alexander, C.M.O'D. (2018) High-temperature dust
2160 condensation around an AGB star: evidence from a highly pristine presolar corundum. The
2161 Astrophysical Journal Letters, 862, L13. doi: 10.3847/2041-8213/aadlf5

2162 Taylor, B.J. (1996) Supermetallicity at the quarter-century mark: A conservative statistician's
2163 review of the evidence. The Astrophysical Journal Supplement, 102, 105.

2164 Timmes, F.X., Woosley, S.E., and Weaver, T.A. (1995) Galactic chemical evolution: Hydrogen
2165 through zinc. The Astrophysical Journal Supplement Series, 98, 617–658.

2166 Timmes, F.X., Woosley, S.E., Hartmann, D.H., and Hoffman, R.D. (1996) The production of
2167 ^{44}Ti and ^{60}Co in supernovae. The Astrophysical Journal, 464, 332–341.

2168 Tominga, N., Umeda, H., and Nomoto, K. (2007) Supernova nucleosynthesis in population III
2169 13-50 Msolar stars and abundance patterns of extremely metal-poor stars. Astrophysical
2170 Journal, 660, 516-540.
2171 Travaglio, C., Gallino, R., Amari, S., Zinner, E., Woosley, S., and Lewis, R.S. (1999) Low-
2172 density graphite grains and mixing in type II supernovae. The Astrophysical Journal, 510,
2173 325–354.
2174 Treffers, R. and Cohen, M. (1974) High-resolution spectra of cool stars in the 10- and 20-micron
2175 regions. The Astrophysical Journal, 188, 545-552.
2176 Truran, J.W. and Heger, A. (2003) Origin of the elements. In H.D. Holland and K.K. Turekian
2177 [Editors]. Treatise on Geochemistry, 1st edition, 1, 1-15. New York: Elsevier.
2178 Verchovsky, A.B., Fisenko, A.V., Semjonov a, L.F., Bridges, J., Lee, M.R., and Wright, I.P.
2179 (2006) Nanodiamonds from AGB stars: A new type of presolar grain in meteorites. The
2180 Astrophysical Journal, 651, 481-490.
2181 Vollmer, C., Hoppe, P., Brenker, F.E., and Hozapfel, C. (2007) Stellar $MgSiO_3$ perovskite: A
2182 shock-transformed stardust silicate found in a meteorite. The Astrophysical Journal, 666, L49-
2183 L52.
2184 Vollmer, C., Hoppe, P., Stadermann, F.J., Floss, C., and Brenker, F.E. (2009) NanoSIMS
2185 analysis and Auger electron spectroscopy of silicate and oxide stardust from the carbonaceous
2186 chondrite Acfer 094. Geochimica et Cosmochimica Acta, 73, 7127–7149.
2187 Vollmer, C., Hoppe, P. and Brenker, F.E. (2013) Transmission electron microscopy of Al-rich
2188 silicate stardust from asymptotic giant branch stars. The Astrophysical Journal, 769, 61 (8 pp).
2189 Waters, L.B.F.M., Molster, F.J., de Jong, T., Beintema, D.A., Waelkens, C., and 32 others (1996)
2190 Mineralogy of oxygen-rich dust shells. Astronomy & Astrophysics, 315, L361-L364.

Wood, J.A. and Hashimoto, A. (1993) Mineral equilibrium in fractionated nebular systems. Geochimica et Cosmochimica Acta, 57, 2377-2388.

Woolf, N.J. and Ney, E.P. (1969) Circumstellar infrared emission from cool stars. The Astrophysical Journal, 155, L181.

Wopenka, B., Jadhav, M., and Zinner, E. (2011a) Raman analysis of high-density presolar graphite grains from the Orgueil carbonaceous chondrite. Lunar and Planetary Science Conference, 42, #1162.

Wopenka, B., Groopman, E., and Zinner, E. (2011b) Orgueil low-density presolar carbon ain't graphite but glassy carbon. Meteoritics & Planetary Science, 46, A252.

Yada, T., Floss, C, Stademann, F.J., Zinner, E., Nakamura, T., Noguchi, T., and Lea, A.S. (2008) Stardust in Antarctic micrometeorites. Meteoritics & Planetary Science, 43, 1287-1298.

Yoneda, S. and Grossman, L. (1995) Condensation of CaO-MgO-Al_2O_3-SiO_2 liquids from cosmic gases. Geochimica et Cosmochimica Acta, 59, 3413-3444.

Zega, T.J., Alexander, C.M.O'D., Nittler, L.R., and Stroud, R.M. (2011) A transmission electron microscopy study of presolar hibonite. The Astrophysical Journal, 730, 83-93.

Zega, T.J., Nittler, L.R., Gyngard, F., Alexander, C.O.M'D., Stroud, R.M., and Zinner, E.K. (2014a) A transmission electron microscopy study of presolar spinel. Geochimica et Cosmochimica Acta, 124, 152-169.

Zega, T.J., Haenecour, P., Floss, C., and Stroud, R.M. (2014b) Extraction and analysis of presolar grains from the LAP 031117 CO3.0 chondrite. Lunar and Planetary Science Conference, 45, #2256.

Zega, T.J., Haenecour, P., Floss, C., and Stroud, R.M. (2015) Circumstellar magnetite from the LAP 031117 C03.0 chondrite. The Astrophysical Journal, 808, 55.

2214 Zinner, E.K. (2014) Presolar grains. In Treatise on Geochemistry, Vol. 1: Meteorites, Comets,
2215 and Planets, Second Edition. A.M. Davis, H.D.Holland, and K.K.Turekian [Editors], pp.17-
2216 39. Oxford: Elsevier-Pergamon.

2217 Zinner, E.K., Fahey, A.J., Goswami, J.N., Ireland, T.R., and McKeegan, K.D. (1986) Large ^{48}Ca
2218 anomalies associated with ^{50}Ti anomalies in Murchison and Murray hibonites. The
2219 Astrophysical Journal Letters, 311, L103-L107.

2220 Zinner, E.K., Ming, T., and Anders, E. (1987) Large isotopic anomalies of Si, C, N, and noble
2221 gases in interstellar silicon carbide from the Murray meteorite. Nature, 330, 730-732.

2222 Zinner, E.K., Amari, S., Wopenka, B., and Lewis, R.S. (1995) Interstellar graphite in meteorites:
2223 Isotopic compositions and structural properties of single graphite grains from Murchison.
2224 Meteoritics, 30, 209–226.

2225 Zinner, E.K., Nittler, L.R., Gallino, R., Karakas, A.I., Lugaro, M., Straniero, O., and Lattanzio,
2226 J.C. (2006) Silicon and carbon isotopic ratios in AGB stars: SiC grain data, models, and the
2227 Galactic evolution of the Si isotopes. The Astrophysical Journal, 650, 350-373.

2228 Zinner, E.K., Amari, S., Guinness, R., Jennings, C., Mertz, A.F., Nguyen, A.N., Gallino, R.,
2229 Hoppe, P., Lugaro, M., Nittler, L.R., and Lewis, R.S. (2007) NanoSIMS isotopic analysis of
2230 small presolar grains: Search for Si_3N_4 grains from AGB stars and Al and Ti isotopic
2231 compositions of rare presolar SiC grains. Geochimica et Cosmochimica Acta, 71, 4786-4813.

2232 Zinner, E.K., Moyniuer, F., and Stroud, R.M. (2011) Laboratory technology and
2233 cosmochemistry. Proceedings of the National Academy of Sciences USA, 108, 19135-19141.

2234
2235

This is a preprint, the final version is subject to change, of the American Mineralogist (MSA)
Cite as Authors (Year) Title. American Mineralogist, in press.
DOI: https://doi.org/10.2138/am-2020-7173

Table 1. Diagnostic properties of stardust minerals and other condensed phases. Unconfirmed phases appear in [brackets].

Group	Species (Formula)	Natural Kind	Characteristics	References
NATIVE ELEMENTS				
	Diamond (C)	AGB diamond	high $^{12}C/^{13}C$; low $^{14}N/^{15}N$; possibly high ^{22}Ne	1,2
		SN-II diamond	low $^{12}C/^{13}C$; possibly high Xe	2,3
	Graphite (C)	AGB graphite	high $^{12}C/^{13}C$; high Zr, Mo, Ti	4-8
		SN-II graphite	low $^{14}N/^{15}N$; high $^{18}O/^{16}O$; ^{26}Mg, ^{44}Ca, and ^{49}Ti	7,9,10
		CNova graphite	very low $^{12}C/^{13}C$; high $^{30}Si/^{28}Si$; high ^{22}Ne	8,11,12
	Amorphous Carbon (C)	Stellar amorphous C	amorphous to electron diffraction; anomalous $^{12}C/^{13}C$	13,14
	Iron (Fe)	SN-II iron	nano-scale inclusions in SN-II graphite	4,5,10,15-17
	Taenite (Fe,Ni)	SN-II taenite	nano-scale inclusions in SN-II graphite	4,5,10,15-17
	Ruthenium (Ru)	SN-II ruthenium	nano-scale inclusion in SN-II graphite	5,15
	Osmium (Os)	SN-II osmium	nano-scale inclusion in SN-II graphite	5,15
	Other Native Elements (?)	[Nickel, Ni]	nano-scale inclusion in graphite, alloyed with Fe	18,19
CARBIDES				
	Moissanite (SiC)	AGB moissanite	typically low $^{12}C/^{13}C$; often with elevated Zr, Mo, Ti	19-29
		SN-II moissanite	low $^{14}N/^{15}N$; high $^{29}Si/^{28}Si$ & $^{30}Si/^{28}Si$; elevated ^{26}Mg; ^{44}Ca	30-33
		CNova moissanite	low $^{12}C/^{13}C$; high $^{30}Si/^{28}Si$; high ^{22}Ne	11,31,34
	Khamrabaevite (TiC)	AGB khamrabaevite	enriched in *s*-process elements V, Zr, Mo, and Ru	6,35
		SN-II khamrabaevite	grains embedded in graphite; enriched in V, but not Zr, Mo, Ru	17,36
	Mo-Zr Carbide [(Mo,Zr)C]	AGB Mo-Zr carbide	nano-inclusions in AGB graphite; usually with Ti	4,37
	Cohenite (Fe_3C)	SN-II cohenite	nano-inclusions in SN-II graphite	38
	Iron Carbide [$(Fe,Cr)_7C_3$]	SN-II iron carbide	nano-inclusions in SN-II graphite	5

Other Carbides (?)	[Ti-Al carbide]	subgrains in SN-II graphite	37	
SILICIDES				
$(Fe,Ni)_2Si$	~[$(Fe,Ni)_2Si$]	nano-inclusions in SiC; unknown structure and composition	19	
$(Fe,Ni)_3Si$	~[$(Fe,Ni)_3Si$]	nano-inclusions in SiC; unknown structure and composition	19	
PHOSPHIDES				
Schreibersite (Fe_3P)	[schreibersite]	Unconfirmed, but predicted to be a stellar condensate	39	
NITRIDES				
Nierite (Si_3N_4)	SN-II nierite	low $^{14}N/^{15}N$; and low $^{30}Si/^{28}Si$	33,40,41	
Other Nitrides (?)	[Ti(N,C)]	local concentrations in SiC	16,42	
	[(Mg,Al)N]	local concentrations in SiC	16,42	
	[Al nitride]	local concentrations in SiC	19,43	
SULFIDES				
Oldhamite (CaS)	AGB oldhamite	nano-scale inclusions in moissanite	39,44	
Troilite (?) (FeS)	SN-II (?) troilite	nano-scale inclusions in graphite, negative delta^{33}S and ^{34}S	12	
Other Sulfides (?)	[Niningerite, MgS]	Unconfirmed, but predicted to be a stellar condensate	39	
OXIDES				
Corundum (Al_2O_3)	AGB corundum	typically with high $^{17}O/^{16}O$; low $^{18}O/^{16}O$	45-50	
	SN-II corundum	low $^{17}O/^{16}O$; high$^{18}O/^{16}O$; ^{26}Mg, ^{44}Ca	47,50	
	CNova corundum	very high $^{17}O/^{16}O$, low $^{18}O/^{16}O$	50	

This is a preprint, the final version is subject to change, of the American Mineralogist (MSA)
Cite as Authors (Year) Title. American Mineralogist, in press.
DOI: https://doi.org/10.2138/am-2020-7173

Amorphous Al_2O_3	AGB amorphous Al_2O_3	amorphous in TEM; high $^{17}O/^{16}O$; low $^{18}O/^{16}O$; ^{26}Mg	49,51
Eskolaite (Cr_2O_3)	SN-II eskolaite	occurs as subgrains in SN-II graphite	18
Rutile (TiO_2)	AGB TiO_2	high $^{17}O/^{16}O$ [structure not yet confirmed]	50,52,53
	SN-II rutile	high $^{18}O/^{16}O$; occurs as subgrains in SN-II graphite	37,42
Magnetite (Fe_3O_4)	AGB magnetite	elevated $^{17}O/^{16}O$; occurs as subgrains in graphite	18,54
Spinel ($MgAl_2O_4$)	AGB spinel	high $^{17}O/^{16}O$; low $^{18}O/^{16}O$	47,55,56
	SN-II spinel	high $^{18}O/^{16}O$, low ^{25}Mg, and high ^{26}Mg	50,56
	CNova spinel	extreme enrichments in ^{17}O, ^{25}Mg, and ^{26}Mg	56
Chromite ($Fe^{2+}Cr_2O_4$)	AGB chromite	high $^{17}O/^{16}O$; low $^{18}O/^{16}O$	55,57
Hibonite [$(Ca,Ce)(Al,Ti,Mg)_{12}O_{19}$]			
	AGB hibonite	high $^{17}O/^{16}O$; high ^{26}Mg	50,52,58,59
	SN-II hibonite	high $^{18}O/^{16}O$; low ^{25}Mg; high ^{26}Mg	50,52
Other oxides (?)	[Fe oxide]	unknown structure/composition;	60,61
	[Cr oxide]	cubic structure, unknown composition	18
	[Ca-Al oxide]	unknown structure/composition	50
	[Mg chromate]	unknown structure/composition	50
	["hexagonal Al_2O_3"]	unknown structure	51
SILICATES			
Forsterite [$(Mg,Fe)_2SiO_4$]	AGB forsterite	high $^{17}O/^{16}O$	62-67
	SN-II forsterite	low $^{17}O/^{16}O$; high $^{18}O/^{16}O$	68
Enstatite [$(Mg,Fe)SiO_3$]	AGB enstatite	high $^{17}O/^{16}O$	62,69
	SN-II enstatite	normal $^{17}O/^{16}O$; very high $^{18}O/^{16}O$	53,62,69-72
Bridgmanite ($MgSiO_3$)	AGB bridgmanite	high $^{17}O/^{16}O$; probably a post-stellar shocked enstatite grain	73

This is a preprint, the final version is subject to change, of the American Mineralogist (MSA)
Cite as Authors (Year) Title. American Mineralogist, in press.
DOI: https://doi.org/10.2138/am-2020-7173

Amorphous Silicate	AGB amorphous Mg-Fe silicate	high $^{17}O/^{16}O$		74-76

References: 1. Verchovsky et al. 2006; 2. Lewis et al. 2018; 3. Lewis et al. 1987; 4. Bernatowicz et al. 1996; 5. Croat et al. 2005; 6. Bernatowicz et al. 2006; 7. Jadhav et al. 2013; 8. Jadhav et al. 2008; 9. Nittler et al. 1996; 10. Stadermann et al. 2005; 11. Amari et al. 2001c; 12. Haenecour et al. 2016; 13. Stroud et al. 2011; 14. Wopenka et al. 2011b; 15. Croat et al. 2013; 16. Gyngard et al. 2018; 17. Croat et al. 2003; 18. Croat et al. 2008; 19. Hynes et al. 2010; 20. Davis 2011; 21. Stroud et al. 2004a; 22. Hoppe et al. 1995; 23. Amari et al. 2001b; 24. Fujiya et al. 2013; 25. Liu et al. 2017c; 26. Nguyen et al. 2018; 27. Hoppe et al. 1994; 28. Amari et al. 2001a; 29. Hoppe et al. 1997; 30. Croat et al. 2010; 31. Liu et al. 2016; 32. Liu et al. 2018; 33. Lin et al. 2010; 34. José and Hernanz 2007; 35. Soker and Harpez 1999; 36. Groopman et al. 2012; 37. Croat et al. 2011; 38. Bernatowicz et al. 1999; 39. Lodders & Amari 2005; 40. Nittler et al. 1995; 41. Hoppe et al. 1996; 42. Groopman and Nittler 2018; 43. Stroud and Bernatowicz 2005; 44. Hynes et al. 2011; 45. Hutcheon et al. 1994; 46. Nittler et al. 1997; 47. Choi et al. 1998; 48. Takigawa et al. 2014; 49. Takigawa et al. 2018; 50. Nittler et al. 2008; 51. Stroud et al. 2004b; 52. Zega et al. 2011; 53. Bose et al. 2010a; 54. Zega et al. 2015; 55. Zega et al. 2014a; 56. Gyngard et al. 2010c; 57. Nittler et al. 2005; 58. Choi et al. 1999; 59. Nittler et al. 2011; 60. Floss et al. 2008; 61. Bose et al. 2010b; 62. Mostefaoui and Hoppe 2004; 63. Busemann et al. 2009; 64. Vollmer et al. 2009; 65. Zega et al. 2014b; 66. Nguyen and Messenger 2014; 67. Nittler et al. 2018a; 68. Messenger et al. 2005; 69. Floss and Stademann 2009; 70. Floss and Stademann 2012; 71. Vollmer et al. 2013; 72. Nguyen et al. 2016; 73. Vollmer et al. 2007; 74. Kemper et al. 2004; 75. Messenger et al. 2003; 76. Zinner 2014.